THE UNIVERSITY *of* EDINBURGH

Electrospun nanofibre veils and carbon fibre-based veils for enhanced electrical conductivity of carbon fibre reinforced polymer composites

Muhammad Waqas

A thesis presented for the degree of

Doctor of Philosophy

University of Edinburgh

School of Engineering

February 2023

Declaration of Originality

I hereby declare that this thesis and the work contained in and presented throughout this document have been made by myself, including those sections deriving from an article under review for which I am the first author. I confirm that this work has not been previously submitted for any other degree or professional qualification.

Muhammad Waqas

February 2023

Abstract

Carbon fibre reinforced polymer (CFRP) composites are comprised of high performance reinforcement carbon fibres and a polymer resin matrix. CFRP composites have been used by the commercial aerospace industry to manufacture structural composites due to their high mechanical strength, impact resistance, and thermo-mechanical properties. Carbon fibres are electrically conductive, however, epoxy-carbon fibre laminates have limited electrical conductivity in the through-thickness direction due to the insulating nature of the epoxy matrix. Enhanced through-thickness electrical conductivity is now desired for modern composites applications requiring lightning strike protection, electrostatic dissipation, and electromagnetic shielding.

Various technologies and materials such as resin modification, fibre surface modification, and interleaving have been investigated with the target to increase CFRP performance and through-thickness electrical conductivity. Interleaving, where a thin interleaving material is inserted between the dry carbon fabric plies or prepreg layers, is a common method for improving the interlaminar fracture toughness (IFT) and electrical conductivity of CFRP. Interleaves are also easy to add to the production process. Interleaving reinforcement is expected to improve the mechanical performance of composites under structural loads.

This thesis addresses the effect of conductive veil interlayers on enhancing the through-thickness electrical conductivity of CFRP composites. The research work carried out in this thesis was focused on investigating the use of electrospun nanofibres and microfibrous carbon fibre-based veils interleaved in carbon fibre reinforced polymer composites. These materials were used to assess the potential of the veils to improve the through-thickness electrical properties without compromising the mechanical properties of the composites. Electrospun nanofibre veils are well suited to resin infusion due to their high porosity, which makes it easier for resin to flow and wet well the nanofibres, providing favourable interfacial properties and mechanical robustness to the end-product.

The research work started with the design and development of a low cost nozzle-free electrospinning setup that can efficiently and evenly deposit the electrospun nanofibres at a higher production rate over a large surface of carbon fibre fabric. The equipment uses a rotating mandrel partially immersed within a polymer solution to produce fibres in an upward motion by inducing the formation of multiple Taylor cones and subsequently multi-jetting out of an electrified open surface. This lab-scale, high-throughput device has provided an alternative, economical route for nozzle-free electrospinning research, in contrast to the high costs associated with industrially available upscaling equipment. Among the device's technical specifications, a key feature is a cryo-collector mandrel capable of collecting nanofibres at sub-zero temperatures, which can induce ultra-porous nanostructures with wider pores. A multi-channel gas chamber allows the conditioning of the atmosphere, temperature, and airflow, while the chamber's design averts user exposure to the high-voltage components.

The processability of conductive polymers is an important research area in the field of polymer science. There have been several techniques reported in the literature on this topic. However, the scalability of many of those techniques and their manufacturability on an industrial scale are not always practically viable. The electrospinning of conductive polymers, in particular, has not been extensively studied, despite the potential commercial applications of electrospun nanofibers in areas such as sensors, anti-static coatings, membranes, biocompatibility, and energy storage. Polyaniline (PANI) has significant advantages among conducting polymers, it based on a low-cost aniline monomer. This polymer is easy to synthesise, has tuneable electrical conductivity, and high environmental stability. PANI has a low molecular weight, low solubility, an infusible nature, and a rigid backbone structure, which makes it necessary to be blended with other electrospinnable polymers to produce nanofibres. The conductive forms of PANI, polyaniline emeraldine base (PANI-EB), and polyaniline emeraldine salt (PANI-ES) were synthesised and characterised. Polyvinylpyrrolidone (PVP) has good solubility, mechanical strength, film forming, electrospinability, high molecular compatibility with other polymers, and the ability to form thermally stable composites. The PVP chemical interaction with resin could

provide good compatibility and enhance the mechanical properties of the CFRP composites.

In order to achieve the conductive electrospun nanofibres, polyaniline (PANI) in its emerald base (PANI-EB) and salt (PANI-ES) forms was combined with PVP to produce nanofibres in a one-step electrospinning process using a nozzle-free electrospinning setup to achieve the conductive electrospun nanofibres. The surface morphologies and chemical structures of the PANI-EB/PVP and PANI-ES/PVP nanofibres were characterised using different techniques. The incorporation of different contents of PANI-EB and PANI-ES in the PVP solution and their impact on the structure and properties of the nanofibres were investigated. Through electrical characterisation, It was found that a high amount of PVP compared to PANI (18:1 W/W) was required in order to electrospin the PANI/PVP solutions into nanofibres. This could be the reason that PANI/PVP electrospun nanofibre veils and their interleaved CFRP composites were not conductive; the presence of an insulating carrier polymer restricted the nanofibre veils' ability to reach the required electrical conductivity percolation threshold and their possible use in aerospace applications requiring higher electrical conductivity. A higher amount of PANI in the PANI/PVP solution was found to be unsuitable for electrospinning due to PANI's higher viscosity and electrical conductivity. Therefore, an alternative route was explored based on prefabricated veils.

As the electrospun nanofibre veils were not conductive, pre-fabricated microfibrous carbon fibre-based veils were used as interleaving in CFRP composites. These veils were made from loosely connected carbon fibre and nickel-coated carbon fibre with a binder, and their random orientation forms a porous network. Carbon fibre (CF) or nickel-coated carbon fibre (NiCF) veils were used as interlayers between standard carbon fibre reinforcement fabrics. The through-thickness electrical conductivity of the interleaved composites with CF or NiCF veils improved over 50 fold, from 0.18 to 9.47 and 9.16 S/cm, respectively, compared to the control composites. The introduction of conducting veils facilitated the creation of electrical pathway between the carbon fabric plies by reducing the non-conducting resin rich zone in the

interlaminar region. However, the interleaved specimens exhibited a ca. 20-24% reduction in their interlaminar shear strength (ILSS) and flexural strength.

In conclusion, the development of a nozzle-free electrospinning setup has proven its ability to overcome limitations and drawbacks associated with single and multi-nozzle spinneret configurations, such as low yield, limited production capacity, non-uniform electric field distribution, and clogging. This lab-scale high-throughput device can provide an alternative, economical route for needleless electrospinning research, in contrast to the high costs associated with industrially available upscaling equipment. This can help electrospun materials advance research in tissue engineering, wound healing, energy storage, energy harvesting, and other applications in a wide range of industrial sectors. This research revealed the difficulties associated with the production of conducting electrospun veils based on PANI, but other types of veils such as the prefabricated microfibrous carbon fibre-based veils show considerable promise. This research shows that conducting veil-interleaved CFRP composites can meet the functional integration requirement of the aerospace sector for electrical properties and can find applications in lightning strike protection, electromagnetic shielding, electrostatic dissipation, and structural health monitoring. The interdisciplinary work presented in this thesis opens up new pathways for exploration in regards to the fields of materials science, composites, and nanotechnology.

Lay Summary

Carbon fibre reinforced polymer (CFRP) composites are made up of carbon fibre reinforcements and a polymer resin matrix. CFRP composites have been used by the commercial aerospace industry to make structural composites because they are strong, don't break easily, and can withstand higher temperatures without losing their shape. Carbon fibres are electrically conductive, but due to the insulating nature of epoxy, they are not conductive in the through-thickness direction. Modern composites structures needs lightning strike protection, electrostatic dissipation, and electromagnetic shielding, which require electrical conductivity in all directions of the material.

CFRP composites performance and through-thickness electrical conductivity can be improved using various technologies and materials. Resin modification, fibre surface modification, and interleaving can be used to improve the electrical conductivity of composites. Resin modification and fibre surface modification can improve conductivity. However, the addition of nanoparticles (carbon nanotubes and other nanofillers) in the resin and fibre modification creates some issues, i.e., increase in viscosity of the resin, poor fibre wetting, fibre weakening, and porosity, which results in poor mechanical properties.

Interleaving reinforcement is a third phase, and in theory, it should improve the mechanical performance of composites when they are subjected to structural loads. In this thesis, we investigated how well electrospun nanofibre veils and microfibrous carbon fibre-based veils could improve the through-thickness electrical conductivity of CFRP composites without compromising their mechanical properties.

Electrospinning is commonly used to create nanofibrous veils ranging from micrometre thin membranes to thick non-woven fabrics. A very high voltage is used to propel liquid jets from a polymer solution towards a charged collector. The polymer elongates and twists as the jets travel to the collector, resulting in a collection of micron-sized or even finer fibres on the collector's surface. Electrospun nanofibre veils are good for resin flow because of their porosity.

The research began with the design and development of a low-cost electrospinning setup that can produce electrospun fibres at a high production rate. This lab-scale, high-throughput device has given researchers an alternative, and cheaper way to produce nanofibres. This setup is in contrast to the high costs of upscaling equipment used in the industry. One of the most important parts of the device's technical specs is a cryo-collector mandrel that can collect nanofibres at temperatures below zero, which can lead to ultra-porous nanostructures with larger pores. A multi-channel gas container allows the user to control the atmosphere, temperature, and airflow while also protecting the user from high-voltage shock.

Polyaniline (PANI) is a low cost conducting polymer, and with its tuneable electrical conductivity. In this research, polyaniline emeraldine base (PANI-EB) and polyaniline emeraldine salt (PANI-ES) were synthesised. PANI is difficult to electrospin, so it needs to be mixed with other polymers that can be electrospun to make nanofibres. Polyvinylpyrrolidone (PVP) has good solubility, mechanical strength, film formation, electrospinability, and high molecular compatibility with other polymers.

Polyaniline (PANI) in its emerald base (PANI-EB) and salt (PANI-ES) forms were mixed with PVP to make conductive electrospun nanofibres on carbon fibre fabric in a one-step electrospinning process. Different methods were used to characterise the surface morphology and chemical structures of PANI-EB/PVP and PANI-ES/PVP nanofibres. PANI/PVP electrospun nanofibres veils interleaved CFRP composites were made. However, the electrospun nanofibre veils were not conductive enough, so pre-fabricated microfibrous carbon fibre-based veils were also used. The carbon fibre and nickel-coated carbon fibre-based veils were used as interlayers and increased their through-thickness electrical conductivity.

Conducting veil-interleaved CFRP composites has significant implications for the modern commercial aerospace industry due to their electrical properties, and they can provide protection from lightning strike protection, electromagnetic shielding, electrostatic dissipation, and monitoring the health of structures.

Acknowledgements

First and foremost, I would like to thank Allah for all the blessings He has bestowed upon me. Without faith in Him, and the patience and perseverance He has granted me, I would not be where I am today.

Over the course of my PhD, I had the pleasure of working closely with many people, and I'd like to take this opportunity to thank them. Firstly, I would like to thank Prof. Vasileios Koutsos, my Principal Supervisor. He has provided me with support and guidance, which I have held in the highest regard. His scientific mind, and professional and personal guidance have been invaluable. I am deeply thankful for all the patience, insight, expertise, and belief in me throughout, and especially through the tougher times of COVID-19. I would also like to thank Dr Dipa Roy, my second supervisor I've truly liked my time in the composites lab, as well as the intelligent discussions and continued feedback on my work. I'd like to thank Dr. Norbert Radacsi in particular. Norbert has been instrumental in my research and learning process, and I cannot thank him enough. Thank you so much, Norbert.

I'd also like to thank all of the amazing scientists I've had the pleasure of working with in the past and now. It would be too many names to list each of you, but thank you for everything. Particularly, I would like to thank Dr James Davidson, Dr Wini Obande, Dr Adeel Shafi, James Quinn, Dr Aris Papasavvas, Zafar Iqbal, Urwah Arif, Haris Hussain, Junaid Ahmad, Faraz Fazal, Dr Rahmat Ullah, Fraz Saeed Butt, Hibbah Akhtar, Muhammad Nafees, Dr Antonios Keirouz, Dr Michael Chung, and Dr Ammara Akram. You made the beginning of my PhD so much easier, it was never going to be an easy task to cross disciplines, and I thank you both profusely for your patience, training, insightful discussions, and most importantly, your time. Dr. Francisco Javier Diaz Sanchez, I sincerely thank you for your assistance and support during the building of the nozzle-free setup. Dr Colin Robert, thank you for the time and effort you put into composites testing and data analysis. I would also like to thank Dr Thomas S. Glen for his patience, time, and experience in using the cryogenic focused-ion-beam scanning electron microscope. It was a pleasure to share those experiences with you.

I am fortunate enough to have some good friends in Edinburgh. My friends, Arslan Sohail and Muhammad Kaleem have made my PhD journey an exciting one, and I thank them for all the good times we have shared. The numerous positive experiences I had in Edinburgh opened doors for me, for which I will be eternally grateful.

To my brothers; Abdul Rauf, Farooq, Mahboob, Waqar, and Awais. I have always truly appreciated the bond we share together and the relationship I hold with each of you individually. I know I can always count on you. A special thanks to Abdul Rauf and Farooq for your valuable guidance and unique method of encouragement, which have always made me happy. I have truly appreciated your exceptional mechanisms of support, as well as drawing upon your scientific help, Thank you.

To my parents, there are not enough words that I could write to express how much you mean to me and how important your guidance has been in my life. Your hard work and your countless sacrifices have allowed me to be in the position I am in today. Your unconditional love, support, emphasis on the importance of education, and being the best man I can be have always pushed me to strive to build a better life for myself and us. There is nothing I could ever give you to repay you for all that you have done for me, but each day I will always strive to show you.

Table of Contents

List of Figure

List of Tables

List of abbreviations

AC	Alternating current
CAD	Computer aided design
CF	Carbon Fibre
CFRP	Carbon fibre-reinforced composites
DC	Direct current
DMF	N, N-dimethylformamide
FTIR	Fourier-transform infrared Spectroscopy
EDX	Energy-dispersive X-ray spectroscopy
EMI	Electromagnetic interference
ICPs	Intrinsically conducting polymers
ILSS	Interlaminar shear strength
NiCF	Nickel-coated carbon fibre
LE	Leucoemeraldine base
NF	Nanofibres
PAA	Poly(acrylic acid)
PAN	Polyacrylonitrile
PANI	Polyaniline
PANI-EB	Polyaniline emeraldine base
PANI-ES	Polyaniline emeraldine salt
PCL	Polycaprolactone
PE	Pernigraniline
PEEK	polyether ether ketone
PEDOT	Poly (3, 4-ethylene dioxythiophene)
PGS	Poly(glycerol sebacate)
POM	Polyoxymethylene
PPY	Polypyrrole
PVDF	Polyvinylidene fluoride
PPV	Poly (p-phenylenevinylene)
PVP	Polyvinylpyrrolidone
SEM	Scanning electron microscopy
XRD	X-ray diffraction
2D	Two-dimensional
3D	Three-dimensional
RPM	Revolutions per minute
wt%	Weight percentage
VARTM	Vacuum assisted resin transfer molding
mL	Millilitre

List of Symbols

Mpa	Mega Pascal
Tanδ	Damping parameter
ρ	Volume resistivity
L	Thickness of specimen
R	Electrical resistance
A	Area of sample
nm	Nano metre
mm	Millimetre
cm	Centimetre
σ	Surface charge
Q	Flow rate
k	Electrical conductivity of the fluid
ρ	Density of the fluid
E	Strength of the electric field
I	Current passing through the jet
r_0	Initial radius of the jet
h	Thickness of the layer
D	Diameter covered by the Taylor cone
F	Electrostatic force
M_w	Molecular weight
Ω	Ohms
kN	Kilo Newton
AWG	American wire gauge
Vf	Fibre volume fraction
M_f	Final mass of the specimen after combustion
M_i	Initial mass of the specimen
ρ_c	Density of the carbon fibre
ρ_r	Density of the cured resin
m	Metre
M	Molarity
N	Newton
P	Power
Pa	Pascal
S	Seconds
W	Watt
θ	Phase shift
g	Gram

Chapter 1 Introduction

1.1 Project background and motivation

Multifunctional materials have the potential to be used in lighter components made from composite materials, which are particularly advantageous for weight-sensitive applications in aircraft, automotive, sports utilities, and lightweight structures. The additional functionality should ideally neither increase the mass of a structure nor alter its mechanical properties [1]. Fibre-reinforced composite materials in particular offer great strength and stiffness at very low weights. Furthermore, they have a significant potential for multifunctionality, making them excellent for a wide range of high performance structural applications. Carbon fibre-reinforced polymer (CFRP) composites are pervasive in current commercial aerospace structures and gaining popularity in the automobile industry. However, despite the remarkable physical qualities of CFRP, the polymer matrices commonly employed are quite brittle and have limited electrical conductivity. Therefore they do not provide enough protection against lightning strikes or electromagnetic forces. Due to the aerospace industry's significant susceptibility to lightning strikes, these properties are very critical. In recent decades, extensive research has been conducted to develop technologies that can improve the mechanical and electrical properties of laminated composites using various methods. Researchers have looked into ways to make CFRP more electrically conductive in the through-thickness direction. Some of these methods include modifying the resin by mixing conductive materials into it or using a conductive resin,

changing the surface of the carbon fibre through grafting, growth, or chemical treatment, or using interleaves in the composites to add conductive materials between the layers of carbon fibres [2, 3].

Interleaving is a method to improve the electrical conductivity of CFRP composites in through-thickness direction. This is done by putting a thin interleaving material between the dry carbon fabric plies or prepreg layers. It's also easy to add interleaves during the manufacturing process. Interleaving improves the conductivity of CFRP in different ways, depending on the type and shape of the material used for the interleaving. An interleave with higher conductivity and density will increase the conductivity. A lack of interpenetration of resin in dense conductive interleaves will create resin-rich zones above and below it [4]. Electrospun nanofibres can be a good interleaving material because they have high porosity and can improve their mechanical properties, such as strength and stiffness [5]. While a solid interleave prevents penetration unless it is actively altered by sanding or drilling, metal-coated polymer fibre veils allow for interpenetration of the interleave. The compatibility of the matrix and interleaving material is very important. A good chemical affinity for one another will increase the interpenetration and enhance mechanical properties.

Electrospun nanofibres (NFs) have unique properties because of their high surface-to-volume ratio, fibre length-to-diameter aspect ratio, and high porosity [5]. Because of these properties, electrospun materials can be important materials in several areas of structural engineering. Incorporating conductive electrospun nanofibre veils into the CFRP composite could help to improve interfacial interactions for efficient load transfer from polymer matrix to nanofibre reinforcement; it is also possible to enhance its electrical conductivity without significantly affecting its other properties. The literature shows that interleaved nanofibre veils in polymer matrix composites could generally improve some mechanical properties such as delamination and impact resistance behaviour [6-8]. One of the main challenges is ensuring that the fibres are evenly distributed throughout the carbon fibre fabric. If the fibres are not evenly distributed, it can lead to variations in the mechanical and electrical properties of the composites, which can reduce their overall performance. Another challenge is ensuring that the electrospun fibres are securely attached to the layers of carbon fibre.

If the fibres are not properly attached, they may be prone to delamination, which can reduce their effectiveness. A nozzle-free electrospinning setup can produce nanofibres at a higher production rate which is a significant advantage for the applications considered.

In this thesis, a step-by-step guide for the design and construction of a temperature-controlled nozzle-free electrospinning device is described. It can permit researchers to conduct lab-scale research on high-throughput fibre production at a low cost. This setup enabled us to produce large electrospun veils at a higher production rate [9].

Previous investigations used electrospun interleaved veils as structural reinforcement to increase the mechanical properties of CFRP composites, but no research has been done to enhance the through-thickness electrical conductivity of CFRP composites using the conductive electrospun veils. Consequently, there is a huge potential for research in this area, which could be of great benefit to fundamental polymer science and CFRP composites.

1.2 PhD aims and scope

The research covered in this thesis aimed to investigate the use of conductive electrospun nanofibres veils and microfibrous carbon fibre-based veils as interlayers in carbon fibre-reinforced polymer composites and assess their potential to improve electrical properties without compromising their mechanical properties. The research planned to develop a method for efficiently collecting, evenly distributing, and manipulating the electrospun nanofibres on carbon fibre fabric. A nozzle-free electrospinning device was designed and constructed for the production of conductive electrospun veils by directly depositing them on carbon fibre fabric. The conductive electrospun veils were synthesised using polyaniline (PANI) and polyvinylpyrrolidone (PVP), and the effects of varying PANI concentrations on the structure and characteristics of the fibres were investigated. Furthermore, the research aimed also to investigate the use of pre-fabricated interleaving conductive veils to improve the electrical conductivity of CFRP materials without deteriorating their mechanical

properties. The resulting CFRP laminates with interleaved conductive veils were characterised in terms of their electrical and mechanical properties.

1.3 Thesis structure

This thesis contains seven chapters. Chapter 2 of this thesis provides a literature review on the topic of CFRP composites, interleaving conductive veils, electrospinning of conductive polymers, nozzle-free electrospinning, electrospun veils and their role in enhancing the through-thickness electrical conductivity of CFRP composites.

The literature review begins by discussing the general properties and characteristics of carbon fibre-reinforced plastics, including their high strength-to-weight ratio and their potential applications in a range of fields such as aerospace, automotive, and sporting goods. Further, it discusses the methods of enhancing the through-thickness electrical conductivity of CFRP composites; the use of interleaving conductive veils in CFRP composites, and the challenges associated with their production and incorporation into composite structures. It discusses the various methods that have been developed for the incorporation of electrospun veils into CFRP composites, and the challenges that remain in optimising their performance.

The literature review then discusses the use of electrospinning as a technique for the production of conductive veils, including both traditional nozzle-based electrospinning and nozzle-free electrospinning. The literature review focuses on nozzle-free electrospinning, a technique that allows for the production of fine, continuous fibres without the use of a traditional nozzle. It examines the various factors that can affect the structure and properties of electrospun veils, such as the concentration of the polymer solution and the electric field strength used during electrospinning. The next section of the literature review focuses on conductive polymers, such as polyaniline (PANI) and polypyrrole (PPy), etc., and their possibilities for electrospinning.

Overall, the literature review provides a comprehensive overview of the current state of research and development in the fields of CFRP composites, pre-fabricated conductive veils, nozzle-free electrospinning, and electrospun veils. It identifies common areas of research and development and highlights the potential benefits of

using these materials and techniques in the production of high-performance multifunctional CFRP composites.

Chapter 3 describes the experimental methods and apparatus that were used for each experiment in the thesis. A discussion is presented regarding the CFRP composites substrates used in the experiments and a detailed outline of the sample preparation methods and subsequent characterisation techniques.

Chapter 4 presents a step-by-step guide for the design and construction of a nozzle-free electrospinning device. Nozzle-free electrospinning can overcome limitations and drawbacks associated with single and multi-nozzle spinneret configurations, such as low yield, limited production capacity, non-uniform electric field distribution, and clogging. Most importantly, this lab-scale high-throughput device can provide an alternative economical route for nozzle-free electrospinning research, in contrast to the high costs associated with industrially available equipment. The device's technical features, including a cryo-collector mandrel and a multi-channel gas chamber, are extensively discussed in this chapter. The chapter also presents results from experiments using the nozzle-free electrospinning device to produce nanofibres using different polymers. These results demonstrate the device's ability to produce high-quality nanofibres with uniform diameter and morphology using different polymers at its high production yield and throughput. Large parts of this chapter have previously been presented in the following article:

Waqas, Muhammad, Antonios Keirouz, Maria Kana Sanira Putri, Faraz Fazal, Francisco Javier Diaz Sanchez, Dipa Ray, Vasileios Koutsos, and Norbert Radacsi. "Design and development of a nozzle-free electrospinning device for the high-throughput production of biomaterial nanofibers." Medical Engineering & Physics 92 (2021): 80-87.

Chapter 5 presents polyaniline emeraldine base (PANI-EB) and polyaniline emeraldine salts (PANI-ES) that were combined with polyvinylpyrrolidone (PVP) to produce nanofibres in a one-step electrospinning process using a nozzle-free electrospinning setup. The surface morphologies and chemical structures of the composite nanofibres were characterised. Four PANI/PVP electrospun nanofibres with

different PANI concentrations were prepared to investigate the effect of PANI concentration on the structure and properties of the nanofibres. The incorporation of different contents of PANI-EB and PANI-ES in the PVP solution and their impact on the fibre morphology were investigated. These findings are valuable for researchers interested in exploring the potential of nozzle-free electrospinning for the production of conductive nanofibres for various applications. Furthermore, PANI-EB/PVP and PANI-ES/PVP electrospun nanofibres were directly deposited on carbon fibre fabric. These electrospun-coated carbon fibre fabrics were used in the production of unidirectional interleaved CFRP laminates. The method of using electrospun nanofibre veils to increase the electrical conductivity of CFRP composites was not successful, possibly because the PANI/PVP electrospun veils were not electrically conductive due to the low concentration of polyaniline used in the electrospinning solution, and the insulating nature of PVP which is required in sufficient quantities for the successful electrospinning process. Some parts of this chapter will be presented in the following article:

Muhammad Waqas, Francisco Javier Diaz Sanchez, Valentin C. Menzel, Ignacio Tudela, Norbert Radacsi, Dipa Ray, and Vasileios Koutsos. "Polyaniline / Polyvinylpyrrolidone nanofibers via nozzle-free electrospinning." (Submitted, 2023).

Chapter 6 of this thesis presents the improvement in the through-thickness electrical conductivity of CFRP composites using interleaved conducting veils. Carbon fibre (CF) and nickel-coated carbon fibre (NiCF) veils were used in the experiments, and the results showed that the through-thickness electrical conductivity of the interleaved composites with CF or NiCF veils improved by over 50-fold. In addition, interlaminar shear strength (ILSS) and flexural strength testing were performed on the interleaved CFRP specimens, and the results showed that the introduction of conducting veils did not significantly affect the mechanical properties of the composites. Overall, the results of these experiments demonstrate the potential of conducting veils as interleaving materials for improving the through-thickness electrical conductivity of CFRP composites. Large parts of this chapter have previously been presented in the following article:

Waqas, Muhammad, Colin Robert, Urwah Arif, Norbert Radacsi, Dipa Ray, and Vasileios Koutsos. "Improving the through-thickness electrical conductivity of carbon fiber reinforced polymer composites using interleaving conducting veils." Journal of Applied Polymer Science 139, no. 43 (2022): e53060.

Chapter 7 of this thesis presents the overall findings of the preceding investigations and discusses prospective areas for future research. The findings of the previous chapters are summarised, and the potential implications and applications of these findings are discussed.

1.4 References

1. Harnden, R., David Carlstedt, Dan Zenkert, and Göran Lindbergh, Multifunctional Carbon Fiber Composites: A Structural, Energy Harvesting, Strain-Sensing Material. ACS applied materials & interfaces, 2022. 14(29): p. 33871-33880.

2. Baharozu, E., G. Soykan, and M.B. Ozerdem, Future aircraft concept in terms of energy efficiency and environmental factors. Energy, 2017. 140: p. 1368-1377.

3. Vallack, N. and W.W. Sampson, Materials systems for interleave toughening in polymer composites. Journal of Materials Science, 2022: p. 1-28.

4. Brown, S.C., Colin Robert, Vasileios Koutsos, and Dipa Ray, Methods of modifying through-thickness electrical conductivity of CFRP for use in structural health monitoring, and its effect on mechanical properties – A review. Composites Part A: Applied Science and Manufacturing, 2020. 133.

5. Palazzetti, R. and A. Zucchelli, Electrospun nanofibers as reinforcement for composite laminates materials–a review. Composite Structures, 2017. 182: p. 711-727.

6. Shakil, U.A., Shukur BA Hassan, Mohd Y. Yahya, and Saad Nauman, Mechanical properties of electrospun nanofiber reinforced/interleaved epoxy matrix composites—A review. Polymer Composites, 2020. 41(6): p. 2288-2315.

7. Wang, G., Demei Yu, Ajit D. Kelkar, and Lifeng Zhang, Electrospun nanofiber: Emerging reinforcing filler in polymer matrix composite materials. Progress in Polymer Science, 2017. 75: p. 73-107.

8. Palazzetti, R. and A. Zucchelli, Electrospun nanofibers as reinforcement for composite laminates materials – A review. Composite Structures, 2017. 182: p. 711-727.

9. Waqas, M., Antonios Keirouz, Maria Kana Sanira Putri, Faraz Fazal, Francisco Javier Diaz Sanchez, Dipa Ray, Vasileios Koutsos, and Norbert Radacsi, Design and development of a nozzle-free electrospinning device for the high-throughput production of biomaterial nanofibers. Med Eng Phys, 2021. 92: p. 80-87.

Chapter 2 Literature review

2.1 Composites

In its simplest form, a composite material comprises at least two elements that interact together to provide material qualities that are distinct from those of the individual constituents. They are not multiphase materials in which the different phases form naturally as a result of reactions, phase transformations, or other processes. In practice, most composites are made up of a bulk material's matrix with some form of reinforcement applied to increase the matrix's strength and stiffness [1].

Today's most prevalent manufactured composites can be classified into three categories. The most popular are polymer matrix composites. The matrix of these materials is a polymer-based resin. At the same time, the reinforcement is a range of fibres such as glass, carbon, and aramid. Polymers with fibre reinforcement are also known as fibre-reinforced polymers (FRP). Metal matrix composites: These materials employ a metal like aluminium as the matrix and reinforce it with fibres or particles like silicon carbide. They are becoming more common in the automotive sector. Ceramic matrix composites: These materials incorporate ceramics as the matrix which is refines with short fibres or whiskers such as silicon and boron nitride. They are used in applications involving very high temperature conditions [2].

2.2 Polymer Matrix composites

Polymer-matrix composites are easier to make than metal-matrix, carbon-matrix, or ceramic-matrix composites, regardless of whether the polymer is thermoset or thermoplastic. A thermoset begins with a non-polymerised resin as a precursor. The resin fully polymerises when heated, and this is known as curing. On the other hand, a thermoplastic polymer is fully polymerised before composite fabrication begins. The thermoplastic polymer softens above its glass transition temperature (T_g). It flows above its melting temperature during composite manufacture, allowing it to adhere to the shape of the mould cavity, especially while under pressure [3]. The relative simplicity of producing polymer-matrix composites is due to their low processing temperatures necessary for polymer-matrix composites fabrication. Processing temperatures for thermosets, such as epoxy and phenolic resin, typically range from room temperature to around 200°C; processing temperatures for thermoplastic polymers, such as polyimide (PI), polyphenyl sulphide (PPS), polyetheretherketone (PEEK), polyetherimide (PEI), and polyethersulfone (PES), typically range from 300 to 400°C.

In the last 40 years, the need for structural materials with high strength, high stiffness, and low density has grown quickly. Fibre-reinforced polymer (FRP) composites are more desirable materials for structural applications than conventional materials due to their high stiffness and strength-to-weight ratio [4]. FRP composites also perform well in terms of fatigue resistance and corrosion resistance; they also possess considerable design flexibility [5]. Numerous FRP composites structures have been used in a variety of industries, including aeronautics and aerospace, civil engineering, marine engineering, sports equipment, and many others [6, 7]. For example, the use of FRP composites in commercial aircraft has grown a lot over the past 20 years, as shown in Figure 2.1. The Boeing 787 and Airbus A350 XWB's structural weight is made up of composites materials to a more than 50% extent [7].

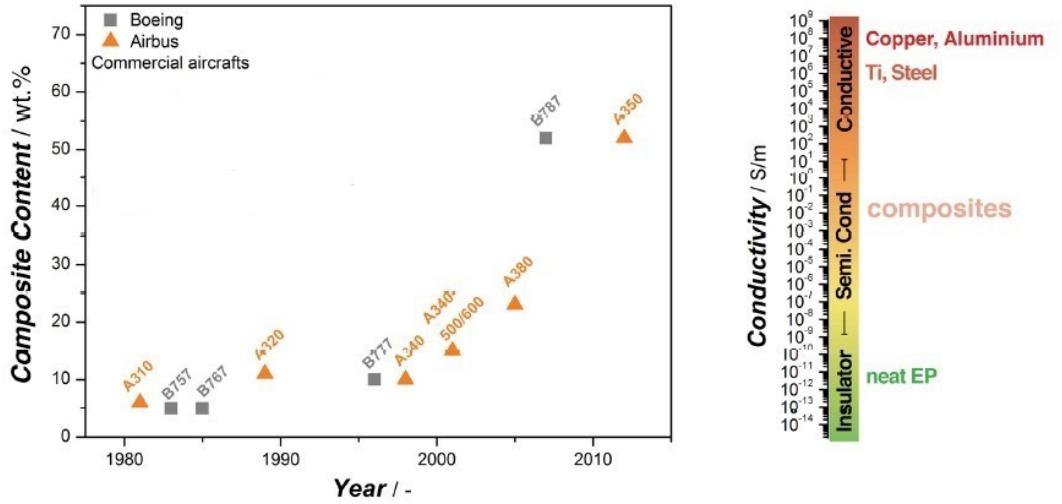

Figure 2-1 Trends in the use of composite materials in commercial aircrafts Airbus and Boeing since 1975 and the scale of electrical conductivity with relevant materials [7].

Carbon fibre polymer-matrix composites are attractive because of their favourable mechanical characteristics, high electrical and thermal conductivity, and low thermal expansion. Carbon fibres, despite their brittleness, have high strength and modulus, making them suitable as a reinforcement for polymers, metals, and ceramics. Apart from these properties, another important reason for the use of carbon fibres in commercial aircraft is their light-weight, which helps operators to reduce harmful emissions as directed by relevant environmental legislation. Effective reinforcing necessitates good fibre-to-matrix adhesion, especially for short fibres. The longitudinal tensile strength of a unidirectional composite (one with continuous fibres all pointing in the same direction) is unaffected by fibre-matrix bonding, but the transverse tensile strength and flexural strength (for bending in longitudinal or transverse directions) increase as fibre-matrix bonding increases [8]. Carbon fibre composites applications are rapidly expanding due to the decreasing cost of carbon fibres. This situation exerts an unprecedented demand on carbon fibre composites research and development. Carbon fibre composites are made up of at least one carbon fibre type, which can be short or long, unidirectional or multidirectional, woven or nonwoven. A polymer, metal, ceramic, or a mixture of materials is commonly used as the matrix. The matrix is a three-dimensionally continuous medium, except for sandwich composites,

whereas the filler might be three-dimensionally discontinuous. Unless the fibres are three-dimensionally joined by weaving or the application of a binder, such as graphite, carbon fibre fillers are typically three-dimensionally discontinuous [1].

Carbon-fibre reinforced polymer (CFRP) composites are increasingly used in renewables, automotive, and aerospace industries due to their high specific strength compared to metals. For example, modern aircraft are planned and built as a multi-material system combining mechanical and electrical structures that provide strength, lightning protection, and electromagnetic shielding [8, 9].

2.3 Through-thickness electrical conductivity of CFRP composites

Carbon fibre-reinforced polymer (CFRP) composites provide manufacturers and builders with an alternative to traditional metal alloys. The introduction of polymer composites in mainframes of modern structures, however, poses unique challenges and issues in terms of their multifunctional properties (e.g., electrical and thermal conductivities) [8, 9], as well as the potential risk of interlaminar damage extension under impact and fatigue loading due to the brittle nature of the matrix resins [10, 11]. To achieve the same electrical and environmental (temperature, humidity, pressure) performance offered by the metallic aeroplane structures, different electrical networks must be developed and implemented in the composite fuselage and other elements of the aircraft, such as the tail cone (electrostatic discharge protection) and wing (electrical conductivity against lightning strikes) [12].

The Electrical Structure Network (ESN) in the composite fuselage provides the electrical and environmental conditions required. Owing to the distinct physical and electrical properties of carbon compared to a metallic fuselage, maintaining the ESN system's performance during the life of the aircraft should be given particular attention. The ESN is a passive and metallic redundant network with thousands of metallic structural elements and specific ESN components. The aircraft designer must ensure the structural integrity of the aircraft due to the inherent electrical link between the ESN and CFRP structures. Even with the ESN, composite fuselages provide the best

weight and electrical performance solution while lowering airline operations & maintenance expenses and resulting in a smaller carbon footprint. The Metallic Bonding Network (MBN) acts as a failure current return path for equipment bonding and prevents lightning, electrostatic discharge, and electromagnetic interference shielding [13]. The two networks must be electrically connected to create a fully electrical and environmentally friendly aircraft system [9]. CFRP-designed aero-structures must be multifunctional, with high electrical conductivities comparable to metals and good mechanical qualities. Furthermore, the aircraft designer would have a simpler time not just installing the electrical system but also dealing with difficulties like electromagnetic interference (EMI), electromagnetic shielding (EMS), and lightning strike protection (LSP) of composite fuselage aircraft.

Although carbon fibres are electrically conductive (58.8 kSm^{-1} to 142.9 kSm^{-1}) [14], the matrix is electrically insulating. The carbon fibre composites have anisotropic electrical properties due to high conducting fibre, resulting in a high conductivity along the fibre direction (~2×10^4 Sm^{-1}). In contrast, the through-thickness conductivity is often low (~10^{-3} Sm^{-1}) due to the insulating resin-rich regions obstructing the current passage [15]. Because CFRP must meet safety criteria for LSP and EMI, their usage in aircraft is limited. The carbon fibre composite is currently bonded to copper or aluminium mesh to provide a conductive outer layer in aeroplanes to meet these specifications [16].

Recently in November 2021, a dispute between civilian aircraft manufacturer Airbus and Qatar Airways took a serious turn over paint and surface flaws on A350 jets. Five other airlines also raised the same issue regarding the paint. The paint is peeling off from different areas of fuselage and window of A350 aircraft as shown in Figure 2.2. The paint peeling and cracking exposed the copper foil which was aimed to provide the lightning strike protection. The exposed surface leaves open the carbon fibre fuselage for further structural and weather damages [17]. The weak adhesion between copper mesh and paint might be the reason for paint damage. The use of conductive interleaving within the composites might solve the insulating nature of CFRP composites in the through-thickness direction and enhance further the conduction in the long fibre axis direction.

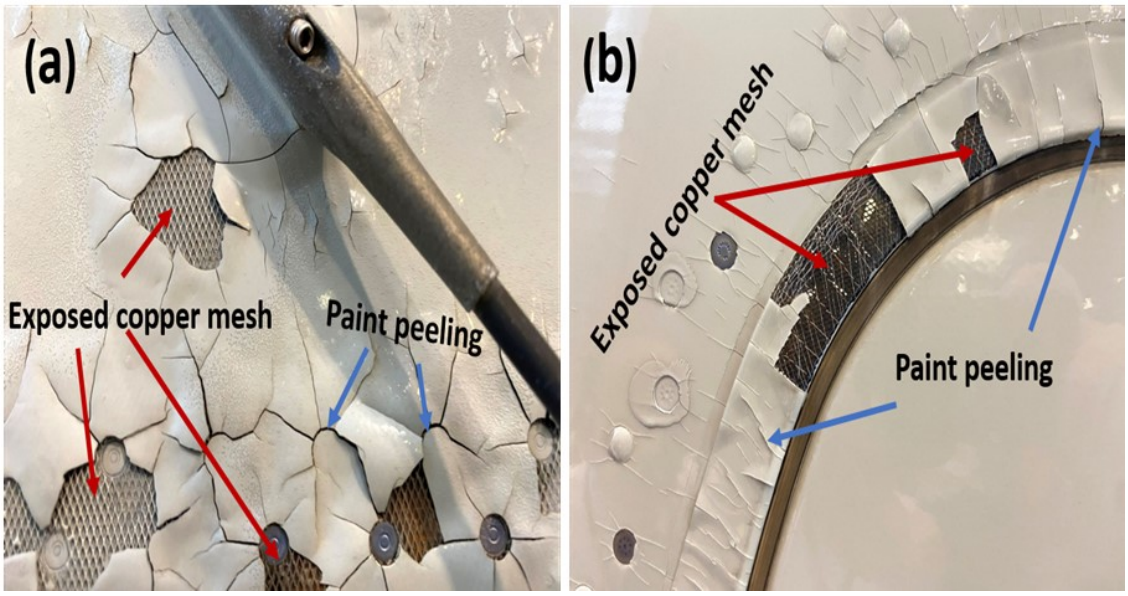

Figure 2-2 (a) Paint peeling, cracking and exposed copper foil on the fuselage of a Qatar Airways A350 aircraft (b) paint peeling, cracking and exposed copper foil on the window of a Qatar Airways A350 aircraft [17].

Recently, the through-thickness electrical conductivity of CFRP composites has gained huge popularity. As a result, the publication of works related to the through-thickness electrical conductivity of CFRP composites increased over the years. A survey of the publications associated with the electrical conductivity of CFRP composites in the past 10 years is given in Figure 2.3. These literature data were obtained based on the Scopus search system. The statistics indicate the development of research in the field of electrical conductivity of CFRP composites.

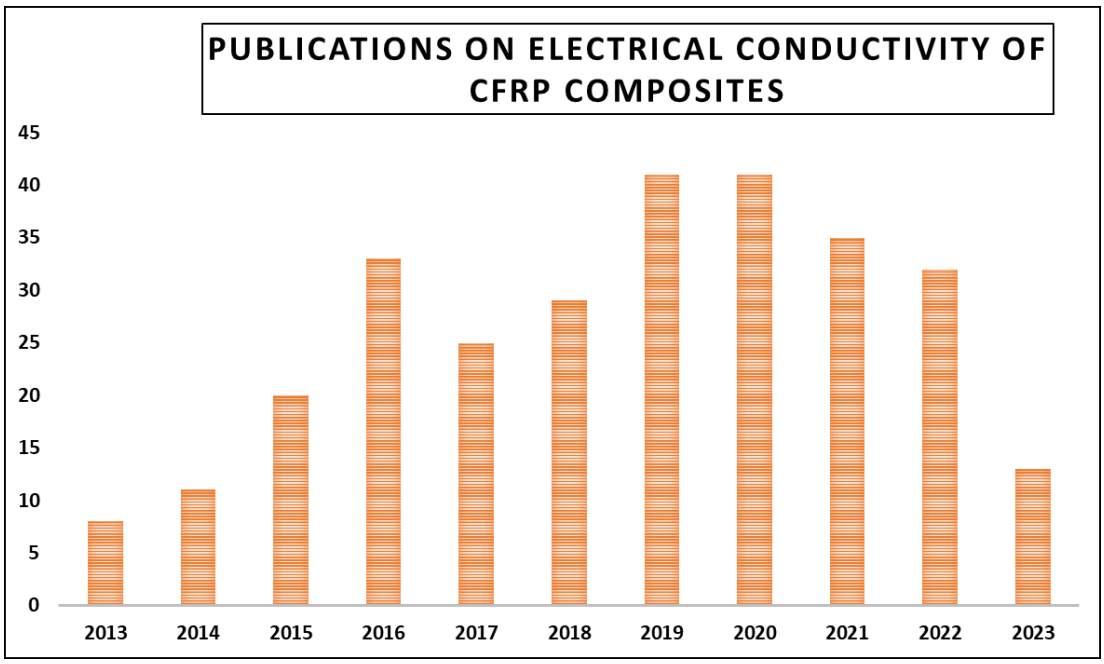

Figure 2-3 Comparison of the annual number of scientific publications related to the through-thickness electrical conductivity of CFRP composites since 2013 using the Scopus search system with the term "electrical conductivity of CFRP composites" as of May 2023.

Various technologies and materials have been investigated to increase CFRP performance and through-thickness electrical conductivity. Resin modification involves dispersing conductive material in a resin matrix or using a conductive polymer resin [18-25], fibre surface modification involves grafting, growth, or chemical action on the carbon fibre surface to improve conductivity [26-33], and interleaving involves adding conductive material between carbon fibre plies [34-50]. The resin modification method has a tendency to improve the conductivity by nine orders of magnitude. However, incorporating nanoparticles (carbon nanotubes and other nanofillers) in the resin generates some issues, such as higher resin viscosity, poor fibre wetting, porosity, and poor mechanical properties [51]. The fibre surface modification aimed to improve the interfacial interaction between the fibre and the matrix. However, additives on the carbon fibre tend to weaken the fibres, and decreased fibre wetting by the resin results in high surface tension regions near the dry fibre. These are the main problems associated with this method [30].

Interleaving is a common method for improving the interlaminar fracture toughness and electrical conductivity of CFRP by inserting a thinner interlayer between dry fibre reinforcement or prepreg layers. Interleaves are simple to add to the production process. However, the addition of additional layers reduces the fibre content and can also deteriorate the overall mechanical properties [9, 45, 52].

2.4 Interleaving

Interleaving, where a thin interleaving material is inserted between the dry carbon fabric plies or prepreg layers, is a common method for improving the interlaminar fracture toughness (IFT) and electrical conductivity of CFRP. Interleaves are also easy to add to the production process [53, 54]. Interleaving reinforcement is considered a third phase, and in principle, it is expected to improve the mechanical performance of composites under structural loads. However, the processes and phenomena by which nano-reinforcements produce their effects may be entirely distinct from those of micro-dimension reinforcement. For example, when the effectiveness of traditional reinforcement decreases over time, it may bring a larger surface area of nanofibres or nanoparticles into contact with the matrix, causing nano-scale dormant responses. On this scale, the interaction between two species, such as polymeric chains and nano-reinforcement, can be described by its own set of properties [55].

A variety of materials, including polymer films, adhesives, resins, and nonwoven mats or veils, are used to form interleaves for composites. Nonwoven interleaves were constructed using a variety of fibres, including carbon, and thermoplastic fibres. Depending on their structure, the interleaves can be divided into three categories: films, micro-fibres, and nanofibres. These can be further divided based on the material, typically but not always a polymer or carbon. Interleaves are formed from a combination of fibre types and carbon nanotube (CNT) based and hybrid interleaves that combine two or more different materials [54]. Polymers are the most common material used in composite interleaving. The most common polymers are polyamide (PA) [56], polystyrene (PES) [57], polyimide [50], polyether sulfone (PES) [58], polycaprolactone (PCL) [36], polyaryletherketone Cardo (PEK-C) [59], and polyvinylidene fluoride (PVDF) [60], in the form of loose fibres, films, or nonwoven

veils. Other fibre types, such as carbon and aramid, are occasionally combined in hybrid interleaves to improve their toughening or electrical properties.

Recently, Vallack et al. [54] summarized the different type of interleaves and their impact on various properties of CFRP composites Figure 2.4. The microfibre veil interleaves and electrospun nanofibre veil interleave were found to increase the interlaminar fracture toughness and maintain the in-plane mechanical properties. In addition, these micro and nanofibre veils are inexpensive, light, and provide ease of manufacturing. The interleaving of metal-coated polymer veils and hybrid CNT-based veils increased CFRP composites' mechanical properties and through-thickness electrical conductivity.

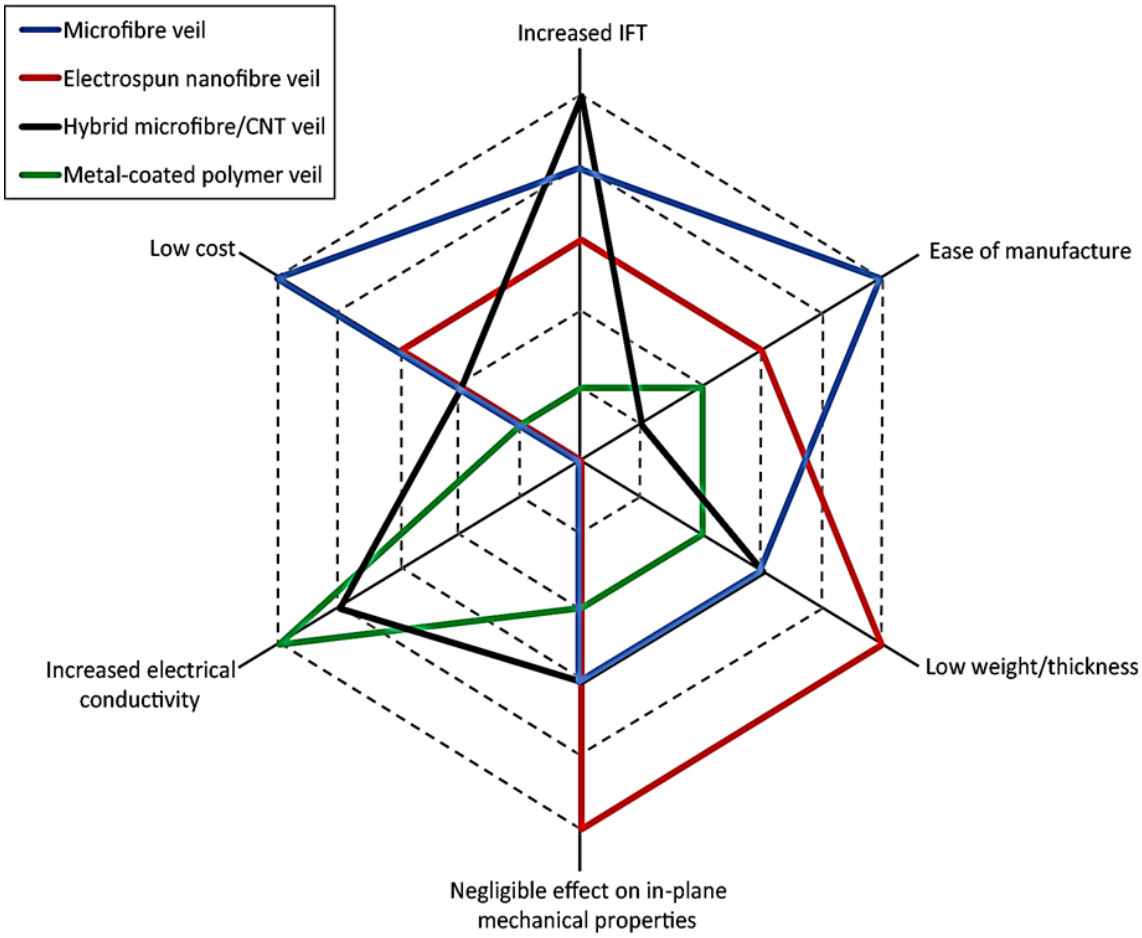

Figure 2-4 Image showing the effect of different types of interleaves on the properties of CFRP composites (reproduced with permission from Copyright 2022 Springer Nature) [54].

Interleaves can reduce delamination by bridging the cracks along matrix-rich interlaminar regions and making cracks follow a more complicated path, which uses more energy in the process [61]. Nonwoven interleaves can be used in composites laminates to provide electrical conductivity, EMI shielding, corrosion resistance, improved fracture toughness, fire protection, as a surface carrier, as a resin flow medium, or as a surface finish [62]. Interleaves are used in the aerospace industry for several reasons, such as to improve acoustic damping in metal structures and stop fatigue cracks from spreading in carbon fibre-reinforced plastics [63]. Interleaves can be inexpensive ways to make the space between layers stronger. They are typically easy to add to a composite lay-up. On the other hand, they add unwanted weight and thickness and can reduce electrical conductivity. Furthermore, if film interleaves are not porous enough, they can stop the resin from flowing during infusion [64]. Since the main benefit of carbon fibre composites in aircraft is their strength-to-weight ratio and stiffness-to-weight ratio, it makes sense that if more plies are added to the laminate for aerospace structures, they should be as light and thin as possible [55].

2.4.1 Veil interleaved CFRP composites

Vipin Kumar and co-researcher [45] used interleaved multiwall carbon nanotube (MWCNT) buckypaper (BP) to replace resin-rich areas in CFRP laminates. The BP paper interleaved laminates had a through-thickness electrical conductivity of 0.52 S/cm compared to 0.07 S/ cm in the control sample. The flexural strength of 1 BP paper interleaved laminate was 581.75 MPa, compared to 584.5 MPa for the control laminate. Flexural strength starts to decline when the number of interleaving BP papers in the laminate increases. The flexural strength of 4 BP paper interleaved laminate was 378.25 MPa. The use of MWCNT-BP has limited capacity to increase the through-thickness electrical conductivity, while an increasing number of interleaving BP paper deteriorates the mechanical properties.

Li et al. [52] used polyamide 12 (PA12) films loaded with MWCNT as interleave between carbon fibre prepreg layers to improve the electrical conductivity of CFRP composites. The stacking order of the laminates was $[0°]_{12}$, with MWCNT modified PA12 films and unmodified films inserted between each ply. The through-thickness

electrical conductivity of control was 8.6×10^{-5} S/cm, and 1.8×10^{-3} S/cm for 10 wt.% MWCNTs/PA12 films interleaved samples. The Mode I and Mode II fracture toughness of 10 wt.% MWCNT doped film laminates increased by 59.3% and 112.8%, respectively.

Guo and Yi [39] used AgNW (silver nanowires) coated paper interleaves for improving the electrical conductivity of CFRP composites. The AgNW coated paper interleaved laminates had a through-thickness electrical conductivity of 0.179 S/cm compared to 0.047S/ cm in control samples. Overall, the through-thickness electrical conductivity improved, but the Mode I and Mode II interlaminar fracture toughness decreased by 67.3% and 66.9%, respectively. The AgNW coated papers were too densely packed to allow the resin to pass through uniformly, which might have adversely affected the wetting. This indicates that a porous interleave with better resin compatibility could be more useful.

In another work, Guo et al. [9] employed Ag coated interleaves made of nylon and Kevlar veils to increase in-plane and through-thickness electrical conductivity of CFRP composites. The nylon veils were made from long continuous nylon fibres, while the Kevlar veils were made from chopped Kevlar fibres that were randomly placed. The through-thickness electrical conductivity of control was 0.122 S/cm, while for both Ag plated nylon and Kevlar veils, interleaved samples was 3.45 S/cm. The addition of the Ag coated nylon, and Kevlar veil interleaves in the CFRP improved the Mode I (Mode II) fracture toughness by 92% (221%) and by 37% (130%), respectively. The veil interleaves acted as obstacles arresting crack propagation between the plies.

Hu et al. [65] recently used unidirectional carbon fibre and epoxy prepreg along with copper-nickel polyester veils (CNPVs) as functional interlayers. The stacking order of the laminates was $[+45/0/45/90]_{4s}$, with CNPVs inserted between each ply. The through-thickness electrical conductivity of the control sample and the CFRP laminate with copper-nickel polyester veils were 1.5×10^{-3} S/cm and 3.25 S/cm, respectively, exhibiting a three order of magnitude improvement. In addition, Mode I and Mode II fracture toughness increased by 59% and 31%, respectively.

Recently Liu et al. [53] reported that a nickel-coated carbon fibre (NiCF) veil improves the electrical conductivity and fracture toughness of carbon fibre/epoxy composites. The unidirectional carbon fibre/epoxy prepregs were used for manufacturing the laminates. A layer of NiCF veil was inserted into mid-plane to fabricate 24 plies unidirectional composite with a layup of $[0°]_{24}$. The control sample had 2.4×10^{-3} S/cm through-thickness electrical conductivity, whereas CFRP laminates with NiCF veil of areal densities of 17 g/m^2 and 34 g/m^2 achieved values of 5.5×10^{-3} S/cm and 7.7×10^{-3} S/cm, respectively. Interleaved specimens increased their Mode I and Mode II fracture toughness by 75% and 34%, respectively.

2.5 Conductive polymers

Intrinsically conductive polymers (CPs) are an intriguing class of organic materials that are manufactured with a wide range of chemical structures and micro and nano-morphologies to produce materials with specific macroscopic physical and chemical properties. In 1977, Heeger, MacDiarmid, and Shirakawa made the ground-breaking discovery of polyacetylene, the first conducting polymer [66]. For this work, they were jointly awarded the Nobel Prize in Chemistry in 2000. This discovery created an entirely new area of study that focused on the frontiers between polymer chemistry and solid-state physics. Since then, interest in this fascinating class of polymers has steadily grown, establishing itself as a thriving field of research that is both exciting and multidisciplinary [67, 68].

CPs are π-conjugated organic polymers, their molecules having their skeletal carbon atoms linked by both π-bonds and the prolonged overlap of π-electron orbitals. Consequently, neutral CPs exhibit a semiconductor electronic structure with a completely filled π-band (valence band) and an empty π^*-band (conduction band), which are separated by an energy gap of the order of 1 eV. The intrinsic conductivity results from doping, i.e., when electrons are withdrawn from or injected into the conjugated polymeric chain, while the overall electroneutrality is maintained by the inclusion of counter ions, also known as dopants. The doped state is obtained through simple oxidation or reduction events that result in the development of delocalized charged structural defects (polarons, bipolarons, and solitons) that are energetically

positioned within the energy gap and function as charge carriers. Through simple and reversible chemical or electrochemical doping/de-doping, it is possible to control the electrical conductivity of these polymers across the entire spectrum from insulating to metallic [67, 69]. The movement of neutral soliton, positive and negative soliton of polyacetylene (PA) is shown in Figure 2.5.

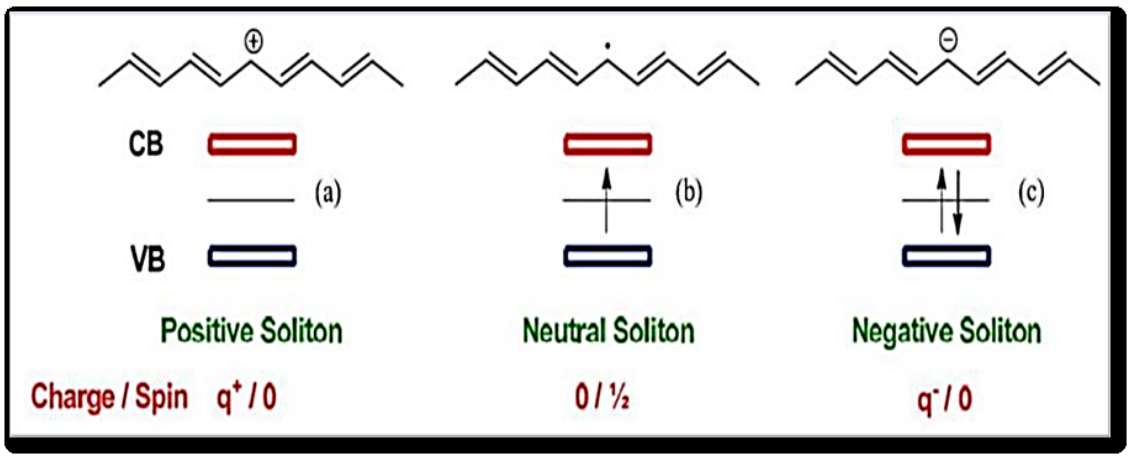

Figure 2-5 The boundary condition (neutral soliton) of two degenerate ground states of t-PA and charged solitons (positive and negative) (a) positive soliton, (b) neutral soliton, and (c) negative solution [70].

In conjunction with simple control of the doping level, the electronic structure of CPs can be reversible by designing novel chemical structures at the molecular level using synthetic chemical or electrochemical strategies. This enables them with a range of optical, electronic, and redox/electrochemical properties. This approach has grown to provide a massive library of chemically varied, lightweight, and flexible polymer structures with desirable qualities for a wide range of properties and significant technological impact, many of which have reached the market see Figure 2.6 [69].

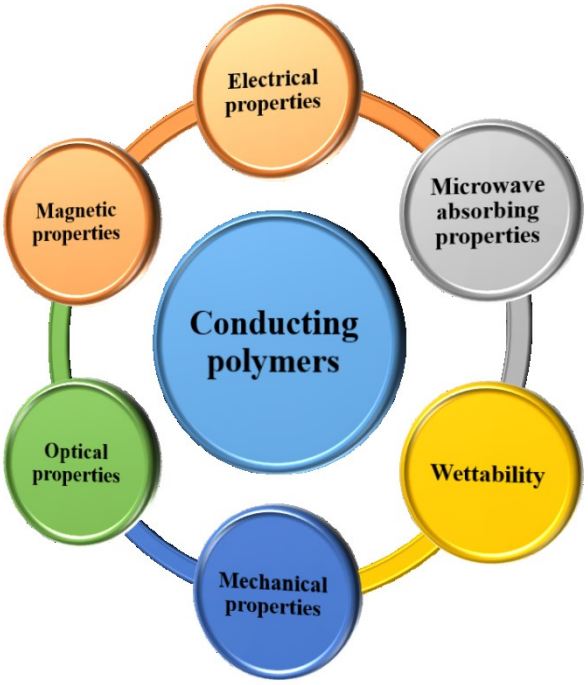

Figure 2-6 Properties of conductive polymers (adapted from [71]).

CPs have significant advantages over their inorganic semiconducting and metallic counterparts in terms of chemical diversity, tuneable conductivity, low density, cost, and flexibility. However, plenty of work is to be done to overcome their inherent problems with solubility/processability, conductivity, and long-term stability. Therefore, the development of CP-based hybrid composites with increased characteristics and controlled shape and morphology has become a prominent area of research within the discipline. CPs nanocomposites with various carbon nanomaterials, metal oxide nanoparticles, or hydrogel inorganic matrices are typical examples [68].

2.6 Electrospinning

Electrospinning is a versatile process used for producing fibres with diameters in the order of tens of nanometres to micrometres using electrostatic forces. The one-dimensional (1D) and two-dimensional (2D) structured materials produced from electrospinning have attracted significant attention due to their ease of synthesis, promising properties, and possibilities of functionalization [72]. Polymer electrospun fibres have unique properties due to their high surface-to-volume ratio, fibre-length-to-diameter aspect ratio [73], and porosity (generally ≥70%) [74]. Nanofibres can be used for diverse applications such as filtration [75], electronic textiles [76], drug delivery [73], tissue engineering [77], wound dressing [78], sensors [79, 80], composites [81], and so on.

Zeleny first outlined the electrospinning principle in his published work on the behaviour of fluid droplets at the end of metal capillaries [82, 83]. Later, in 1934, Formhals patented the marketed electrospinning technique for the production of textile yarns in the United States under patent number 195704 [84, 85]. In 1936, Norton received a patent for an improved method of electrospinning that used an air blast to aid in the creation of fibres rather than a polymer solution [86, 87]. Electrospinning is based on using an external electric field to induce polymer fluid change by the elongation and whipping of the jet, which is the electrospinning principle. Taylor established the concept of the Taylor cone in 1969, which is connected with the electric field-induced deformation of a liquid surface into a distinctive shape. The theoretical analysis of the disintegration of liquid drops in electric fields, the computation of the electric force acting on fine jets, the critical voltage for inducing jet elongation, and the voltage values at which Taylor cones are generated are detailed in next section [88, 89].

2.6.1 Basic principle of electrospinning

Electrospinning is an electro-fluid dynamics process that causes electrified liquid jets to whip and elongate to form fine fibres [90]. A standard laboratory-scale setup consists of four main components: a high-voltage DC (or AC) power supply, a syringe

pump, a nozzle (usually metallic capillary), and a collector that can simply be a metallic foil/plate/disc [91]. Figure 2.7 (a) is a schematic illustration of the electrospinning system, which consists of a disposable syringe with a metallic nozzle, a high-voltage power supply unit, and a collector. Typically, the nozzle (electrode) is charged to a high voltage, such as +30 kV, while the collector is charged to a high voltage in the opposite direction, such as -10 kV. During conventional electrospinning, electrostatic forces accumulate by applying a high voltage to a polymer solution extruded through a nozzle-spinneret. As a result, they induce a conically shaped geometry referred to as the 'Taylor cone' at the nozzle's orifice. The repulsive electric forces overcome the surface tension of the polymer solution, leading to vigorous whipping and splitting motions due to the bending instabilities generated, enabling a jet stream of fibres to travel towards a neutral (or oppositely charged) collector see Figure 2.7 (b) [92]. A collector, which receives the deposition of electrospun nanofibres from the charged jets, is positioned at a predetermined distance from the metallic capillary nozzle.

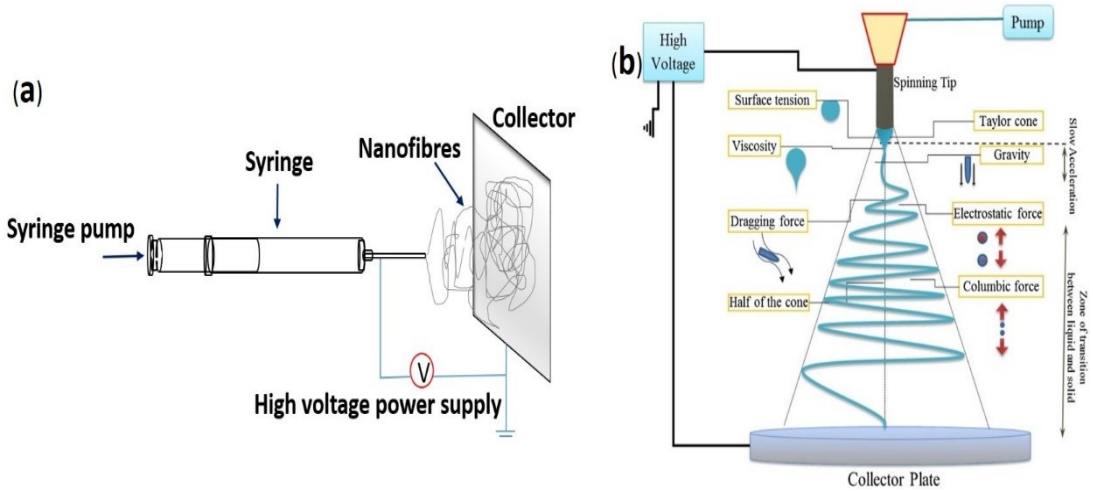

Figure 2-7 (a) Schematic diagram of a nozzle-based electrospinning setup (b) Image showing the formation of Taylor cone at the tip of nozzle spinneret [93].

The jet initially follows a nearly straight line for a certain distance away from the tip of the spinneret. The viscoelastic qualities of the fluid should be able to inhibit the Rayleigh instability, which would otherwise cause the jet to fragment into droplets. Surface charges travel with the jet, producing a current that flows through it. In the straight segment, the velocity, length, and diameter of the jet are measurable. It was

estimated that the jet's velocity at the end of the straight segment was 1-15 m/s [94]. The critical straight segment length (L) can be determined using the following equation:[95, 96]

$$L = \frac{4kQ^3}{\pi\rho^2 I^2}\left[\frac{1}{R_0^2} - \frac{1}{r_0^2}\right]$$

Where $R_0 = (2\sigma Q/\pi k\rho E)^{1/3}$, σ is a surface charge, Q is flow rate, k is the electrical conductivity of the fluid, ρ is the density of the fluid, E is the strength of the electric field, I is the current passing through the jet and r_0 is the initial radius of the jet.

The polymer jet, after leaving the spinneret experience surface tension and viscoelastic force which tend to prevent it from moving ahead. As a result, the acceleration decelerates gradually. As the jet is continuously stretched, the diameter of the jet in the straight segment drops monotonically with the distance from the tip. When the acceleration falls to zero or remains constant, even a minor disturbance might disrupt the straight movement. As a result, instability can readily occur due to the electrostatic repulsion between the surface charges living on the jet as it enters the far-field regime [96].

An electrically charged jet may experience three different forms of instabilities in the far-field area. The first type is axisymmetric, known as Rayleigh instability, which may result in droplet formation. It is controlled by surface tension and can be inhibited by a high electric field [97-99]. The second type is also axisymmetric and is produced by an electric field stronger than the first type. Finally, non-axisymmetric is the third type, often known as whipping or bending instability. It defines long wave jet disturbances as being caused by aerodynamic instability and the "lateral electrostatic force" in a radial direction relative to the jet, as a result of electrostatic repulsion between surface charges in a strong electric field [97, 100].

Whipping instability drastically decreases jet diameter because it greatly lengthens the path over which the jet speeds up and stretches before it is deposited on the collector. During the whipping process, the length of the jet can increase by as much as 10,000 times in a brief period of 0.05 seconds or less. The elongation (drawing) rate is

extraordinarily high (up to 1,000,000 s^{-1}). As a result, the diameter of the jet is lowered by several orders of magnitude, resulting in the creation of fibres with sub-micron and even nanometre scale diameters [101].

Typically, nozzle-based electrospinning apparatus is primarily employed for manufacturing nanofibres in small quantities in the laboratory, evaluating the spinnability of new materials, and optimising electrospinning parameters prior to large-scale production. However, it will be challenging to accurately control the shape of the deposited nanofibres when whipping instability is present. Considering that the production output of nozzle -based electrospinning devices is commonly meagre, ranging at 0.01 – 0.3 g/h, scaling up the process has been progressively studied as a suitable approach to industrialising this fabrication process [92]. Over the years, this was generally achieved by scaling up the spinneret's structure while retaining an energetically stable and well distributed configuration. Unlike multi-nozzle electrospinning, where the electric field around a given nozzle is affected by the nearby jets, which can produce inhomogeneous fibres, free-surface electrospinning is an alternative method capable of producing fibres at high throughput with no constraints of clogged nozzles [102].

2.6.2 Nozzle-free electrospinning

The concept behind free-surface electrospinning was initially described by Yarin and Zussman back in 2004 [103]. The self-organisation of electrified liquid jets from an open flat surface was mathematically delineated by Lukas et al. in 2008 [104]. However, research surrounding needleless electrospinning equipment accounts for less than 1.3% of the available literature. During nozzle-free electrospinning, the polymer solution is sub-merged in a bath containing a rotating cylinder electrode against a biased rotating collector electrode [103, 105]. By controlling the motor, the rotating speed of the roller can be changed. High-voltage power with a potential greater than 40 kV needs to be applied between the two rotating electrodes, which induces the formation of multiple Taylor cones emerging from the rotating electrode surface immersed in the solution bath [106, 107]. When voltage is applied on the roller, the

liquid changes to a conical shape and forms a considerable number of Taylor cones (Figure 2.8) on the surface of the rotating spinneret.

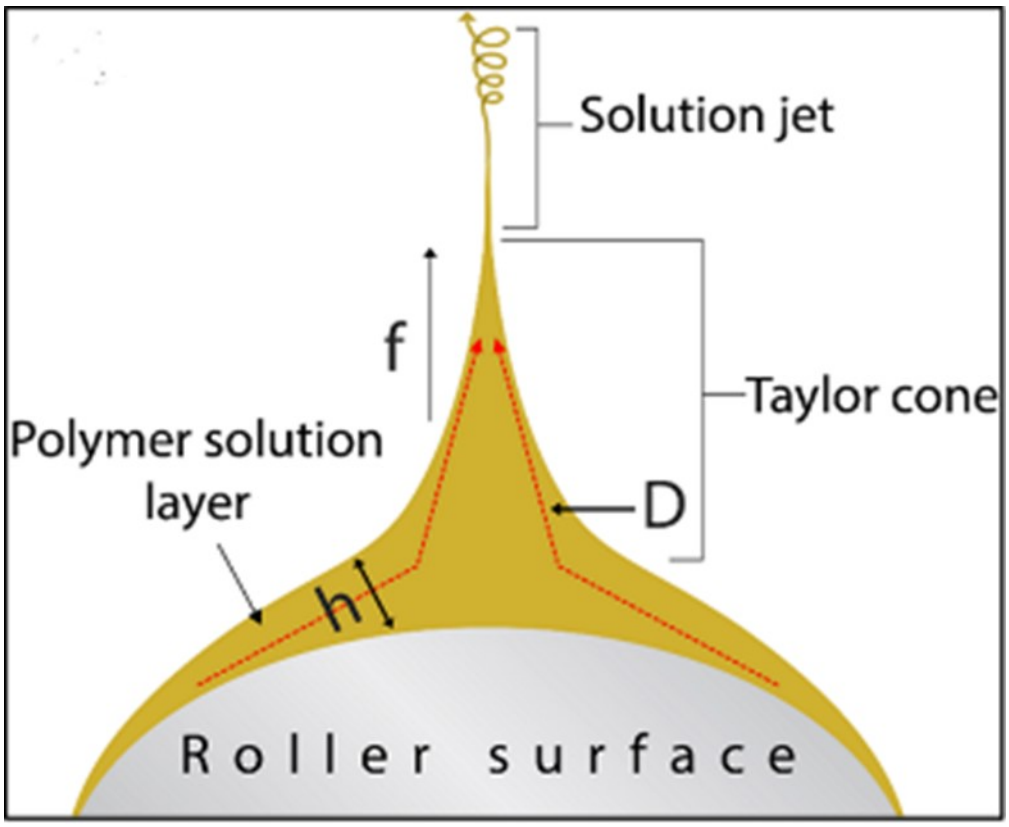

Figure 2-8 A schematic diagram of a free-surface electrospinning Taylor cone formation, where h is the thickness of the layer, D is the diameter covered by the Taylor cone, and f is the electrostatic force [108].

The roller electrospinning method has been proven to be a continuous and efficient process for fabricating NFs. This could be possibly attributed to the high number of patents associated with free-surface electrospinning setups and the extravagant costs of the commercially available equipment. For instance, products such as Nanospider TM (Elmarco, Ltd., Czech Republic[109], an industrial-scale electrospinner, where a high-voltage potential (up to 80 kV) facilitates the formation of fibres out of a polymer-layered thread at a defined rate, cost anywhere between 170,000 to 300,000 USD [109, 110]. Ultimately the prevalence of conventional electrospinning prevents the clinical translation of several exciting and innovating advancements in the field, which present no real-world impact.

2.6.3 Factors influencing the nozzle-free electrospinning process

In nozzle-free electrospinning, the electrospinning parameters are classified as independent and dependent. The independent parameters are further classified as primary and secondary independent parameters, e.g., the type of solvent, polymer, molecular weight, the type and amount of additives, and the concentration of the polymer solution are primary independent parameters. However, the solution properties e.g., viscosity, conductivity, and surface tension, which have a direct impact on the electrospinning process, are secondary independent parameters.

Table 2-1. Parameters of nozzle-free electrospinning [111, 112].

Independent parameters	**Dependant parameters**
o Polymeric solution properties (molecular weight, electrical conductivity, surface tension, viscosity) o Geometry of electrode o Velocity of rotating spinneret o Velocity of collector o Ambient conditions (relative humidity, temperature) o Distance between electrodes	o Number of Taylor cones, density of jets o Life of jets o Thickness of polymer solution layer on the surface of roller o Force acting on a jet o Spinning area o Distance between jets o Jet length in stable zone o Fibre diameter and distribution o Non-fibrous area o Launching time of jets o Total average current, current/jet

2.6.4 Electrospinning of conductive polymers

Intrinsically conducting polymers (ICPs) have drawn considerable attention because of their controllable electrical conductivity, ease of synthesis, low cost, magnetic and optical properties [71, 113]. A variety of conducting polymers, e.g., polypyrrole (PPY) [114], poly (p-phenylenevinylene) (PPV) [115], polyaniline (PANI) [76], poly (3, 4-ethylene dioxythiophene) (PEDOT) [116], polythiophene (PTh) [117], and other derivatives, etc.), have unique electronic structures as shown in Figure 9. These unique properties confer ICPs their electrical conductivity, high electron affinity, and low ionization potentials. Furthermore, ICPs are organic polymers; they have a reversible

doping/dedoping process and have controllable chemical and electrochemical properties depending on their synthesis method [118].

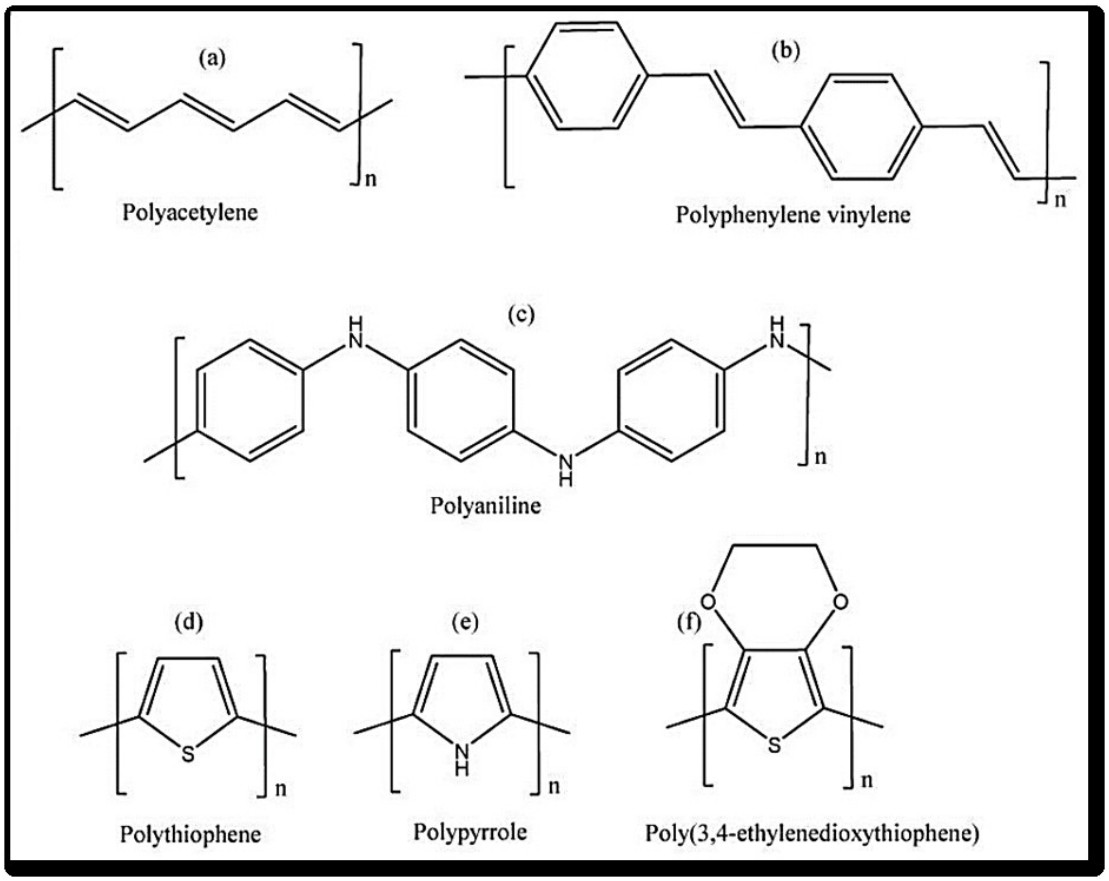

Figure 2-9 Chemical structures of the mostly studied conductive polymers (a) Polyacetylene (b) polyphenylenevinylene (c) polyaniline (d) polythiophene, (e) polypyrrole and (f) poly (3, 4-ethylenedioxythiophen) [70].

Polymer nanostructures (fibres and tubes) can be made using various techniques, including electrospinning, self-assembly, interfacial polymerization, chiral reactions, and template synthesis. In comparison to other synthetic methods, the electrospinning process appears to be the only one capable of mass-producing continuous long nanofibres [113]. In general, conductive polymers are not easy to electrospun because they have low molecular weights, do not dissolve well, and have rigid backbone structures. These properties limit the polymers' spinnability [119]. In order to address the processability issues of conductive polymers, numerous research groups have attempted a variety of strategies, including the introduction of side chains, the regulation of main-chain architecture, the invention of new monomer types, and the

incorporation of functional dopants. Blending conductive polymers with other polymers to produce composite structures and coatings are the most frequent ways. Blending with a polymer that can be easily electrospun is a common method of compensating for poor spinnability. Nonetheless, the presence of an insulating carrier polymer provides a conductivity percolation threshold that restricts their use in applications requiring high conductivity values [119, 120].

PANI has significant advantages among conducting polymers, such as low-cost aniline monomer, ease of synthesis, tunable electrical conductivity, and high environmental stability [121]. Conducting electrospun polymer mats provides the possibility of electrical conductivity while having a three-dimensional (3D) network of fibres. These electrospun mats have high porosity, high surface area, and enhanced surface functionalities than the original material or any other known form of the material [122, 123].

PANI's electrospinning produces nanofibre-based nonwoven mats with attractive features and enhanced properties compared to bulk materials. Due to their conjugated structures, all the conducting polymers are insoluble in common solvents. PANI has a low molecular weight, low solubility, infusible nature, and rigid backbone structure, which makes it necessary to blend it with other non-conducting electrospinnable polymers to produce nanofibres. PANI exists in three isolable oxidation states, fully reduced leucoemeraldine base (LE), the half oxidized emeraldine base (EB), and fully oxidized pernigraniline (PE). The polyaniline emeraldine base (PANI-EB) is usually doped by protonic acids to obtain a conducting form of polyaniline emeraldine salt (ES) and then blended with other to be electrospun [124]. Many researchers have reported the electrospinning of blends containing a mixture of PANI and other polymers such as polyvinylpyrrolidone (PVP) [76], polystyrene [125], polyacrylonitrile (PAN) [126], polyvinylidene fluoride (PVDF) [122] and polyethylene glycol (PEO) [127].

Polyvinylpyrrolidone (PVP) is a water-soluble polymer that has stability, higher degree of compatibility with other polymers on a molecular level, and high mechanical strength. It can be thermally cross-linked and can make thermally stable composites. PVP is used as a steric stabilizer to intercept the agglomeration of colloids. It imparts

properties such as hardness, high crystallinity, low solubility, and thermal resistance and thermal resistance to the composites [128]. PANI and PVP blends are of particular interest because they exhibit the electrical properties of PANI and the mechanical properties of PVP [129]. In PANI/PVP polymer blends, a hydrogen bonding develops between the carbonyl group of PVP and Nitrogen-hydrogen of PANI, which is responsible for PANI's dispersion in the blend [130].

Recently, the electrospinning process has gained huge popularity, and the publication of works related to electrospinning increased over the years. A survey of the publications related to electrospun PANI nanofibres in the past 17 years is given in Figure 2.10. These literature data were obtained based on the Scopus search system. The statistics indicate the development of research with PANI nanofibres generated through electrospinning. Furthermore, the growth of patents for various uses shows the electrospinning process's growing popularity.

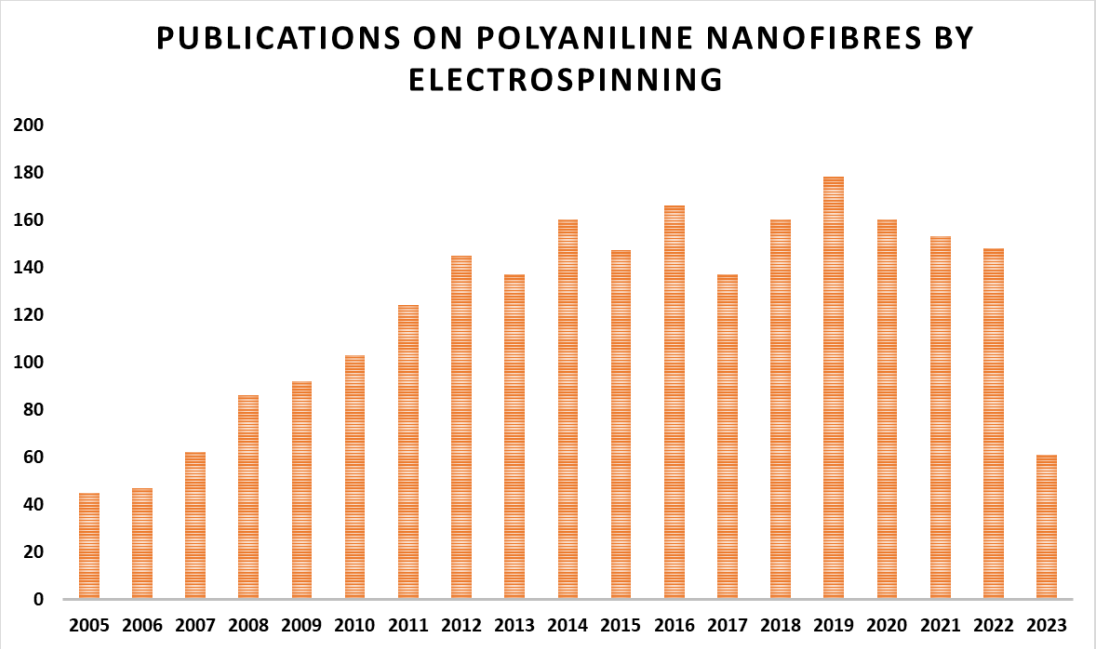

Figure 2-10 Comparison of the annual number of scientific publications related to electrospinning polyaniline nanofibres since 2005 using the Scopus search system with the term "Polyaniline nanofibres" as of May 2023.

2.7 References

1. Chung, D.D.L., Introduction to Carbon Composites, in Carbon Composites. 2017. p. 88-160.

2. Mercier, J.P., G. Zambelli, and W. Kurz, Chapter 16 - Composite materials, in Introduction to Materials Science, J.P. Mercier, G. Zambelli, and W. Kurz, Editors. 2002, Elsevier: Oxford. p. 401-420.

3. Sengupta, R., Mithun Bhattacharya, S. Bandyopadhyay, and Anil K. Bhowmick, A review on the mechanical and electrical properties of graphite and modified graphite reinforced polymer composites. Progress in Polymer Science, 2011. 36(5): p. 638-670.

4. Iyer, S.L., and Rajan Sen. Advanced composites materials in civil engineering structures. 1991. ASCE.

5. Gu, J., W. Dong, Y. Tang, Y. Guo, L. Tang, J. Kong, S. Tadakamalla, B. Wang, and Z. Guo, Ultra-low dielectric, fluoride-containing cyanate ester resins combining with prominent mechanical properties and excellent thermal and dimension stabilities. J Mater Chem C, 2017. 5(28): p. 6929-6936.

6. Khandan, R., Siamak Noroozi, Philip Sewell, and John Vinney, The development of laminated composite plate theories: a review. Journal of Materials Science, 2012. 47(16): p. 5901-5910.

7. Xu, Y., et al., A review on the design of laminated composite structures: constant and variable stiffness design and topology optimization. Advanced Composites and Hybrid Materials, 2018. 1(3): p. 460-477.

8. Brown, S.C., Colin Robert, Vasileios Koutsos, and Dipa Ray, Methods of modifying through-thickness electrical conductivity of CFRP for use in structural health monitoring, and its effect on mechanical properties – A review. Composites Part A: Applied Science and Manufacturing, 2020. 133.

9. Guo, M., Xiaosu Yi, Chris Rudd, Xiaoling Liu., Preparation of highly electrically conductive carbon-fiber composites with high interlaminar fracture toughness by using silver-plated interleaves. Composites Science and Technology, 2019. 176: p. 29-36.

10. Kravchenko, O.G., Diego Pedrazzoli, Vahab Solouki Bonab, Ica Manas-Zloczower., Conductive interlaminar interfaces for structural health monitoring in composite laminates under fatigue loading. Materials & Design, 2018. 160: p. 1217-1225.

11. Wang, S., Zhen Mei, D. D. L. Chung., Interlaminar damage in carbon fiber polymer-matrix composites, studied by electrical resistance measurement. International Journal of Adhesion and Adhesives, 2001. 21(6): p. 465-471.

12. Ye, L., Functionalized interleaf technology in carbon-fibre-reinforced composites for aircraft. Natl Sci Rev, 2014. 1(1): p. 7-8.

13. Lochot, C., and Damien Slomianowski, A350 XWB electrical structure network, in Airbus technical magazine. 2014, Bruno Piquet. p. 20-25.

14. Newcomb, B.A., and Han G. Chae, The properties of carbon fibers, in Handbook of properties of textile and technical fibres. 2018, Elsevier. p. 841-871.

15. Senis, E.C., Igor O. Golosnoy, Janice M. Dulieu-Barton, and Ole T. Thomsen, Enhancement of the electrical and thermal properties of unidirectional carbon fibre/epoxy laminates through the addition of graphene oxide. Journal of Materials Science, 2019. 54(12): p. 8955-8970.

16. Kumar, V., Tomohiro Yokozeki, Takao Okada, Yoshiyasu Hirano, Teruya Goto, Tatsuhiro Takahashi, and Toshio Ogasawara, Effect of through-thickness electrical conductivity of CFRPs on lightning strike damages. Composites Part A: Applied Science and Manufacturing, 2018. 114: p. 429-438.

17. Cornwell, T.H.a.A., Costly Airbus paint flaw goes wider than the Gulf. 2021, Reuters.

18. Cheng, X., Tomohiro Yokozeki, Lixin Wu, Haopeng Wang, JinMeng Zhang, Jun Koyanagi, Zixiang Weng, Qingfu Sun., Electrical conductivity and interlaminar shear strength enhancement of carbon fiber reinforced polymers through synergetic effect between graphene oxide and polyaniline. Composites Part A: Applied Science and Manufacturing, 2016. 90: p. 243-249.

19. Tehrani, M., M. Safdari, A. Y. Boroujeni, Z. Razavi, S. W. Case, K. Dahmen, H. Garmestani, M. S. Al-Haik., Hybrid carbon fiber/carbon nanotube composites for structural damping applications. Nanotechnology, 2013. 24(15): p. 155704.

20. Tehrani, M., A. Y. Boroujeni, T. B. Hartman, T. P. Haugh, S. W. Case, M. S. Al-Haik., Mechanical characterization and impact damage assessment of a woven carbon fiber reinforced carbon nanotube–epoxy composite. Composites Science and Technology, 2013. 75: p. 42-48.

21. Gojny, F.H., Malte HG Wichmann, Bodo Fiedler, Wolfgang Bauhofer, Karl Schulte., Influence of nano-modification on the mechanical and electrical properties of conventional fibre-reinforced composites. Composites Part A: Applied Science and Manufacturing, 2005. 36(11): p. 1525-1535.

22. Han, X., Yan Zhao, Jian-ming Sun, Ye Li, Jin-dong Zhang, Yue Hao., Effect of graphene oxide addition on the interlaminar shear property of carbon fiber-reinforced epoxy composites. New Carbon Materials, 2017. 32(1): p. 48-55.

23. Wang, Y., Suresh Kumar Raman Pillai, Jianfei Che, Mary B. Chan-Park., High Interlaminar Shear Strength Enhancement of Carbon Fiber/Epoxy Composite through Fiber- and Matrix-Anchored Carbon Nanotube Networks. ACS Appl Mater Interfaces, 2017. 9(10): p. 8960-8966.

24. Beckermann, G.W., Nanofiber interleaving veils for improving the performance of composite laminates. Reinforced Plastics, 2017. 61(5): p. 289-293.

25. Fan, Z., Michael H. Santare, Suresh G. Advani., Interlaminar shear strength of glass fiber reinforced epoxy composites enhanced with multi-walled carbon

nanotubes. Composites Part A: Applied Science and Manufacturing, 2008. 39(3): p. 540-554.

26. Delamar, M., G. Desarmot, O. Fagebaume, R_ Hitmi, J. Pinsonc, J-M. Savéant., Modification of carbon fiber surfaces by electrochemical reduction of aryl diazonium salts: Application to carbon epoxy composites. Carbon, 1997. 35(6): p. 801-807.

27. Pozegic, T.R., Ian Hamerton, José V. Anguita, Winnie Tang, Paolo Ballocchi, Philip Jenkins, S. Ravi P. Silva., Low temperature growth of carbon nanotubes on carbon fibre to create a highly networked fuzzy fibre reinforced composite with superior electrical conductivity. Carbon, 2014. 74: p. 319-328.

28. Qin, W., Frederic Vautard, Lawrence T. Drzal, Junrong Yu., Mechanical and electrical properties of carbon fiber composites with incorporation of graphene nanoplatelets at the fiber–matrix interphase. Composites Part B: Engineering, 2015. 69: p. 335-341.

29. Gangineni, P.K., Sagar Yandrapu, Sohan Kumar Ghosh, Abhijeet Anand, Rajesh Kumar Prusty, Bankim Chandra Ray., Mechanical behavior of Graphene decorated carbon fiber reinforced polymer composites: An assessment of the influence of functional groups. Composites Part A: Applied Science and Manufacturing, 2019. 122: p. 36-44.

30. Bedi, H.S., Srikant S. Padhee, Prabhat K. Agnihotri., Effect of carbon nanotube grafting on the wettability and average mechanical properties of carbon fiber/polymer multiscale composites. Polymer Composites, 2018. 39(S2): p. E1184-E1195.

31. Yan, F., Liu Liu, Ming Li, Mengjie Zhang, Lei Shang, Linghan Xiao, Yuhui Ao., One-step electrodeposition of Cu/CNT/CF multiscale reinforcement with substantially improved thermal/electrical conductivity and interfacial properties of epoxy composites. Composites Part A: Applied Science and Manufacturing, 2019. 125.

32. Yao, H., Guodong Zhou, Weitao Wang, Mao Peng., Effect of polymer-grafted carbon nanofibers and nanotubes on the interlaminar shear strength and flexural strength of carbon fiber/epoxy multiscale composites. Composite Structures, 2018. 195: p. 288-296.

33. Park, J.K., Jae Yeol Lee, Lawrence T. Drzal, Donghwan Cho., Flexural properties, interlaminar shear strength and morphology of phenolic matrix composites reinforced with xGnP-coated carbon fibers. Carbon letters, 2016. 17(1): p. 33-38.

34. Beylergil, B., Metin Tanoğlu, Engin Aktaş., Enhancement of interlaminar fracture toughness of carbon fiber-epoxy composites using polyamide-6,6 electrospun nanofibers. Journal of Applied Polymer Science, 2017. 134(35).

35. Sohn, M.S., X. Z. Hu, Jang Kyo Kim, and L. Walker, Impact damage characterisation of carbon fibreepoxy composites with multi-layer reinforcement. Composites: Part B 31, 2000. 31: p.) 681-691.

36. van der Heijden, S., Lode Daelemans, Bert De Schoenmaker, Ives De Baere, Hubert Rahier, Wim Van Paepegem, and Karen De Clerck, Interlaminar toughening of resin transfer moulded glass fibre epoxy laminates by polycaprolactone electrospun nanofibres. Composites Science and Technology, 2014. 104: p. 66-73.

37. Wang, G., Demei Yu, Ajit D. Kelkar, Lifeng Zhang., Electrospun nanofiber: Emerging reinforcing filler in polymer matrix composite materials. Progress in Polymer Science, 2017. 75: p. 73-107.

38. Aruchamy, K., Ashesh Mahto, S. K. Nataraj., Electrospun nanofibers, nanocomposites and characterization of art: Insight on establishing fibers as product. Nano-Structures & Nano-Objects, 2018. 16: p. 45-58.

39. Guo, M., Xiaosu Yi., Effect of Paper or Silver Nanowires-Loaded Paper Interleaves on the Electrical Conductivity and Interlaminar Fracture Toughness of Composites. Aerospace, 2018. 5(3).

40. Koirala, P., Nekoda van de Werken, Hongbing Lu, Ray H. Baughman, Raquel Ovalle-Robles, and Mehran Tehrani., Using ultra-thin interlaminar carbon nanotube

sheets to enhance the mechanical and electrical properties of carbon fiber reinforced polymer composites. Composites Part B: Engineering, 2021. 216.

41. Guo, M., Xiaosu Yi., The production of tough, electrically conductive carbon fiber composite laminates for use in airframes. Carbon, 2013. 58: p. 241-244.

42. Guo, M., Xiaosu Yi, Gang Liu, Lipeng Liu., Simultaneously increasing the electrical conductivity and fracture toughness of carbon–fiber composites by using silver nanowires-loaded interleaves. Composites Science and Technology, 2014. 97: p. 27-33.

43. Beckermann, G.W., Kim L. Pickering., Mode I and Mode II interlaminar fracture toughness of composite laminates interleaved with electrospun nanofibre veils. Composites Part A: Applied Science and Manufacturing, 2015. 72: p. 11-21.

44. García-Rodríguez, S.M., J. Costa, K. E. Rankin, R. P. Boardman, Vicky Singery, J. A. Mayugo., Interleaving light veils to minimise the trade-off between mode-I interlaminar fracture toughness and in-plane properties. Composites Part A: Applied Science and Manufacturing, 2020. 128.

45. Kumar, V., Sushant Sharma, Abhishek Pathak, Bhanu P. Singh, Sanjay R. Dhakate, Tomohiro Yokozeki, Takao Okada, Toshio Ogasawara., Interleaved MWCNT buckypaper between CFRP laminates to improve through-thickness electrical conductivity and reducing lightning strike damage. Composite Structures, 2019. 210: p. 581-589.

46. Ognibene, G., Alberta Latteri, Salvatore Mannino, Lorena Saitta, Giuseppe Recca, Fabrizio Scarpa, Gianluca Cicala., Interlaminar Toughening of Epoxy Carbon Fiber Reinforced Laminates: Soluble Versus Non-Soluble Veils. Polymers (Basel), 2019. 11(6).

47. Wu, Y., Xiuyan Cheng, Shaoyun Chen, Bo Qu, Rui Wang, Dongxian Zhuo, and Lixin Wu., In situ formation of a carbon nanotube buckypaper for improving the interlaminar properties of carbon fiber composites. Materials & Design, 2021. 202.

48. Quan, D., Chiara Mischo, Xiping Li, Gennaro Scarselli, Alojz Ivanković, Neal Murphy., Improving the electrical conductivity and fracture toughness of carbon fibre/epoxy composites by interleaving MWCNT-doped thermoplastic veils. Composites Science and Technology, 2019. 182.

49. Cortes, L.Q., Sebastien Racagel, Antoine Lonjon, Eric Dantras, Colette Lacabanne., Electrically conductive carbon fiber / PEKK / silver nanowires multifunctional composites. Composites Science and Technology, 2016. 137: p. 159-166.

50. Dydek, K., Anna Boczkowska, Paulina Latko-Durałek, Małgorzata Wilk, Karol Padykuła, and Rafał Kozera, Effect of the areal weight of CNT-doped veils on CFRP electrical properties. Journal of Composite Materials, 2020. 54(20): p. 2677-2685.

51. Bauhofer, W., and Josef Z. Kovacs. , A review and analysis of electrical percolation in carbon nanotube polymer composites. Composites Science and Technology, 2009. 69(10): p. 1486-1498.

52. Li, W., Dong Xiang, Lei Wang, Eileen Harkin-Jones, Chunxia Zhao, Bin Wang, Yuntao Li., Simultaneous enhancement of electrical conductivity and interlaminar fracture toughness of carbon fiber/epoxy composites using plasma-treated conductive thermoplastic film interleaves. RSC Advances, 2018. 8(47): p. 26910-26921.

53. Liu, H., Yunli Guo, Yong Zhou, Guoshun Wan, Zhongli Chen, Yuxi Jia., Multifunctional nickel-coated carbon fiber veil for improving both fracture toughness and electrical performance of carbon fiber/epoxy composite laminates. Polymer Composites, 2021.

54. Vallack, N. and W.W. Sampson, Materials systems for interleave toughening in polymer composites. Journal of Materials Science, 2022: p. 1-28.

55. Shakil, U.A., Shukur BA Hassan, Mohd Y. Yahya, and Saad Nauman, Mechanical properties of electrospun nanofiber reinforced/interleaved epoxy matrix composites—A review. Polymer Composites, 2020. 41(6): p. 2288-2315.

56. De Schoenmaker, B., Sam Van der Heijden, Ives De Baere, Wim Van Paepegem, and Karen De Clerck, Effect of electrospun polyamide 6 nanofibres on the mechanical properties of a glass fibre/epoxy composite. Polymer Testing, 2013. 32(8): p. 1495-1501.

57. Ozden, E., Y.Z. Menceloglu, and M. Papila, Engineering chemistry of electrospun nanofibers and interfaces in nanocomposites for superior mechanical properties. ACS applied materials & interfaces, 2010. 2(7): p. 1788-1793.

58. Li, G., Xiaolong Jia, Zhibin Huang, Bo Zhu, Peng Li, Xiaoping Yang, and Wuguo Dai, Prescribed morphology and interface correlation of MWNTs-EP/PSF hybrid nanofibers reinforced and toughened epoxy matrix. Materials Chemistry and Physics, 2012. 134(2-3): p. 958-965.

59. Zhang, J., T. Lin, and X. Wang, Electrospun nanofibre toughened carbon/epoxy composites: Effects of polyetherketone cardo (PEK-C) nanofibre diameter and interlayer thickness. Composites science and technology, 2010. 70(11): p. 1660-1666.

60. Saghafi, H., T. Brugo, G. Minak, and A. Zucchelli, The effect of PVDF nanofibers on mode-I fracture toughness of composite materials. Composites Part B: Engineering, 2015. 72: p. 213-216.

61. Tsotsis, T.K., Interlayer toughening of composite materials. Polymer composites, 2009. 30(1): p. 70-86.

62. TFP Ltd. [cited 2022 22 November]; Available from: https://www.tfpglobal.com/products/composite-materials.

63. Shivakumar, K.N., R. Panduranga, and M. Sharpe. Interleaved polymer matrix composites-a review. in 54th AIAA/ASME/ASCE/AHS/ASC structures, structural dynamics, and materials conference. 2013.

64. Cheng, C., Zhang, C., Zhou, J., Jiang, M., Sun, Z., Zhou, S., Liu, Y., Chen, Z., Xu, L., Zhang, H. and Yu, M, Improving the interlaminar toughness of the carbon fiber/epoxy composites via interleaved with polyethersulfone porous films. Composites Science and Technology, 2019. 183: p. 107827.

65. Hu, D., Xiaosu Yi, Minqiang Jiang, Genghong Li, Xiaoye Cong, Xiaoling Liu, Chris Rudd., Development of highly electrically conductive composites for aeronautical applications utilizing bi-functional composite interleaves. Aerospace Science and Technology, 2020. 98.

66. Chiang, C.K., C. R. Fincher Jr, Yung W. Park, Alan J. Heeger, Hideki Shirakawa, Edwin J. Louis, Shek C. Gau, and Alan G. MacDiarmid, Electrical conductivity in doped polyacetylene. Physical review letters, 1977. 39(17): p. 1098.

67. Conductive Polymers : Materials and Applications. Conductive Polymers. 2020: MDPI - Multidisciplinary Digital Publishing Institute.

68. Le, T.-H., Y. Kim, and H. Yoon, Electrical and electrochemical properties of conducting polymers. Polymers, 2017. 9(4): p. 150.

69. Quijada, C., Conductive Polymers. 2020.

70. Mdluli, S.B., et al., π-Conjugated Polymers and Their Application in Organic and Hybrid Organic-Silicon Solar Cells. Polymers (Basel), 2022. 14(4).

71. Das, T.K. and S. Prusty, Review on Conducting Polymers and Their Applications. Polymer-Plastics Technology and Engineering, 2012. 51(14): p. 1487-1500.

72. Radacsi, N., Fernando Diaz Campos, Calum RI Chisholm, and Konstantinos P. Giapis, Spontaneous formation of nanoparticles on electrospun nanofibres. Nat Commun, 2018. 9(1): p. 4740.

73. Cleeton, C., Antonios Keirouz, Xianfeng Chen, and Norbert Radacsi, Electrospun Nanofibers for Drug Delivery and Biosensing. ACS Biomaterials Science & Engineering, 2019. 5(9): p. 4183-4205.

74. Thorvaldsson, A., Hanna Stenhamre, Paul Gatenholm, and Pernilla Walkenström, Electrospinning of highly porous scaffolds for cartilage regeneration. Biomacromolecules, 2008. 9(3): p. 1044-1049.

75. Qin, X. and S. Subianto, Electrospun nanofibers for filtration applications, in Electrospun Nanofibers. 2017. p. 449-466.

76. Perdigão, P., Bruno Miguel Morais Faustino, Jaime Faria, João Paulo Canejo, João Paulo Borges, Isabel Ferreira, and Ana Catarina Baptista, Conductive Electrospun Polyaniline/Polyvinylpyrrolidone Nanofibers: Electrical and Morphological Characterization of New Yarns for Electronic Textiles. Fibers, 2020. 8(4).

77. Keirouz, A., Mariia Zakharova, Jaehoon Kwon, Colin Robert, Vasileios Koutsos, Anthony Callanan, Xianfeng Chen, Giuseppino Fortunato, and Norbert Radacsi, High-throughput production of silk fibroin-based electrospun fibers as biomaterial for skin tissue engineering applications. Mater Sci Eng C Mater Biol Appl, 2020. 112: p. 110939.

78. Keirouz, A., Norbert Radacsi, Qun Ren, Alex Dommann, Guido Beldi, Katharina Maniura-Weber, René M. Rossi, and Giuseppino Fortunato, Nylon-6/chitosan core/shell antimicrobial nanofibers for the prevention of mesh-associated surgical site infection. J Nanobiotechnology, 2020. 18(1): p. 51.

79. Amariei, N., L. R. Manea, A. P. Bertea, R. Cramariuc, A. Bertea, and O. Cramariuc, Electrospinning Polyaniline for Sensors. IOP Conference Series: Materials Science and Engineering, 2017. 209.

80. Souri, H., Hritwick Banerjee, Ardian Jusufi, Norbert Radacsi, Adam A. Stokes, Inkyu Park, Metin Sitti, and Morteza Amjadi, Wearable and Stretchable Strain Sensors: Materials, Sensing Mechanisms, and Applications. Advanced Intelligent Systems, 2020. 2(8).

81. Dodero, A., Marina Alloisio, Silvia Vicini, and Maila Castellano, Preparation of composite alginate-based electrospun membranes loaded with ZnO nanoparticles. Carbohydrate Polymers, 2020. 227: p. 115371.

82. Agarwal, T., Rajan Narayan, Somnath Maji, Shubhanath Behera, Senthilguru Kulanthaivel, Tapas Kumar Maiti, Indranil Banerjee, Kunal Pal, and Supratim Giri, Gelatin/Carboxymethyl chitosan based scaffolds for dermal tissue engineering applications. Int J Biol Macromol, 2016. 93(Pt B): p. 1499-1506.

83. Zeleny, J., The electrical discharge from liquid points, and a hydrostatic method of measuring the electric intensity at their surfaces. Physical Review, 1914. 3(2): p. 69.

84. Agrawal, P. and K. Pramanik, Chitosan-poly(vinyl alcohol) nanofibers by free surface electrospinning for tissue engineering applications. Tissue Eng Regen Med, 2016. 13(5): p. 485-497.

85. Anton, F., Process and apparatus for preparing artificial threads. 1934, Google Patents.

86. Abdelrazek, E.M., H. M. Ragab, and M. Abdelaziz, Physical characterization of poly (vinyl pyrrolidone) and gelatin blend films doped with magnesium chloride. 2013. 2(1): p. 1-8.

87. Norton, C.L., Method of and apparatus for producing fibrous or filamentary material. 1936, Google Patents.

88. Anurag Singh; Sahand P. Shamchi; Carmen Sguazzo; Xiaosu Yi; Z. Zhao; Pedro M.G.P, M. Analysis of Mechanical Behavior of Multi-functional CFRP under bending and DCB mode-I fracture. in Procedia Structural Integrity. 2020.

89. Taylor, G.I., Electrically driven jets. Proceedings of the Royal Society of London. A. Mathematical and Physical Sciences, 1969. 313(1515): p. 453-475.

90. Kong, T., Howard A. Stone, Liqiu Wang, and Ho Cheung Shum, Dynamic regimes of electrified liquid filaments. Proc Natl Acad Sci U S A, 2018. 115(24): p. 6159-6164.

91. Keirouz, A., Michael Chung, Jaehoon Kwon, Giuseppino Fortunato, and Norbert Radacsi, 2D and 3D electrospinning technologies for the fabrication of nanofibrous scaffolds for skin tissue engineering: A review. Wiley Interdiscip Rev Nanomed Nanobiotechnol, 2020. 12(4): p. e1626.

92. Niu, H. and T. Lin, Fiber Generators in Needleless Electrospinning. Journal of Nanomaterials, 2012. 2012: p. 1-13.

93. Khalf, A. and S.V. Madihally, Recent advances in multiaxial electrospinning for drug delivery. European Journal of Pharmaceutics and Biopharmaceutics, 2017. 112: p. 1-17.

94. Xue, J., Tong Wu, Yunqian Dai, and Younan Xia, Electrospinning and Electrospun Nanofibers: Methods, Materials, and Applications. Chemical Reviews, 2019. 119(8): p. 5298-5415.

95. Gañán-Calvo, A.M., Cone-jet analytical extension of Taylor's electrostatic solution and the asymptotic universal scaling laws in electrospraying. Physical review letters, 1997. 79(2): p. 217.

96. He, J.-H., Y. Wu, and W.-W. Zuo, Critical length of straight jet in electrospinning. Polymer, 2005. 46(26): p. 12637-12640.

97. Reneker, D.H., Alexander L. Yarin, Hao Fong, and Sureeporn Koombhongse, Bending instability of electrically charged liquid jets of polymer solutions in electrospinning. Journal of Applied physics, 2000. 87(9): p. 4531-4547.

98. Shin, Y.M., M. M. Hohman, M. P. Brenner, and G. C. Rutledge, Experimental characterization of electrospinning: the electrically forced jet and instabilities. Polymer, 2001. 42(25): p. 09955-09967.

99. Yarin, A.L., S. Koombhongse, and D.H. Reneker, Bending instability in electrospinning of nanofibers. Journal of applied physics, 2001. 89(5): p. 3018-3026.

100. Reneker, D.H. and A.L. Yarin, Electrospinning jets and polymer nanofibers. Polymer, 2008. 49(10): p. 2387-2425.

101. Shin, Y., et al., Electrospinning: A whipping fluid jet generates submicron polymer fibers. Applied physics letters, 2001. 78(8): p. 1149-1151.

102. Williams GH, R.-A.B., Luo C, Moving from bench to the clinic, in Nanofibres in Drug Delivery. 2018, UCL Press: London, UK.

103. Yarin, A.L. and E. Zussman, Upward needleless electrospinning of multiple nanofibers. Polymer, 2004. 45(9): p. 2977-2980.

104. Lukas, D., A. Sarkar, and P. Pokorny, Self-organization of jets in electrospinning from free liquid surface: A generalized approach. Journal of Applied Physics, 2008. 103(8): p. 084309.

105. Niu, H., Xungai Wang, and Tong Lin, Upward Needleless Electrospinning of Nanofibers. Journal of Engineered Fibers and Fabrics, 2012.

106. Niu, H., Xungai Wang, and Tong Lin, Upward needleless electrospinning of nanofibers. 2012. 7(2_suppl): p. 155892501200702S03.

107. Wang, X., Haitao Niu, Tong Lin, and Xungai Wang, Needleless electrospinning of nanofibers with a conical wire coil. Polymer Engineering & Science, 2009. 49(8): p. 1582-1586.

108. Waqas, M., Antonios Keirouz, Maria Kana Sanira Putri, Faraz Fazal, Francisco Javier Diaz Sanchez, Dipa Ray, Vasileios Koutsos, and Norbert Radacsi, Design and development of a nozzle-free electrospinning device for the high-throughput production of biomaterial nanofibers. Med Eng Phys, 2021. 92: p. 80-87.

109. Elmarco. Elmarco Laboratory equipment 2020, February 19; Available from: https://www.elmarco.com/laboratory-equipment.

110. Bhardwaj, N. and S.C. Kundu, Electrospinning: a fascinating fiber fabrication technique. Biotechnol Adv, 2010. 28(3): p. 325-47.

111. Yalcinkaya, F., B. Yalcinkaya, and O. Jirsak, Dependent and independent parameters of needleless electrospinning. Electrospinning–Material, Techniques and Biomedical Applications. 1st ed. Rijeka, Croatia: InTech, 2016: p. 67-93.

112. Yener, F., New methods in the study of roller electrospinning mechanism. Department of Nonwoven and Nanofibrous Materials, 2014: p. 136.

113. Yanılmaz, M. and A.S. Sarac, A review: effect of conductive polymers on the conductivities of electrospun mats. Textile Research Journal, 2014. 84(12): p. 1325-1342.

114. Júnior, L.P., Dáfenes BR dos S. Silva, Maurício F. de Aguiar, Celso P. de Melo, and Kleber GB Alves, Preparation and characterization of polypyrrole/organophilic montmorillonite nanofibers obtained by electrospinning. Journal of Molecular Liquids, 2019. 275: p. 452-462.

115. Okuzaki, H., Spontaneous Formation of Poly(p-phenylenevinylene) Nanofibre Yarns through Electrospinning of a Precursor. Macromolecules 2006(39): p. 4276-4278.

116. Cárdenas-Martínez, J., Beatriz L. España-Sánchez, Rodrigo Esparza, and José A. Ávila-Niño, Flexible and transparent supercapacitors using electrospun PEDOT:PSS electrodes. Synthetic Metals, 2020. 267.

117. Matysiak, W., Tomasz Tański, Weronika Smok, Klaudiusz Gołombek, and Ewa Schab-Balcerzak, Effect of conductive polymers on the optical properties of electrospun polyacrylonitryle nanofibers filled by polypyrrole, polythiophene and polyaniline. Applied Surface Science, 2020. 509: p. 145068.

118. Chauhan, N.P.S. and M. Mozafari, Chapter 1 - Polyaniline: An introduction and overview, in Fundamentals and Emerging Applications of Polyaniline, M. Mozafari and N.P.S. Chauhan, Editors. 2019, Elsevier. p. 1-15.

119. Long, Y.-Z., Meng-Meng Li, Changzhi Gu, Meixiang Wan, Jean-Luc Duvail, Zongwen Liu, and Zhiyong Fan, Recent advances in synthesis, physical properties and applications of conducting polymer nanotubes and nanofibers. Progress in Polymer Science, 2011. 36(10): p. 1415-1442.

120. Hong, K.H. and T.J. Kang, Polyaniline–nylon 6 composite nanowires prepared by emulsion polymerization and electrospinning process. Journal of applied polymer science, 2006. 99(3): p. 1277-1286.

121. Abd Razak, S.I., Izzati Fatimah Wahab, Fatirah Fadil, Farah Nuruljannah Dahli, Ahmad Zahran Md Khudzari, and Hassan Adeli, A Review of Electrospun Conductive Polyaniline Based Nanofiber Composites and Blends: Processing Features, Applications, and Future Directions. Advances in Materials Science and Engineering, 2015. 2015: p. 1-19.

122. Merlini, C., Alessandro Pegoretti, Thiago Medeiros Araujo, Sílvia DAS Ramoa, Wido H. Schreiner, and Guilherme Mariz de Oliveira Barra, Electrospinning of doped and undoped-polyaniline/poly(vinylidene fluoride) blends. Synthetic Metals, 2016. 213: p. 34-41.

123. Wu, J.C.-C., Sudip Ray, Marija Gizdavic-Nikolaidis, Jianyong Jin, and Ralph P. Cooney, Effect of polyvinylpyrrolidone on storage stability, anti-oxidative and anti-bacterial properties of colloidal polyaniline. Synthetic Metals, 2016. 217: p. 202-209.

124. Yılmaz, F., and Zuhal Küçükyavuz, The influence of polymerization temperature on structure and properties of polyaniline e-Polymers, 2009. 9(1): p. 005.

125. Wei, M., Junseok Lee, Bongwoo Kang, and Joey Mead, Preparation of Core-Sheath Nanofibers from Conducting Polymer Blends. Macromolecular Rapid Communications, 2005. 26(14): p. 1127-1132.

126. Heikkilä, P. and A. Harlin, Electrospinning of polyacrylonitrile (PAN) solution: Effect of conductive additive and filler on the process. Express Polymer Letters, 2009. 3(7): p. 437-445.

127. Moutsatsou, P., Karen Coopman, Martin B. Smith, and Stella Georgiadou, Conductive PANI fibers and determining factors for the electrospinning window. Polymer, 2015. 77: p. 143-151.

128. Abdelrazek, E.M., H. M. Ragab, and M. Abdelaziz, Physical characterization of poly (vinyl pyrrolidone) and gelatin blend films doped with magnesium chloride. Plastic and Polymer Technology, 2013. 2(1): p. 1-8.

129. Taghizadeh, M.T. and S. Nasirianfar, Ultraviolet Irradiation Effect on Polyvinylpyrrolidone/Polyaniline Films with Additives. Polymer-Plastics Technology and Engineering, 2018. 57(18): p. 1893-1905.

130. Subramanian, E., G. Anitha, and N. Vijayakumar, Constructive modification of conducting polyaniline characteristics in unusual proportion through nanomaterial blend formation with the neutral polymer poly(vinyl pyrrolidone). Journal of Applied Polymer Science, 2007. 106(1): p. 673-683.

Chapter 3 Materials and Methods

3.1 Introduction

This chapter introduces the main reagents, devices, characterisation techniques, and methods utilised in this dissertation. In the respective chapters, the specific materials and methods required for particular experiments in the specific chapters are detailed therein.

3.2 Materials

3.2.1 Reagents

Table 3-1: The chemicals and other materials used in the thesis are listed in this table

Chemicals		
Product name	**Supplier**	**Description**
N, N-dimethylformamide (DMF)	Sigma-Aldrich Ltd., UK	≥99% pure
Ethanol	Thermo Fisher Scientific, UK	≥99% pure
De-ionised water (DI water)	Cryomed Scientific, UK	Provided by the laboratory
Aniline monomer	Thermo Fisher Scientific, UK	≥99% pure
Ammonium peroxydisulfate	Sigma-Aldrich Ltd., UK	≥98% pure
Acetone	VWR International, France	≥99% pure
Ammonium Hydroxide	Sigma-Aldrich Ltd., UK	24%
Hydrochloric acid	Sigma-Aldrich Ltd., UK	37% pure
Sodium hypochlorite	Thermo Fisher Scientific, UK	5% solution
Potassium biiodate	Thermo Fisher Scientific, UK	≥99.85% pure
Polyvinylpyrrolidone	Alfa-Aesar Ltd., USA	M_w 1,300,000 g mol^{-1}
Unidirectional (UD) carbon fibre fabric	SAERTEX GmbH	TENAX J IMS60 E 13 24K, areal density 274 g/m^2

Epoxy infusion resin	Easy Composites Ltd., UK	IN2 M_w ≤700 g/mol
Slow hardener	Easy Composites Ltd., UK	AT30
Carbon fibre veil	Technical Fiber Products Ltd., UK	Areal density 14 g/m^2
Nickel carbon fibre veil	Technical Fiber Products Ltd., UK	Areal density 20 g/m^2
Silver epoxy adhesive & Hardener	Chemtronics	CW2400
Copper wire	Available in the laboratory	23 American wire gauge (AWG) bare copper

3.2.2 3.2.2 Equipment

Table 3.2: The main and auxiliary equipment used for the characterisation of the properties of the materials and laminates are listed below.

Equipment		
Name	**Manufacturer**	**Model**
Scanning electron microscopy (SEM)	JEOL Ltd.	JEOL JSM-IT100
Sputter coater	Agar Scientific	AGB7341
3D printer	Ultimaker BV	Ultimaker 3
Conductivity metre	Traceable	4063 CC
X-Ray diffraction (XRD)	Bruker Corporation	D2 Phaser

Electrical impedance spectroscopy	Sciospec Scientific Instruments GmbH	ISX-3v2
Fourier transform infrared spectroscopy	Thermo Fisher Scientific, UK	Nicolet iS10
EDX	Zeiss.co.uk	Crossbeam 550
Nozzle-free electrospinner	—	Built in-house
Mechanical testing	Instron	3369
Dynamic mechanical analysis	Perkin Elmer, Inc	DMA 8000
Potentiostat	Metrohm AG	Autolab PGSTAT204
Pneumatic press	Radius Engineering, Incorporation	Customised
Curing Oven	SciQuip Ltd.	SQ Oven-230HT
Muffle furnace	Nabertherm	LT03/13 CR

3.3 Experimental methods for fabrication

3.3.1 Nozzle-free Electrospinning setup

The homemade nozzle-free setup consists of a rotating collector and a drum partially submerged in a Teflon bath containing the polymer solution in a rectangular glass aquarium [1]. The negative and positive high voltage sources are connected to the collector and spinneret. A 6 V DC motor is employed to maintain a constant 5 revolutions per minute (RPM) for the spinneret coil. A brushed 12V DC motor with a 4500 RPM rating and a speed controller module is used to rotate and modulate the collector's RPM. The speed controller module enables the user to accurately set the collector's rotational speed to any number between 100 and the maximum RPM. By altering the maximum current and voltage supplied to a motor, it is possible to attain lower RPM. The motor that rotates the collector is powered by an adjustable DC power source that enables operation in constant current or constant voltage mode. If the user intends to set the collector speed to 100 RPM or higher, the power supply should always be operated in constant voltage mode at 12 V. Depending on the experiment, operational parameters such as voltage and RPM of the collector were altered. These will be described separately in their respective chapters.

The environmental chamber in this electrospinning arrangement can be maintained at a specified temperature and relative humidity (RH %). This can be accomplished by using a heating assembly that enables the pumping of conditioned hot air or gas through a perforated glass lid into the glass chamber.

3.3.2 Electrospinning of PANI and PVP

Preliminary trials were performed to optimise PVP concentrations for dense and thick electrospun veils. The PVP concentration of 10, 12, 14, 18, and 20 wt. % were used to prepare solutions in DMF. The PVP solutions (15 wt. % and 18 wt. %) were prepared by dissolving 12 g PVP and 14.4 g (M_w = 1,300,000 g mol^{-1}) powder in 80 mL of DMF and allowing the mixture to spin at 700 RPM at room temperature overnight. The PANI solution was then prepared by dissolving separately 0.5 or 1 g of PANI-EB and

PANI-ES in 10 mL of DMF at room temperature while stirring continuously at 400 RPM. To prepare the master solution, the PANI-EB and PANI-ES solutions were individually combined with the 18 wt. % PVP/DMF solution. The solution was stirred for 60 minutes in order to obtain maximum homogeneity.

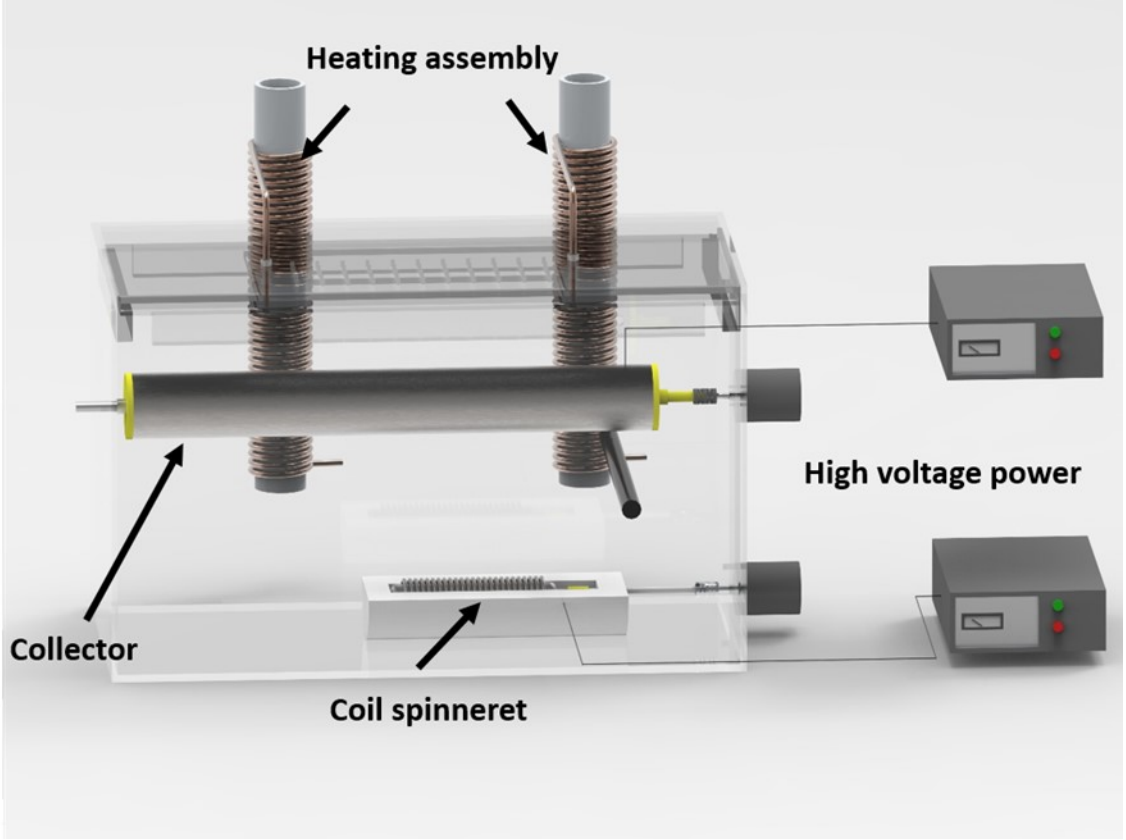

Figure 3-1 Rendered CAD model of the nozzle-free electrospinning setup with a description of each assembly and device component. A heating assembly was used for the conditioning of air. Nanofibres arise from a coil spinneret and are collected at a metallic collector.

All solutions were electrospun using the nozzle-free electrospinning apparatus illustrated in Figure 3.1 and detailed in [1]. The nozzle-free electrospinning apparatus consists of a spiral coil spinneret revolving slowly in a Teflon solution bath. The rotating coil spinneret, which was partially immersed in a solution bath, was coupled to a high voltage source. The collector was wired with an opposing charge to the spinneret. Between the two revolving electrodes, a total DC potential difference ranging from 40 kV to 60 kV was applied. As the coil spinneret slowly rotates, a thin

coating of the polymer solution develops on the spinneret's upper side, allowing fibres to jet from the surface's numerous Taylor cones.

3.3.3 Synthesis of CFRP laminates

The electrospun nanofibres cover around 15 cm × 15 cm area of carbon fibre fabric. These electrospun-coated carbon fibre fabrics were used to produce electrospun veils interleaved CFRP laminates. The unidirectional (UD) laminates were made using a hand layup technique with a stack of 5 plies $[0]_5$ of electrospun coated carbon fibre fabric. For each composition, two laminates were made. After being hand laid up, the laminates were consolidated in a press at 1 bar of pressure and left to cure for 24 hours at room temperature. The resulting composites were post-cured for 2 hours at 40 °C, 2 hours at 50 °C, and 4 hours at 60 °C.

A commercial unidirectional (UD) carbon fibre fabric was used in this study as the dry reinforcement material. The fabric is composed of TENAX J IMS60 E 13 24 K fibres in the 0° direction with an areal density of 274 g/m^2 and a glass fibre stitching in 90°. The fabric was supplied by SAERTEX GmbH. The matrix system used in this study was epoxy infusion resin by Easy Composites Ltd., UK, under the brand name of epoxy resin (IN2) (molecular weight =<700 g/mol) mixed with a slow hardener (AT30 slow). Resin to hardener weight ratio of 100:30 was used as recommended by the supplier.

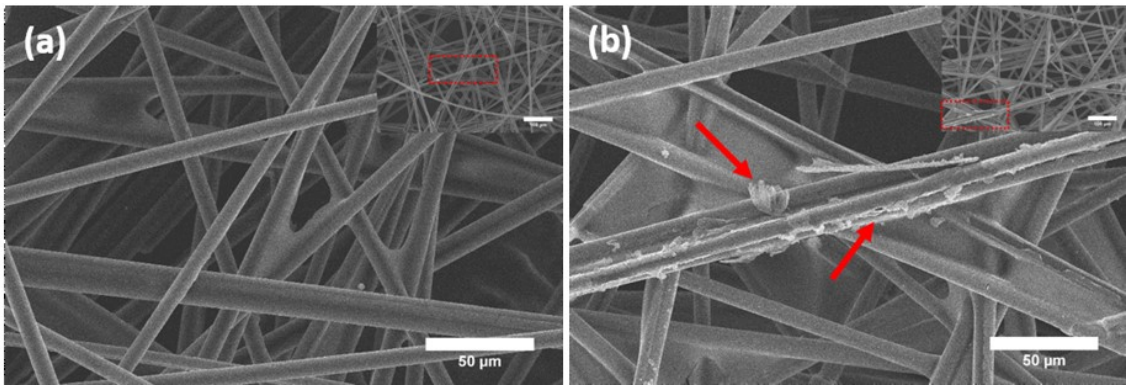

Figure 3-2 SEM images of (a) CF veil with 14 g/m^2 areal density and 7µm average fibre diameter (b) NiCF veil with 20 g/m^2 areal density and 8µm average fibre diameter.

The CF and NiCF veils used in this study are proprietary products of Technical Fibre Products Ltd., UK. The CF veil was made of carbon fibre loosely connected with a cross-linked styrene acrylic binder. The NiCF veil was made of nickel-coated carbon fibre loosely connected with a cross-linked polyester binder. The SEM images of both veils are shown in Figure 3.2. Some nickel particles can be seen (highlighted with red arrows in Figure 3.2 (b) adhering to the fibre surface [2]. The random orientation of the veil fibres forms a uniform porous network structure, which aids in resin impregnation. Both the veils were used as received. The areal density, thickness, and average fibre diameter of the CF and NiCF veils are given in Table 3.3.

Table 3.3: The physical properties, i.e. areal density, dry veil thickness, average fibre diameter, binder type, and electrical resistivity of CF and NiCF veils from technical datasheets (Technical Fibre Products Ltd., UK) [3].

Interleaf	**Area density (g/m^2)**	**Thickness (µm)**	**Fibre diameter (µm)**	**Binder type**	**Resistivity (Ω/sq.)**
Carbon fibre (CF) veil	14	170	7	Cross-linked styrene acrylic	7
Nickel-coated carbon fibre (NiCF) veil	20	180	8	Cross-linked polyester	1.3

The unidirectional (UD) laminates were made using a hand layup technique with a stack of 5 plies $[0]_5$ of carbon fibre fabric, and interleaving veils positioned between each ply. For each composition, two laminates were made. After being hand laid up, the laminates were consolidated in a press at 1 bar of pressure and left to cure for 24 hours at room temperature. The resulting composites were post-cured for 2 hours at 40 °C, 2 hours at 50 °C, and 4 hours at 60 °C.

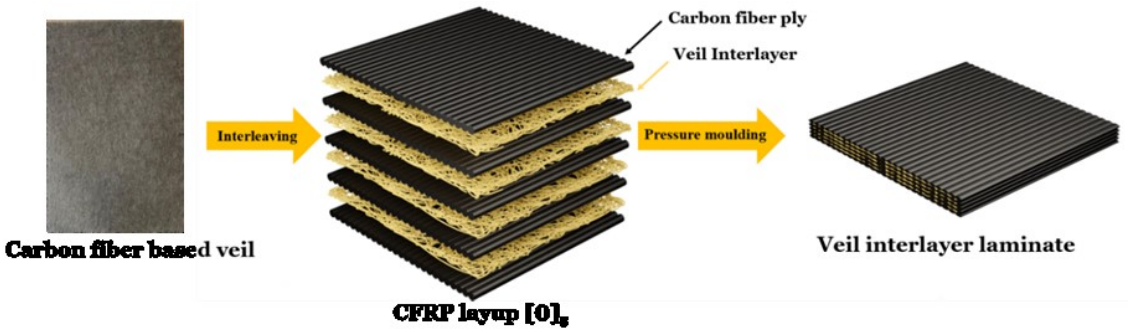

Figure 3-3 Schematic of overall CF based veil interlayer CFRP laminate preparation.

3.4 Experimental methods for characterisation

3.4.1 Scanning electron microscopy

All electrospun fibres and polymer powder samples were examined under a scanning electron microscope (JEOL JSM-IT100, JEOL Ltd., Japan) operating at an accelerating voltage of 10-15 kV. Each SEM sample was prepared by placing it on carbon conductive tape, which was attached to aluminium sample holders. Each sample was sputter-coated with a thin evaporated layer of gold until reaching a thickness of approximately 100 Å using a sputter coater (AGB7341, Agar Scientific, UK). The fibre diameters were measured from the SEM images using the ImageJ software [4].

The fracture surfaces of the CFRP samples from short beam shear (SBS) tests were examined by SEM at an electron excitation voltage of 10 kV. Before the examination, the fracture surfaces were sputter-coated with a thin evaporated layer of gold, until reaching a thickness of approximately 100 Å using an Agar auto sputter coater. The carbon fibre ply and veil interlayer thickness wrere calculated by taking an average of 50 measurements from different SEM images of SBS samples.

3.4.2 X-ray diffraction (XRD)

The crystalline structure of the polymer powders was examined by X-ray diffraction (XRD). The scans were carried out at a rate of 5° per minute throughout a 2θ range of 5° to 60°. For the scans, copper Kα radiation was used.

3.4.3 Fourier transform infrared spectroscopy (FTIR)

A Fourier transform infrared (FTIR) spectrometer, the Nicolet iS10, was used to identify the various functional groups present in the materials. The infrared (IR) spectrometer measures the absorbed and transmitted wavelengths in the infrared region by different functional groups, hence giving the material composition. Before measuring the FTIR spectrum of each sample, a blank (background) scan was recorded. Once the background scan was completed, a small amount of the powder or flat sample was placed in the material window, and the manual press was tightened to make the sample more homogeneous. The FTIR spectra were recorded for the electrospun and CFRP laminate samples (transmittance profiles) between 4000 and 400 cm^{-1}.

3.4.4 Polymer solution conductivity measurement

A model 4063 CC Traceable portable equipment was utilised to measure the conductivity of the various polymer solutions used to make the electrospun fibrous mats and structures. The device's probe, which is always submerged in de-ionized water while not in use, was added to a flask containing DMF, and it was agitated frequently until the reading in the metre stabilised. A steady reading was then acquired by repeatedly stirring the probe inside the flasks holding one of the polymer solutions. Afterward, the probe was removed from the polymer solution and rinsed with DMF. All other polymer solution conductivities were measured using the same procedure.

3.4.5 Electrical conductivity of polyaniline

The electrical conductivity of polyaniline powder was measured using a potentiostat (Metrohm, Autolab PGSTAT204). The four-point probe method (also known as

Kelvin method) was used to measure the electrical conductivity of dry-pressed polyaniline pellets. In a small hydraulic press, pellets were produced by uniaxial pressing the dry polyaniline powders. The die was 13 mm in diameter, and 1-tonne force was put on it for 3 minutes.

According to this theory, the device under test (DUT) is connected to either end by a pair of leads known as "force" and "sense" creating a total of four wires from the measuring equipment. Because the sensing voltage (V) utilised for the meter's $V/I = R$ (I is the current and R is the electrical resistance) calculation is that across the DUT, not across the DUT plus test leads, the relevance of the four wires is that they eliminate lead resistance as a source of error [11].

3.5 Characterisation of CFRP laminates

A few characterisations were specifically performed on CFRP laminates. Further details are written in the following sections.

3.5.1 Dynamic mechanical thermal analysis

Dynamic mechanical analysis (DMA) was performed according to ASTM D4065-12 to investigate the damping properties of the laminates. The test was carried out on samples (dimension: 35 mm × 8 mm × 1.3 mm) using DMA 8000 (Perkin Elmer©) in three-point bending mode, where 20 μm displacement amplitudes were applied at 1 Hz. A temperature sweep from 25 to 150 °C was used at a heating rate of 5 °C/min. Glass transition temperature (T_g) and tan delta were determined and plotted using Pyris software to obtain the damping properties of the CFRP.

Dynamic mechanical thermal analysis (DMTA) is used to determine how the modulus of material changes with temperature. This is accomplished by heating a material specimen while applying a sinusoidal force or displacement. DMTA can measure the elastic and plastic material behaviour of polymeric materials by measuring the complex modulus, In this type of experiment, a motor is used to exert a sinusoidal strain, or stress on a material (in tension, bending, or shear), and the resulting stress is either recorded with a force transducer or the resulting strain with a position sensor. DMTA is better suited to researching polymers in a glassy or rubbery phase as opposed to a liquid state [12].

3.5.2 Mechanical testing

The flexural characteristics of specimens were determined using ISO 14125 specified three-point bend tests. For each laminate, five specimens 50 mm × 15 mm × 1.3 mm were tested. A 5 N pre-load was put on the samples to prevent them from moving. Tests were performed using an Instron 3369, and the crosshead moved at a rate of 1 mm per minute. Each specimen was loaded until cracks propagated across the entire specimen.

Interlaminar shear strength was measured by performing the short beam shear (SBS) tests. The SBS specimens were 20 mm × 10 mm × 1.3 mm, and the tests were done according to ISO 14130. The span to thickness ratio was 15:1. Seven samples were evaluated for each laminate using an Instron 3369 tester at a constant displacement rate of 1 mm/min.

The 3369 series dual column desktop testing equipment performs tensile, compression, and bend tests on elastomers, plastics, medical devices, rope, textiles, and automotive parts when maximum forces are less than 50 kN. The greatest force capacities of accessible models are 5, 10, 30, and 50 kN [13].

3.5.3 Electrical conductivity testing

The through-thickness electrical conductivity of the composite specimens was measured using the two-probe method [14]. A sample size of 75 mm × 75 mm × 1.3 mm was used. The top and bottom surfaces of the laminates were polished to remove the excess epoxy resin and expose the conductive path. A conductive silver epoxy adhesive and hardener (Circuit Works© CW2400) were mixed at a 1:1 ratio and painted onto the plates at 9 equally distributed points with 23 AWG copper wire on both sides prior to curing overnight [15].

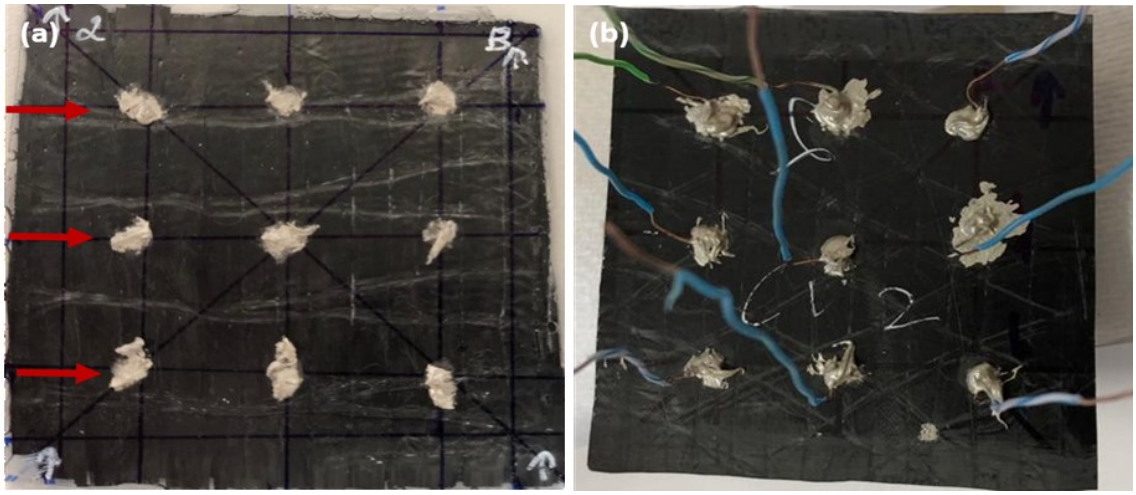

Figure 3-4 Representative images of the test laminates for through-thickness electrical conductivity measurement (a) conductive silver epoxy applied at 9 locations on a laminate, indicated via red arrows (b) copper wires attached to a laminate.

The electrical impedance was measured with a Sciospec ISX-3v2 electrical impedance spectroscopy [16]. For a point electrical resistance in the through-thickness direction, one thousand data points were collected. The volume conductivity was measured by equation 3.1 [17-19].

$$\sigma = \frac{1}{\rho} = \frac{L}{RA} \qquad \text{Equation 3.1}$$

Where ρ is the volume resistivity, L is the thickness of the specimen, R is the measured electrical resistance of the specimen, and A is the area of the sample.

Figure 3-5 Sciospec ISX-3v2 electrical impedance spectroscopy [16].

3.5.4 Fibre volume fractions

Fibre volume fractions (FVF) were determined by the matrix burn-off technique specified in ASTM D3171 in the furnace (Nabertherm, LT03/13 CR). An estimated fibre volume fraction was calculated using equation 3.2.

$$V_f = \frac{M_f}{M_i} \times 100 \times \frac{\rho_c}{\rho_r} \qquad \text{Equation 3.2}$$

Where V_f is fibre volume fraction, M_f is final mass of the specimen after combustion, M_i is initial mass of the specimen, ρ_c is density of the carbon fibre (g/cm^3) and ρ_r is density of the cured resin (g/cm^3).

3.6 References

1. Waqas, M., Antonios Keirouz, Maria Kana Sanira Putri, Faraz Fazal, Francisco Javier Diaz Sanchez, Dipa Ray, Vasileios Koutsos, and Norbert Radacsi, Design and development of a nozzle-free electrospinning device for the high-throughput production of biomaterial nanofibers. Medical Engineering & Physics, 2021. 92: p. 80-87.

2. Liu, H., Yunli Guo, Yong Zhou, Guoshun Wan, Zhongli Chen, Yuxi Jia., Multifunctional nickel-coated carbon fiber veil for improving both fracture toughness and electrical performance of carbon fiber/epoxy composite laminates. Polymer Composites, 2021.

3. TFP Ltd. [cited 2023 16/01/2023]; Available from: https://www.tfpglobal.com/products/composite-materials.

4. Schneider, C.A., W.S. Rasband, and K.W. Eliceiri, NIH Image to ImageJ: 25 years of image analysis. Nature Methods, 2012. 9(7): p. 671-675.

5. Egerton, R.F., Physical principles of electron microscopy. Vol. 56. 2005: Springer.

6. Park, M.-J., Dong Hwan Kim, Keun Park, Dong Young Jang, and Dong-Chul Han, Design and fabrication of a scanning electron microscope using a finite element analysis for electron optical system. Journal of Mechanical Science and Technology, 2008. 22(9): p. 1734-1746.

7. Abd Mutalib, M., M. A. Rahman, M. H. D. Othman, A. F. Ismail, and J. Jaafar, Chapter 9 - Scanning Electron Microscopy (SEM) and Energy-Dispersive X-Ray (EDX) Spectroscopy, in Membrane Characterization, N. Hilal, et al., Editors. 2017, Elsevier. p. 161-179.

8. He, B.B., Two-dimensional X-ray diffraction. 2018: John Wiley & Sons.

9. Cullity, B.D., Elements of X-ray Diffraction. 1956: Addison-Wesley Publishing.

10. Larkin, P., Infrared and Raman spectroscopy: principles and spectral interpretation. 2017: Elsevier.

11. Jones, M., Chapter 4 - Test Equipment Principles, in Building Valve Amplifiers (Second Edition), M. Jones, Editor. 2014, Newnes: Oxford. p. 235-380.

12. Franck, A. and T. Germany, Viscoelasticity and dynamic mechanical testing. TA Instruments, New Castle, DE, USA AN004, 1993.

13. Instron 3369. 2023 [cited 2023 16/01/2023]; Available from: https://www.instron.com/-/media/literature-library/products/2011/06/3300-series-table-model.pdf.

14. Koirala, P., Nekoda van de Werken, Hongbing Lu, Ray H. Baughman, Raquel Ovalle-Robles, and Mehran Tehrani., Using ultra-thin interlaminar carbon nanotube sheets to enhance the mechanical and electrical properties of carbon fiber reinforced polymer composites. Composites Part B: Engineering, 2021. 216.

15. Hu, D., Xiaosu Yi, Minqiang Jiang, Genghong Li, Xiaoye Cong, Xiaoling Liu, Chris Rudd., Development of highly electrically conductive composites for aeronautical applications utilizing bi-functional composite interleaves. Aerospace Science and Technology, 2020. 98.

16. Sciospec ISX-3v2. 2023 [cited 2023 16/01/2023]; Available from: https://www.sciospec.com/en-gb/product/isx-3/.

17. Guo, M., Xiaosu Yi, Chris Rudd, Xiaoling Liu., Preparation of highly electrically conductive carbon-fiber composites with high interlaminar fracture toughness by using silver-plated interleaves. Composites Science and Technology, 2019. 176: p. 29-36.

18. Chung, D.D.L., 3 - Polymer-Matrix Composites: Structure and Processing, in Carbon Composites (Second Edition), D.D.L. Chung, Editor. 2017, Butterworth-Heinemann. p. 161-217.

19. Brown, S.C., Colin Robert, Vasileios Koutsos, Dipa Ray., Methods of modifying through-thickness electrical conductivity of CFRP for use in structural health monitoring, and its effect on mechanical properties – A review. Composites Part A: Applied Science and Manufacturing, 2020. 133.

Chapter 4 Design and development of a nozzle-free electrospinning device

4.1 Introduction

Nanofibres can be made in different ways, such as through centrifugal spinning [1], meltblowing [2], bicomponent spinning [3], electrospinning [4], and bubble electrospinning [5]. Electrospinning is the most common way to make nanofibres when compared to other methods. The nozzle-free electrospinning method has been proven to be a continuous and effective way to make NFs. This could be because there are many patents on free-surface electrospinning setups, and the equipment that can be bought on the market is very expensive. For example, products like the Nanospider TM (Elmarco, Ltd., Czech Republic), an industrial-scale electrospinner where a high-voltage potential (up to 80 kV) helps form fibres out of a polymer-layered thread at a set rate, cost anywhere from 170,000 to 300,000 USD. In fact, traditional electrospinning prevents many exciting and innovative advances in the field from being used in the real world.

This chapter provides a step-by-step guide for the design and construction of a temperature-controlled nozzle-free electrospinning device. The equipment uses a rotating mandrel partially immersed within a polymer solution to produce fibres in an upward motion by inducing the formation of multiple Taylor cones and subsequently

multi-jetting out of an electrified open surface. Free-surface electrospinning can overcome limitations and drawbacks associated with single and multi-nozzle spinneret configurations, such as low yield, limited production capacity, nonuniform electric field distribution, and clogging. Most importantly, this lab-scaled high-throughput device can provide an alternative economical route for needleless electrospinning research, in contrast to the high costs associated with industrially available upscaling equipment. Among the device's technical specifications, a key feature is a cryo-collector mandrel, capable of collecting fibres in sub-zero temperatures, which can induce ultra-porous nanostructures, wider pores, and subsequent in-depth penetration of cells. A multi-channel gas chamber allows the conditioning of the atmosphere, temperature, and airflow, while the chamber's design averts user exposure to the high-voltage components. The cost-effective design, which costs between 1500-2000 USD to assemble, can permit researchers to conduct lab-scaled research on high-throughput fibre production at a low cost.

4.2 Results and discussion

A rendered CAD model of the nozzle-free electrospinning equipment is depicted in Figure 4.1. All the assembled and connected parts/materials used for the manufacturing nozzle-free electrospinning setup are listed in Table A1 of appendix A. The setup consists of five major sub-assemblies

(i) Spinneret

(ii) Collector drum

(iii) Heating assembly

(iv) A three-layer lid assembly

(v) Electronics.

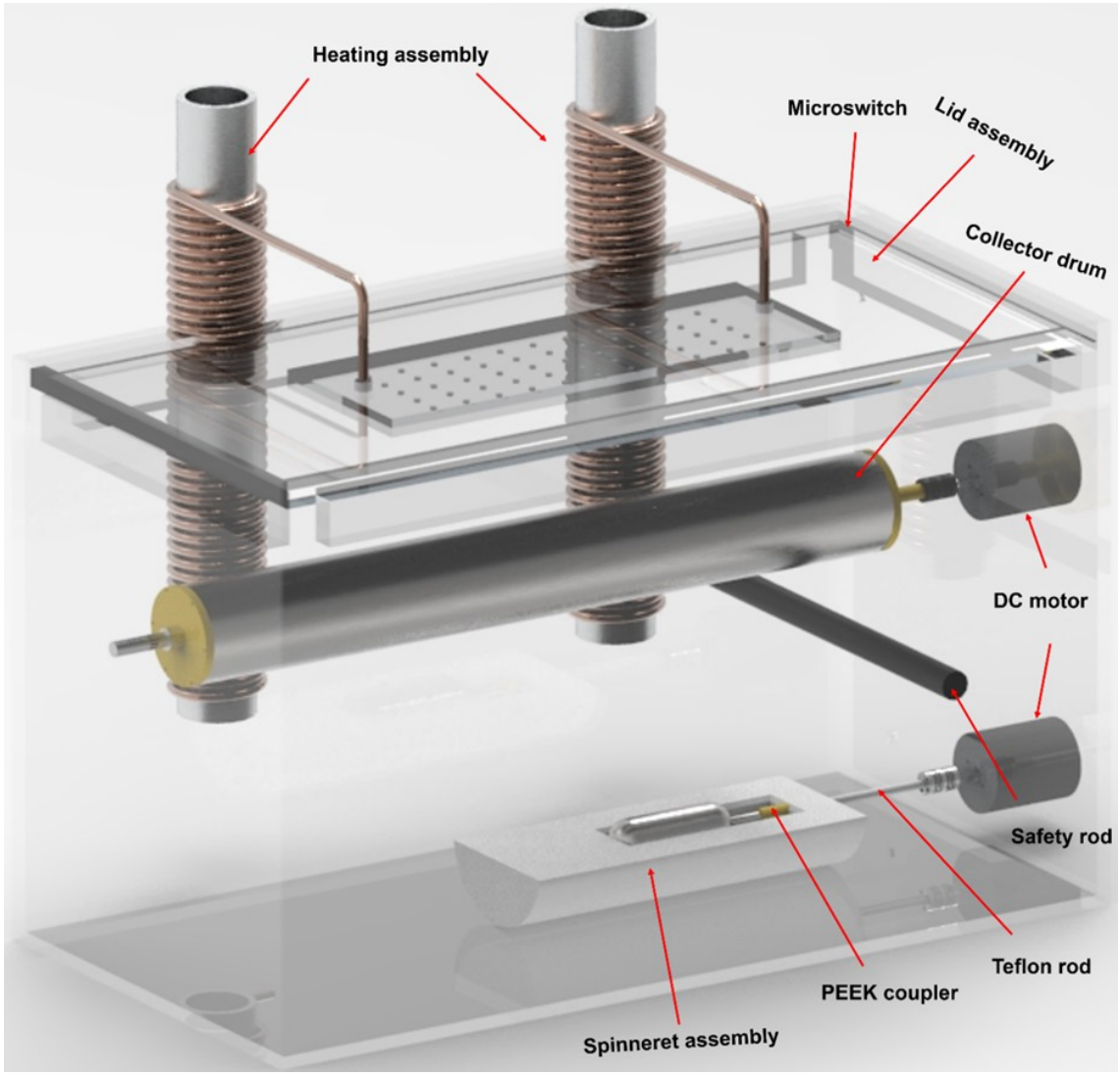

Figure 4-1 Rendered CAD model of the nozzle-free electrospinning setup with a description of each assembly and device component.

An exploded CAD model of the nozzle-free electrospinning setup can be found in Figure 4.2, which gives a better understanding of each major sub-assembly of the device.

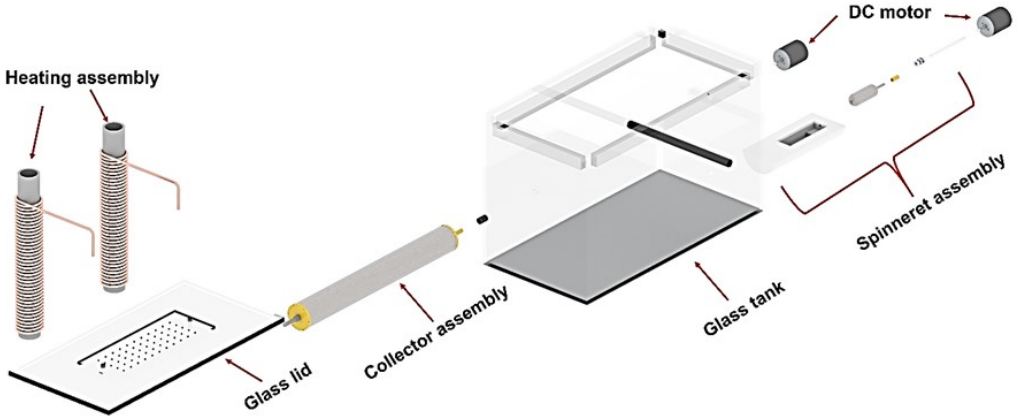

Figure 4-2 Exploded CAD model of the nozzle-free electrospinning setup.

4.2.1 Safety measures

As electrospinning uses high voltage to electrify the polymer solution and produce fibres, an electrically insulating material is required as a safety precaution. As glass presents a very high dielectric strength and resistivity, a low coefficient of thermal expansion, high tensile strength, and is transparent, it was chosen for the casing [6]. For the casing of the electrospinning setup, a rectangular glass tank (aquarium) of 5 mm glass thickness (dimensions: 610 (length) x 308 (width) x 380 (height) mm) was used. In total, 13 holes were carefully drilled in various compartments of the glass aquarium using a circular diamond-tipped drill bit hole saw and drill positioning tools, taking into account the fragility of glass material.

A round plastic (polyoxymethylene; POM) safety rod was placed below and antiparallel to the collector's direction as a safety measure to prevent direct contact between the negative and positive high voltage connections, in the unlike scenario, the collector drum was to detach during the electrospinning process due to high rotation speed.

At the top of the glass tank, four rectangular acrylic pieces were glued on, using epoxy, facing inwards and parallel to each other, to support the placement of the lid. A safety interlock was mounted on one of the rectangular acrylic pieces at the midsection between the top of the aquarium and the lid support, where the interlock (microswitch) was placed, allowing for the automatic shutdown of the high voltage components and prevent the onset of high voltage at the absence of the lid.

4.2.2 Fabrication of the spinneret assembly

The spinneret configuration during free-surface electrospinning plays an imperative part towards the fibre production output. The spinneret's size and geometry, along with the polymer solution properties, ambient parameters, and applied voltage, will direct the number of the emerging Taylor cones from the open surface. Wei et al. [7] found that the electric field intensity reaches the highest values at the ends of the cylinder spinneret and decreases towards the centre, which may hamper jet formation. Electric field profile and intensity simulations using COMSOL have demonstrated that, although the highest electric field profile is generated towards the centre of an annular spinneret, the electric field intensity is at least 5-fold higher at the edges.

In the setup, the spinneret is connected to a high voltage power supply via a high-voltage wire loop and is partially immersed in a solution bath. As the spinneret slowly rotates, a thin film of the polymer solution forms on the upper (open) side of the spinneret that is not immersed, allowing for the jetting of fibres from multiple Taylor cones throughout its surface. There are three spinneret assemblies: a cylinder, a ball, and a spiral coil described in this chapter, Figure 4.3.

Selecting the appropriate material for the spinneret assembly is critical due to the corrosive nature of different solvents. Teflon, stainless steel, and polyether ether ketone (PEEK) are well-documented towards their resistant nature against common solvents [8]. The spinneret assembly consisted of a Teflon bath, a solid stainless-steel cylinder, a Teflon rod, a PEEK coupler, an HV wire loop, and a 12 V DC gear motor.

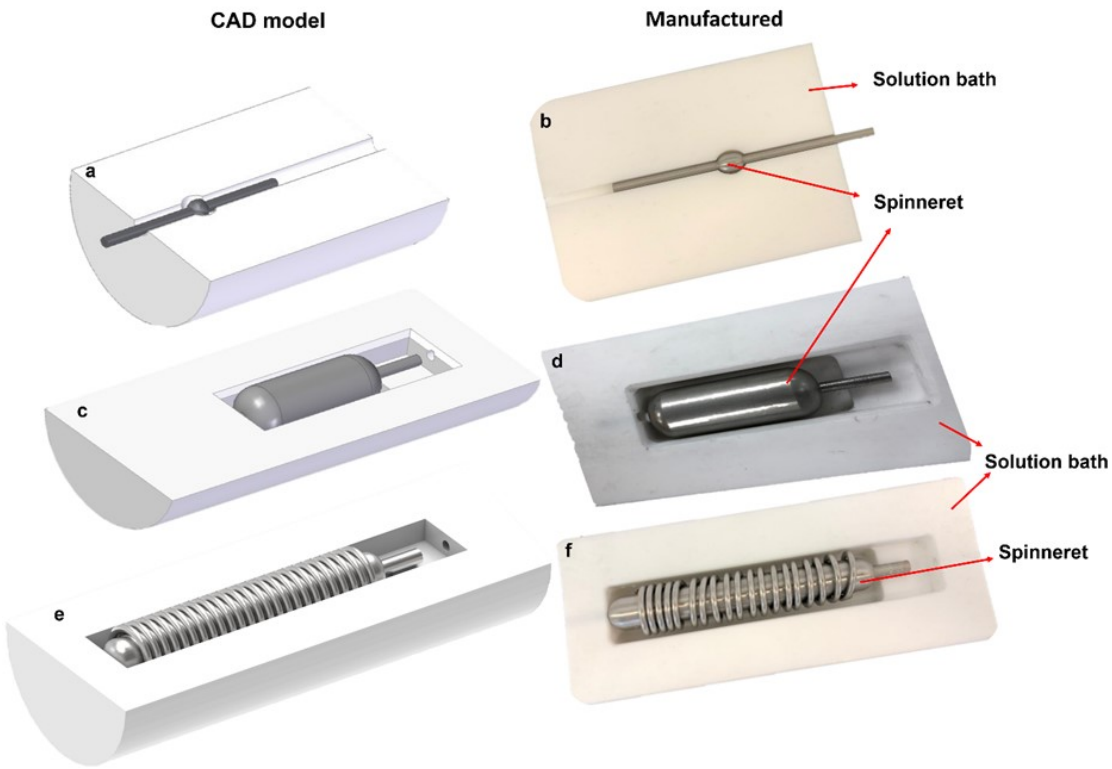

Figure 4-3 CAD models and corresponding photographs of the three spinneret assemblies. (a-b) CAD model and photograph of the small spherical spinneret, (c-d) CAD model and photograph of the medium-size spinneret, (e-f) CAD model, and a photograph of a large spinneret with the coil.

The solution bath refers to the polymer reservoir within which the spinneret rotates. Three different solution baths were made to accommodate different solution volumes. The solution bath was machined from a Teflon rod stock to form a rectangular pot that can facilitate the electrospinning of polymer solutions.

The small Teflon bath (2 mL solution capacity) presents a 5.1 mm diameter semi-cylinder carved out along its length to facilitate the placement of the metallic rod that is used to rotate the spinneret Figure 3 (a-b). The reservoir of 16 mm in diameter and 8 mm in depth was carved in the shape of a semi-sphere out of the Teflon material to contain the polymer solution. The 2 mL Teflon bath was able to accommodate the immersion of a 10 mm stainless-steel metallic sphere capable of rotating along its axis. A 5 mm round shaft attached to the metallic sphere ensured its straight horizontal position along the x-axis.

The medium solution bath was machined from a Teflon rod stock to form a rectangular pot that can facilitate the electrospinning of a 40 mL polymer solution (solution bath dimensions: 90 mm (length) × 30 mm (width) × 20 mm (depth)). A hole was drilled on the upper level of the rectangular pot to position the spinneret with a step for the shaft Figure 3 (c-d). Then, a 6 mm opening was drilled on the Teflon bath, in which a small piece of Teflon rod mounted within the centre (x-axis) of the metallic roller ensured its straight positioning and subsequent ability to rotate. On the opposite side, a 6 mm opening drilled through the Teflon material allowed a 300 mm in length Teflon rod and a PEEK coupler to connect the spinneret with the DC motor. The device was designed to facilitate a stainless-steel metallic roller spinneret (113 mm (length) x 30 mm (width)). The metallic roller has tapered edges to prevent concentrated high electric fields from forming. An exploded CAD model of medium spinneret can be found in Figure 4.4.

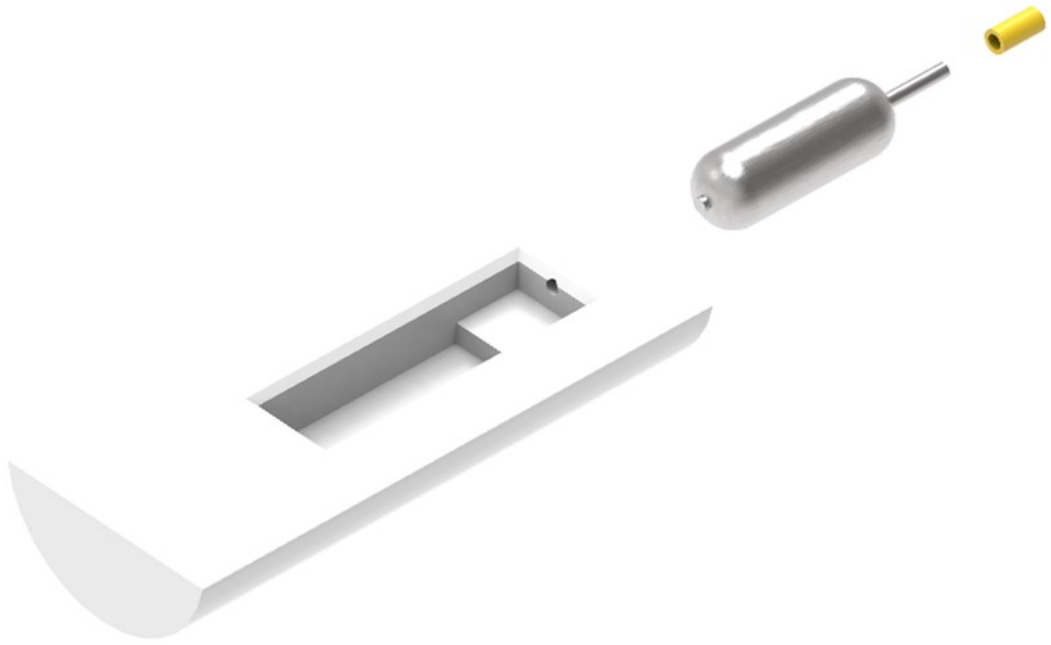

Figure 4-4 Exploded CAD model of the medium spinneret.

The solution bath, within which the spinneret was submerged, provided a 5% margin on each side of the spinneret to allow for its rotation and polymer coating, and a 10% margin on the coupler-rod side for the positioning of the HV loop. Allowing minimal exposure of the polymer solution is an important aspect of the device, which provides

shelter to volatile solvents and allows consistency throughout the electrospinning process.

The large spinneret assembly (60 mL solution capacity), conceptually similar to the 40 mL solution bath, was machined from a Teflon rod stock to form a rectangular cavity with a step for the shaft. As shown in Figure 4.3 (e-f), the spinneret of the large assembly, a stainless-steel metallic roller, consisted of a solid stainless-steel spindle spiral stainless-steel coil is welded around it. The stainless-steel roller's total length was 185 mm, where the diameter along the spiral coil was 21 mm. The spiral coil geometry can increase the number of Taylor cones forming along the spinneret's surface due to the increased curvature that leads to a stronger electric field than the smooth spinneret used in the medium Teflon bath. An exploded CAD model of a large spinneret can be found in Figure 4.5.

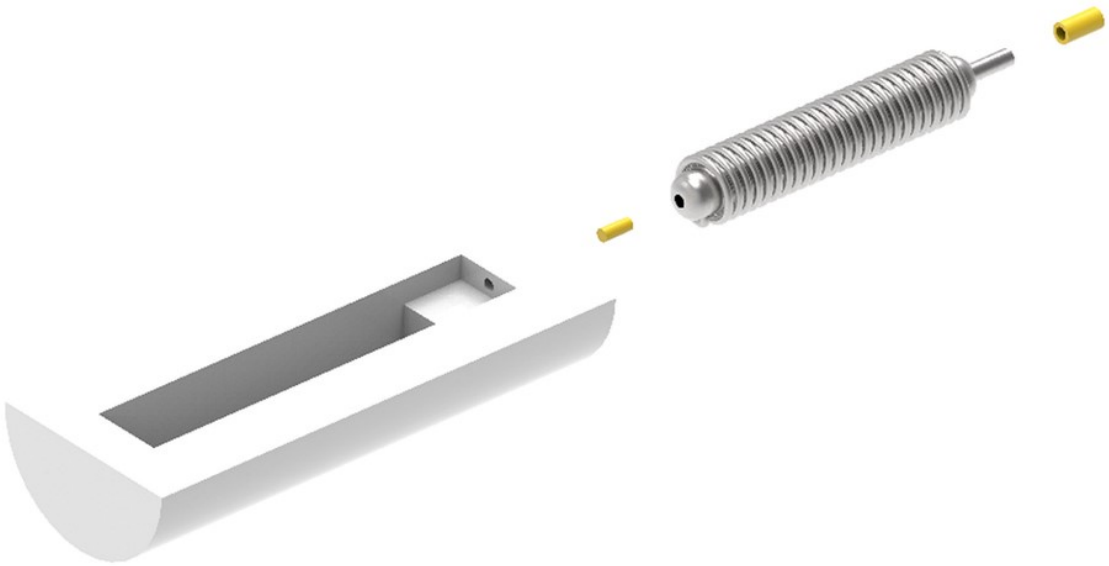

Figure 4-5 Exploded CAD model of large spinneret.

4.2.3 Fabrication of the collector assembly

The collector was manufactured from a stainless-steel cylinder to attain good electrical conductivity and charge distribution along its surface [9]. The collector assembly consisted of five distinct parts: a hollow stainless-steel cylinder, two PEEK discs for positioning the cylinder, and two protruding shafts. Four 20 mm holes on the side of the collector allowed dry ice insertion. The PEEK discs were fixed on the hollow cylinder by six stainless steel screws, while the shafts were mounted on the discs using two stainless steel screws for each Figure 4.6.

The small collector assembly has a diameter of 48 mm and is 500 mm long Figure 4.6 (a-b). The shaft connecting the collector to the electric motor was made out of aluminium Figure 4.6 (c-d). On the opposite side, an aluminium shaft was inserted in the centre of a 10 mm-diameter metallic ball bearing, allowing its rotation.

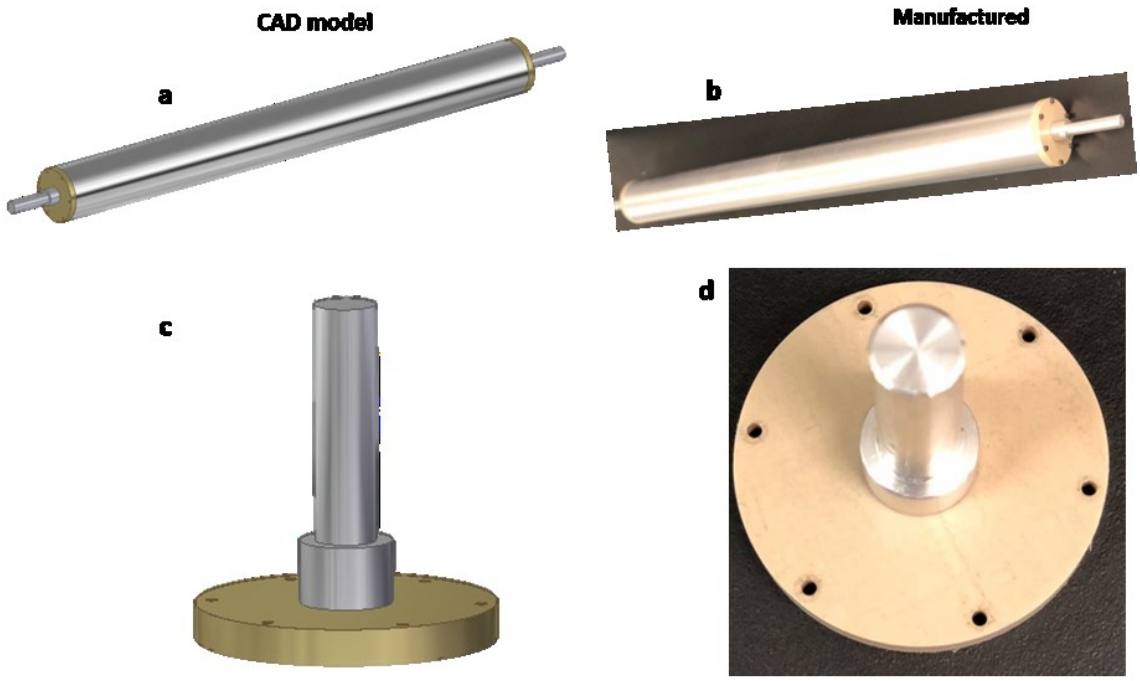

Figure 4-6 CAD model of the small collector assembly (a-b) CAD model and photograph of the manufactured small assembly (c-d) CAD model and photograph of the PEEK disc with four holes with the aluminium shaft

Figure 4-7 Exploded CAD model of cryo-collector assembly

Cryogenic electrospinning is a technique that uses a sub-zero (in °C) temperature collector to facilitate the simultaneous formation of nanofibres and ice crystals. The scaffold's pore size can be adjusted from 10–500 μm, depending on various controllable factors, such as size and the amount of ice crystals. The ice crystals are then removed by freeze-drying the fibrous scaffolds, leaving large void spaces, which create an ultra-porous biomaterial with wide pores that can permit cell infiltration [10]. An exploded CAD model of cryo-collector assembly can be found in Figure 4.7.

The cryo-collector assembly has a diameter of 64 mm and is 500 mm long Figure 4.8 (a-b). The shaft connecting the collector to the electric motor was made out of PEEK Figure 4.8 (c-d) to avoid electrical charges escaping from the collector's surface towards the DC motor. On the opposite side, an aluminium shaft Figure 4.7 (e-f) was inserted in the centre of a 10 mm-diameter metallic ball bearing, allowing its rotation.

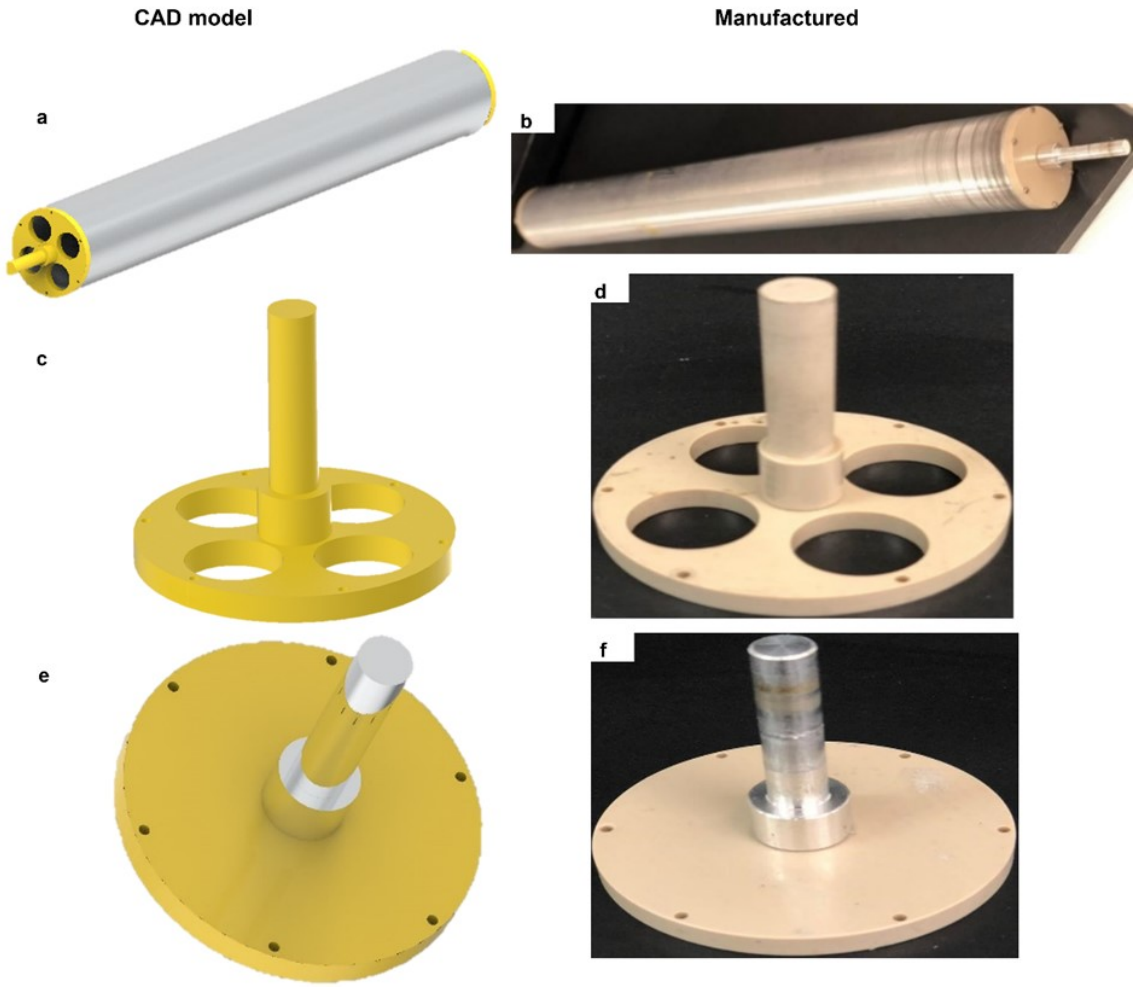

Figure 4-8 CAD model of the cryo-collector assembly (a-b) CAD model and photograph of the manufactured cryo-collector assembly (c-d) CAD model and photograph of the PEEK disc with four holes with the PEEK shaft (e-f) CAD model and photograph of the closing PEEK disc and aluminium shaft.

4.2.4 Heating and lid assembly

The lid assembly consisted of three rectangular glass plates, as shown in Figure 4.9 (a-e). The ambient humidity is a critical factor that can directly affect the electrospinnability of a polymer solution and the subsequent morphology of the fibres. For instance, high humidity can affect the morphology of the fibres by forming defects (e.g., beads), secondary morphologies (e.g., net-like spider webs), or by completely halting a solution from being electrospun. The layered glass assembly allows the uniform distribution of gas (hot air, nitrogen) onto the collector assembly, controlling the humidity and temperature within the electrospinning chamber. Each rectangular glass plate was 590 mm (length) x 295 mm (width) x 5 mm (thickness). The outermost glass layer had 55 holes of 3 mm diameter arranged at five rows and 11 columns, similar to a perforated glass. This allowed for the uniform distribution of air/nitrogen across the glass aquarium, at a constant flow across the holes. A rectangular glass piece was cut out from the middle glass plane at the same position where the 55 holes were presented on the bottom glass plane to allow for the gas distribution and circulation. The top glass plane presented two openings for Swagelok tube fittings from where copper tubing linked to the gas supply was connected to the lid. Heavy-duty suction cups were positioned to lift the lid.

Controlling the electrospinning chamber temperature, by heating the gas was achieved by using two heating assemblies positioned outside the glass aquarium. The heating assembly consisted of a heat sink, made of an aluminium pipe (50 mm (inner pipe diameter) x 400 mm (length)). Then, 6 mm copper tubing was used to wrap the heat sink, as shown in Figure 4.9 (f). Wrapping the aluminium pipes using high-temperature heating and insulation tapes, prevents heat loss to the environment. Two metallic hose clamps were used to stabilize the assembly and hold it together, as shown in Figure 4.9 (g). The high-temperature insulating tapes were heated by an MC 242 electric heating controller.

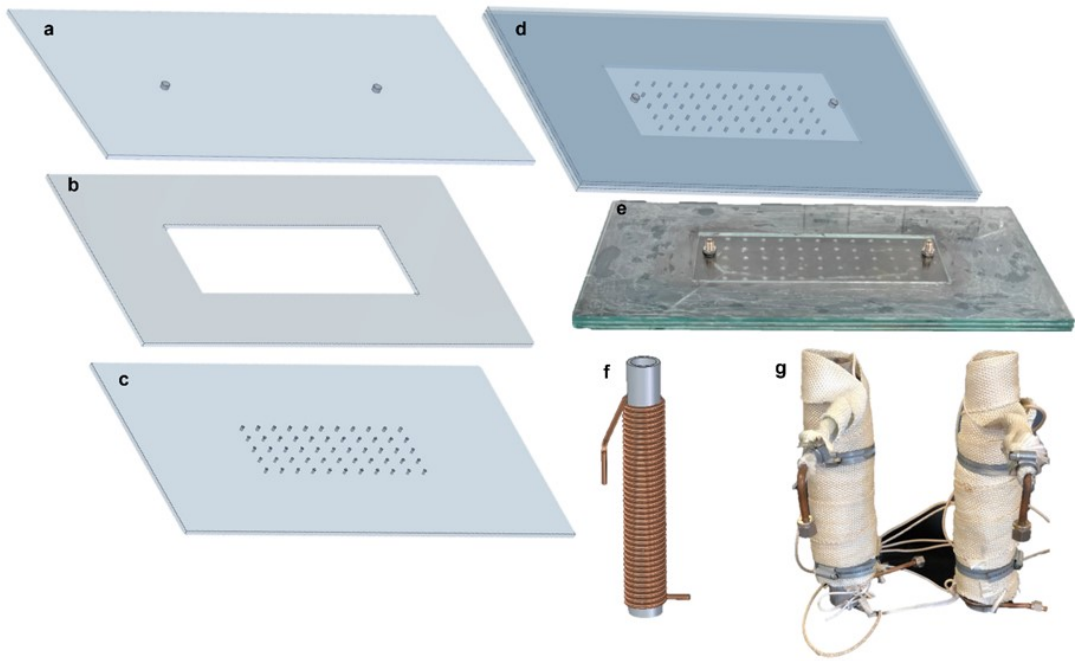

Figure 4-9 CAD model of the glass lid and heating assembly (a) CAD model of top glass plane, (b) CAD model of middle glass plane with the rectangular cut out (c) CAD model of bottom glass plane with 55 holes (d) CAD model (e) photograph of complete 3-layer lid assembly (f) CAD model of the heat sink with the copper coil wrapper around it (g) photograph of heating assembly.

4.2.5 Electronics

Two high-voltage DC power supplies (Information Unlimited, New Hampshire, USA) of adjustable output voltage, one of negative and one of positive voltage output, were utilized to electrify the polymer solution and draw the fibres towards the collector. Both have the capability to be adjusted between 5-35 kV, allowing the users to set a total potential difference of up to 70 kV between the rotating collector and the spinneret.

The rotations of the spinneret and the collector are independently controlled by DC motors. The spinneret rotational speed is constant, controlled by a direct current, 6 V at 5 revolutions per minute (RPM) when no load is coupled to the shaft. The collector is fitted with a brushed DC motor rated at 4500 RPM when unloaded (Bosch,

Germany). The user can adjust the effective RPM utilizing two controlling mechanisms; a speed controller and a DC source feeding the circuit.

The speed controller module used with the proposed setup (Model EM-185, Electromen OY, Finland) regulates the effective voltage fed to the motor, enabling the user to set the rotation of the collector from an estimate of 100 RPM up to its rated maximum RPM value, when no load limitation due to weight is considered. This controller supports only coarse RPM adjustments and will not allow the user to reliably set speeds below 100 RPM. The module can be powered up by any DC source that provides 12-24 V DC, and it can safely source up to 3 A to the motor. Identifying the maximum current that the module can handle is important for the design since the setup is required to operate under heavy load conditions when the hollow collector is filled with dry ice in the cryo-electrospinning mode. In this case, the motor requires a higher current spike for initiating rotation, which can be easily covered by the 3A limit outlined for the selected speed controller.

The power source selected for powering up the collector motor and its control circuit is an adjustable DC power supply (Model HCS 3102, Manson Engineering Industrial Ltd.) with programmable output voltage and current. The user can select an output voltage between 0 and 30 V in 0.1 V increments and an output current between 0 and 5 A with 0.1 increments. The selected source supports constant current and constant voltage supply modes. Users will typically employ the constant voltage supply mode, which will provide the requested voltage to the load while keeping it constant but allows variations in the supplied current.

In some cases, the user might want to set the collector speed below 100 RPM. For this specific task, having a programmable power source for the collector motor has proven to be advantageous. If the user sets the output voltage of the source at a low value and limits the output current to perhaps 0.1 or 0.2A after motor start-up, it is possible to force the collector to rotate at speeds within the range of 30 to 50 RPM. Although the RPM value tends to be unstable when this mode is engaged for long periods of time and the collector may stop inadvertently, this mode of operation will very likely be achieved in a future iteration of the set up.

4.2.6 Fabrication of nanofibres

The current nozzle-free electrospinning setup successfully produced NFs using different polymers. The SEM images of these electrospun NFs are shown in Figure 4.10 (a-f). The nozzle-free electrospinning setup can produce homogenous and uniform electrospun mats over a large area. The higher production rate of electrospun fibres can be achieved in very short time, 1.45 g of nanofibres collected on an aluminium foil in just 18 minutes, as shown in Figure 4.10 (g).

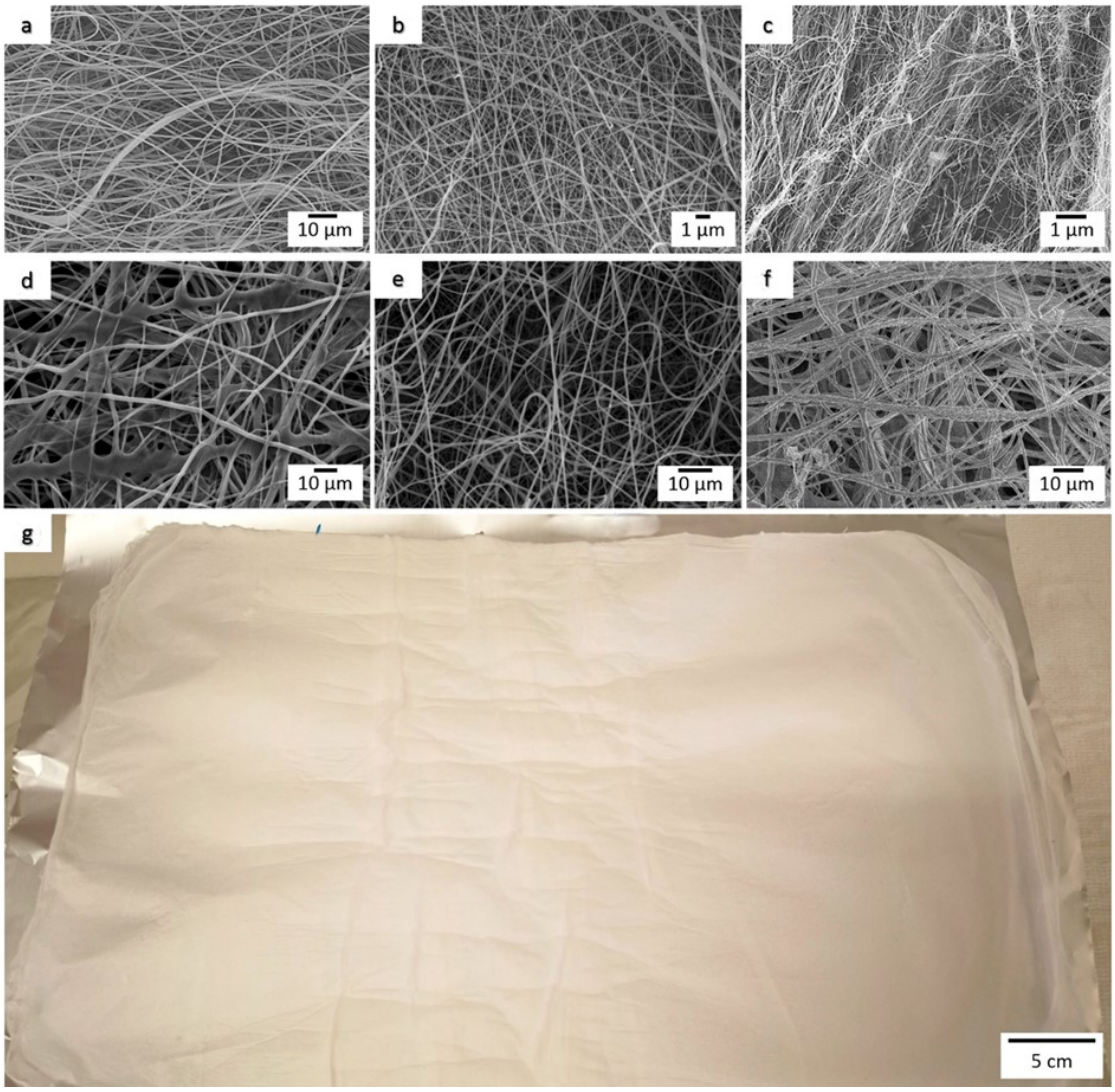

Figure 4-10 Nozzle-free electrospinning setup used to produce electrospun fibres using different polymers (a) Polyvinylpyrrolidone in N,N dimethylformamide (DMF)/Ethanol/distilled water (b) polycaprolactone in trifluoroacetic acid (c) silk

fibroin dissolved in trifluororethylene (d) polyaniline /polyacrylic acid in DMF (e) polyacrylonitrile in DMF (f) polyvinylidene fluoride/polyethylene glycol in DMF/distilled water (g) polyvinylidene fluoride/polyethylene glycol composite material electrospun directly on an aluminium foil. The electrospun mat shown in Figure 4.10 (g) was obtained within 18 minutes of electrospinning.

4.3 Conclusions

Nozzle-free electrospinning is a promising technology for large-scale production of NFs, as free-surface electrodes are not associated with clogging issues and non-uniform electric field distribution, allowing for the formation of multiple Taylor cones across the spinneret's surface. This chapter presents a step-by-step guide for the fabrication of a low-cost, temperature-controlled, nozzle-free electrospinning setup. The setup includes a cryo-collector, which enables cryo-electrospinning for obtaining ultra-porous materials. Three different spinnerets of variable size and geometries allow different solution volumes to be accommodated. In addition, a multi-channel gas lid allows uniform gas circulation, counter to the electrospinning direction, capable of controlling the humidity and temperature, which directly affect the solvent evaporation rate. As indicated, this setup has been successfully tested using several polymers and solvent systems and can be further validated by published works in the fields of drug formulation [11], tissue engineering [12, 13], wound healing [14], energy storage [15], and energy harvesting [16]. By utilising this setup, high-throughput production of fibres can be achieved efficiently and at a low cost, which can benefit the advancement of electrospun materials in health care, energy, and a wide range of industrial sectors.

In the next chapter, the introduction of conductive polymers into nanofibre veil is explored.

4.4 References

1. Zhang, Z.-M., Yao-Shuai Duan, Qiao Xu, and Biao Zhang, A review on nanofiber fabrication with the effect of high-speed centrifugal force field. Journal of Engineered Fibers and Fabrics, 2019. 14: p. 1558925019867517.

2. Drabek, J. and M. Zatloukal, Meltblown technology for production of polymeric microfibers/nanofibers: A review. Physics of Fluids, 2019. 31(9): p. 091301.

3. Naeimirad, M., Ali Zadhoush, Richard Kotek, Rasoul Esmaeely Neisiany, Saied Nouri Khorasani, and Seeram Ramakrishna, Recent advances in core/shell bicomponent fibers and nanofibers: A review. Journal of Applied Polymer Science, 2018. 135(21): p. 46265.

4. Waqas, M., Antonios Keirouz, Maria Kana Sanira Putri, Faraz Fazal, Francisco Javier Diaz Sanchez, Dipa Ray, Vasileios Koutsos, and Norbert Radacsi, Design and development of a nozzle-free electrospinning device for the high-throughput production of biomaterial nanofibers. Medical Engineering & Physics, 2021. 92: p. 80-87.5. Wan, L.Y., Bubble electrospinning and Bubble-spun Nanofibers. Recent Patents on Nanotechnology, 2020. 14(1): p. 10-13.

6. N.A. Othman, M.A.M.P., Z. Adzis, H. Ahmad, N.A. Ahmad, H. Kamarden, A.A. Suleiman, Characterization of charge distribution on the high voltage glass insulator string. Journal of Electrostatics, 2014. 72(4): p. 315-321.

7. Wei, L., et al., Mass production of nanofibers from needleless electrospinning by a novel annular spinneret. Materials & Design, 2019. 179.

8. Zhou, W., et al., Polydopamine-functionalized poly(ether ether ketone) tube for capillary electrophoresis-mass spectrometry. Anal Chim Acta, 2017. 987: p. 64-71.

9. Niu, H., T. Lin, and X. Wang, Needleless electrospinning. I. A comparison of cylinder and disk nozzles. Journal of Applied Polymer Science, 2009. 114(6): p. 3524-3530.

10. Niu, H. and T. Lin, Fiber Generators in Needleless Electrospinning. Journal of Nanomaterials, 2012. 2012: p. 1-13.

11. Keirouz, A., et al., Nylon-6/chitosan core/shell antimicrobial nanofibers for the prevention of mesh-associated surgical site infection. J Nanobiotechnology, 2020. 18(1): p. 51.

12. Keirouz, A., Giuseppino Fortunato, Mei Zhang, Anthony Callanan, and Norbert Radacsi, Nozzle-free electrospinning of Polyvinylpyrrolidone/Poly(glycerol sebacate) fibrous scaffolds for skin tissue engineering applications. Med Eng Phys, 2019. 71: p. 56-67.

13. Muenwacha, T., Oratai Weeranantanapan, Nuannoi Chudapongse, Francisco Javier Diaz Sanchez, Santi Maensiri, Norbert Radacsi, and Wiwat Nuansing, Fabrication of Piezoelectric Electrospun Termite Nest-like 3D Scaffolds for Tissue Engineering. Materials, 2021. 14(24): p. 7684.

14. Keirouz, A., Mariia Zakharova, Jaehoon Kwon, Colin Robert, Vasileios Koutsos, Anthony Callanan, Xianfeng Chen, Giuseppino Fortunato, and Norbert Radacsi, High-throughput production of silk fibroin-based electrospun fibers as biomaterial for skin tissue engineering applications. Mater Sci Eng C Mater Biol Appl, 2020. 112: p. 110939.

15. Radacsi, N., Fernando Diaz Campos, Calum RI Chisholm, and Konstantinos P. Giapis, Spontaneous formation of nanoparticles on electrospun nanofibres. Nat Commun, 2018. 9(1): p. 4740.

16. Sanchez, F.J.D., Michael Chung, Muhammad Waqas, Vasileios Koutsos, Stewart Smith, and Norbert Radacsi, Sponge-like piezoelectric micro- and nanofiber structures for mechanical energy harvesting. Nano Energy, 2022. 98: p. 107286.

Chapter 5 Polyaniline / polyvinylpyrrolidone nanofibres via nozzle-free electrospinning

5.1 Introduction

In this chapter, polyaniline (PANI) in its emeraldine base (PANI-EB) and salt (PANI-ES) forms were combined with polyvinylpyrrolidone (PVP) to produce composite nanofibres using a one-step electrospinning process. Electrospinning is a technique that uses an electric field to draw charged polymer solutions or melts into continuous, nanoscale fibres. The resulting PANI/PVP nanofibres were characterised using various techniques, including scanning electron microscopy (SEM), X-ray diffraction (XRD), Fourier transform infrared spectroscopy (FTIR), and energy-dispersive X-ray spectroscopy (EDX). Four PANI/PVP electrospun nanofibres with different PANI concentrations were prepared to investigate the effect of PANI concentration on the structure and properties of the nanofibres. The incorporation of different contents of PANI-EB and PANI-ES in the PVP solution and their impact on the fibre morphology were investigated. This is the first time that the electrospinning of pure PANI-EB/PVP and PANI-ES/PVP and their electrospun fibres have been studied, and the results of this work may have potential applications in fields such as membrane, biocompatibility, electronics, composites and energy storage.

This chapter also presents the synthesis of CFRP laminates where PANI/PVP electrospun veils are used as interleaving materials after being directly deposited on carbon fibre fabric. These electrospun veils were not conductive enough to be for improving the through-thickness electrical conductivity of interleaving CFRP composites.

5.2 Results and discussion

5.2.1 Morphology and electrical conductivity of synthesized polyaniline

Chemical oxidative polymerization of aniline is the traditional method for preparing polyaniline. The typical fluffy granular powder morphology was observed for the PANI-EB polymer, Figure 5.1 (a). Polyaniline prepared using ammonium peroxydisulfate has a highly aggregated morphology. M. Angelopoulos et al. reported that PANI-EB tends to make inter-chain H-bonding between amine and imine sites resulting in aggregate formation [1]. Huang et al. [2] reported that oxidation of aniline is an exothermic reaction and in early polymerization process polyaniline nanofibres in the range of 30-50 nm are formed. When ammonium peroxydisulfate solution is added to aniline solution, after rapid sedimentation and aggregation the nanofibres become thickened and coarser, and the resulting structure comprises irregularly-shaped agglomerates [3]. Green-coloured PANI-ES was synthesized after mixing aniline with two oxidants, potassium biiodate, and hypochlorite, in 1M HCl solution. The SEM micrograph shown in Figure 5.1 (b) demonstrates that the synthesized PANI-ES consists of an irregular mixture of fibrils and a few granular particles. The sodium hypochlorite's facilitates nanofibre growth and reduces nucleation sites formation on the nanofibre surface [4]. Therefore, thinner and longer nanofibreils of PANI-ES were produced.

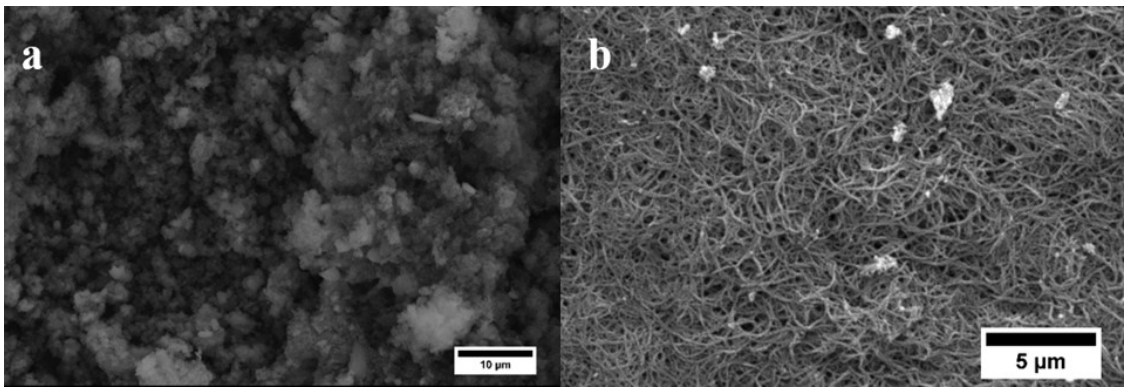

Figure 5-1 SEM micrograph of (a) polyaniline emeraldine base (PANI-EB) (b) polyaniline emeraldine salt (PANI-ES).

The bulk room temperature electrical conductivity of polyaniline pellets was measured using the four-point probe method. The electrical conductivity of PANI-EB is very low, outside of the range of the used Ossila four-point probe. Yilmaz et al. reported the electrical conductivity of PANI-EB in the order of magnitude of 10^{-3} S/cm [5]. The electrical conductivity of PANI-ES is 13.1 ± 1.71 S/cm which is ca. 7 times less than the value reported by A.Rahay [6]. Stejskal et al. reported that 40% standard deviation in polyaniline's conductivity is possible for a set of polymerization even after following the same method [7]. Variable electrical conductivity could be caused by differences in reaction conditions, sample processing, and electrical measurement conditions, such as pellet size and pressure applied to a compressed pellet. The electrical conductivity of polyaniline can be greatly influenced by varying the different parameters of polymerization. To achieve maximum electrical conductivity it is very important to optimize the reaction speed, temperature, oxidant ratio, time of reaction, and the acid ratio of PANI polymerization [8]. In addition to the above parameters, the diameter and length of the nanofibril structure of PANI-ES may have an influence on electrical conductivity. The average diameter and length of synthesized PANI-ES nanofibrils are 124 ± 24 nm, and 1.16 ± 0.28 µm, respectively, while A. Rahy reported fibril average diameter and length of ca. 50 nm and 4 µm, respectively.

5.2.2 X-ray diffraction analysis

The crystallinity and orientation of conducting polymers have been of much interest because more highly ordered systems can display a metallic conductive state [9]. Many

researchers reported that polyaniline has an X-ray diffraction pattern consisting of three peaks at 15°, 20°, and 25° [4, 10, 11]. Figure 5.2 shows that our sample also has three crystalline peaks, at ca. 15°, 20°, and 25°, which indicates that our sample has a crystalline nature. The characteristic peaks appeared at 15°, 20°, and 25°, corresponding to (011), (020), and (200) crystal planes of PANI [3, 8].

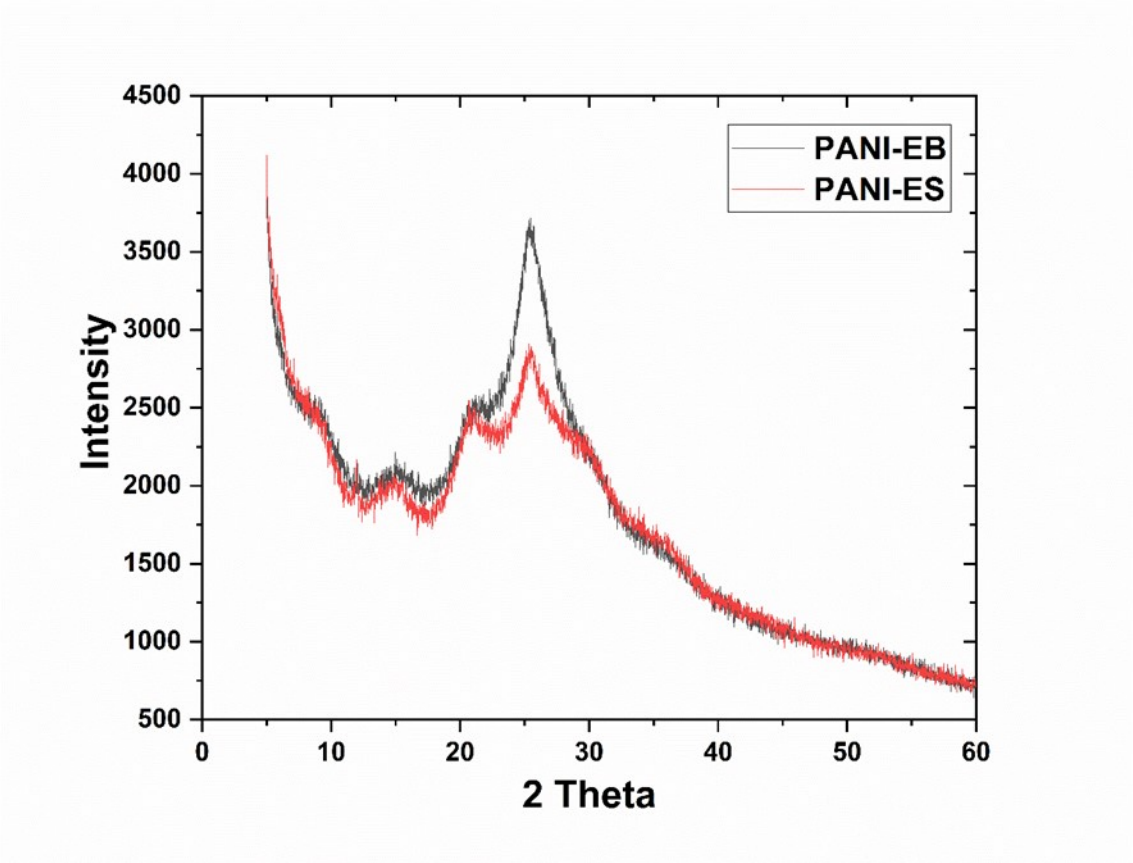

Figure 5-2 XRD graph of PANI-EB (black line) and PANI-ES (red line).

5.2.3 Morphology of electrospun nanofibres composite

PVP, PANI-EB/PVP, and PANI-ES/PVP electrospun fibre composite were prepared employing nozzle-free electrospinning using varying fractions of PANI and PVP in the solution system. The composition of the electrospinning solution, the electrical conductivity of the solution, and the fibre diameter of PVP and PANI/PVP electrospun fibres are reported in Table 5.1. The average fibre diameters observed for the electrospun composite were measured from the SEM micrographs and determined by measuring the diameters of at least 50 random fibres. Two different forms: PANI-EB

Polyaniline / polyvinylpyrrolidone nanofibres via nozzle-free electrospinning and PANI-ES were used with two different concentrations, 5.55 mg mL^{-1} and 11.11 mg mL^{-1} in the PANI/PVP electrospinning solution as given in Table 5 1. It has to be noted that blends containing more than 11.11 mg mL^{-1} PANI-ES were not suitable for electrospinning due to the high viscosity and high electrical conductivity of the solution [12].

Table 5-1 The different investigated concentrations of PANI/PVP and the corresponding electrical conductivity of the solution and average fibre diameter.

Composition of electrospinning solution in DMF	**Name of samples**	**The electrical conductivity of the solution (µS/cm)**	**Average fibre diameter (nm)**
150 mg mL^{-1} PVP	PVP-1	7.22	166 ± 58
180 mg mL^{-1} PVP	PVP-2	7.27	89 ± 15
5.55 mg mL^{-1} PANI-EB	PANI-EB-5/PVP	10.15	366 ± 220
11.11 mg mL^{-1} PANI-EB	PANI-EB-11/PVP	17.81	286 ± 136
5.55 mg mL^{-1} PANI-ES	PANI-ES-5/PVP	37.4	189 ± 61
11.11 mg mL^{-1} PANI-ES	PANI-ES-11/PVP	50.4	219 ± 57

Figure 5.3 illustrates SEM images of the electrospun composite of PVP, PANI-EB/PVP, and PANI-ES/PVP. Histograms of the fibre diameter distributions and the average values for each case are presented in Figure 5.4. The electrospun fibres are randomly oriented fibrous networks. Figure 5.3 (a-b) shows the electrospun fibres of pure PVP; with increasing the concentration of PVP, the average fibre diameter was also reduced from 166 ± 58 nm to 89 ± 15 nm. PVP was dissolved in DMF, which facilitates polymer dissolution by separating the ion pairs. Besides, its presence in the

solution could raise the charge density and generate excessive charges, leading to nanofibre formation with smaller diameters [13].

The morphology of PANI-EB/PVP electrospun fibres is shown in Figure 5.3 (c-f). The incorporation of PANI-EB in PVP solution resulted in an increase in electrospun fibre diameter to 366 ± 220 nm for PANI-EB-5/PVP Figure 5.3 (c-d), in agreement with the increase in PANI-EB/PVP electrospun fibre diameters with PANI-EB previously reported in the literature [14]. It is worth noting that the average fibre diameter of PANI-EB-5/PVP and PANI-EB-11/PVP electrospun fibres decreases from 366 ± 220 nm to 286 ± 136 nm, respectively with increasing PANI-EB content in the blend, as shown in Figure 5.4 (c-d). This behaviour could be attributed to the difference in solution viscosity because of densely entangled polymer chains [15]. The reduction in fibre diameter is related to the high viscosity of the solution that prevents the jet from breaking up into droplets. Moreover, the increase in chain entanglements results in an increase in viscoelastic force, which can be enough to prevent the electrically charged jet's breakup [16]. As a result, the charged jet elongates towards collector by Coulombic stress, and the diameter of the jet decreases [15]. As the PANI-EB content increases in the electrospinning solution, an increased presence of encapsulated micrometre-sized particles is detected attached within the PANI-EB/PVP fibres, as shown in the SEM images Figure 5.3 (c-f) [14]. These particles might be undissolved PANI-EB, which remains in the solution system while electrospinning. Additional reasons for the encapsulation of PANI-EB particles might be the high surface tension of PANI molecules and number of entanglements of PVP chains during the electrospinning process [12, 17]. The presence of micro-sized porous particles of PANI-EB on the fibre surface results in electrospun matrix with a higher surface area. The fibrous mat can be used to trap gaseous agents and might have higher surface interactions with polyaniline particles encapsulated within the electrospun mats [18].

For the PANI-ES/PVP solution, with increasing PANI-ES content, the system electrical conductivity substantially increased, as mentioned in Table 5.1 The PANI-ES may affect the solution's electrical and viscoelastic properties by increasing its concentration in the solution. The higher charge density and ionic conductivity can enhance the jet instability and higher splitting degree, making the overall

Polyaniline / polyvinylpyrrolidone nanofibres via nozzle-free electrospinning electrospinning process challenging to control [19]. The potential difference of the applied voltage was adjusted from 40 kV to 60 kV during the electrospinning process to avoid the PANI-ES/PVP solutions electrospraying. Figure 5.3 SEM images of (a) PVP-1 (b) PVP-2 (c-d) PANI-EB-5/PVP irregularly-shaped undissolved polymer particles are attached to nanofibres (e-f) PANI-EB-11/PVP irregularly-shaped undissolved polymer particles are attached to nanofibres (g) PANI-ES-5/PVP (h) PANI-ES-11/PVP.

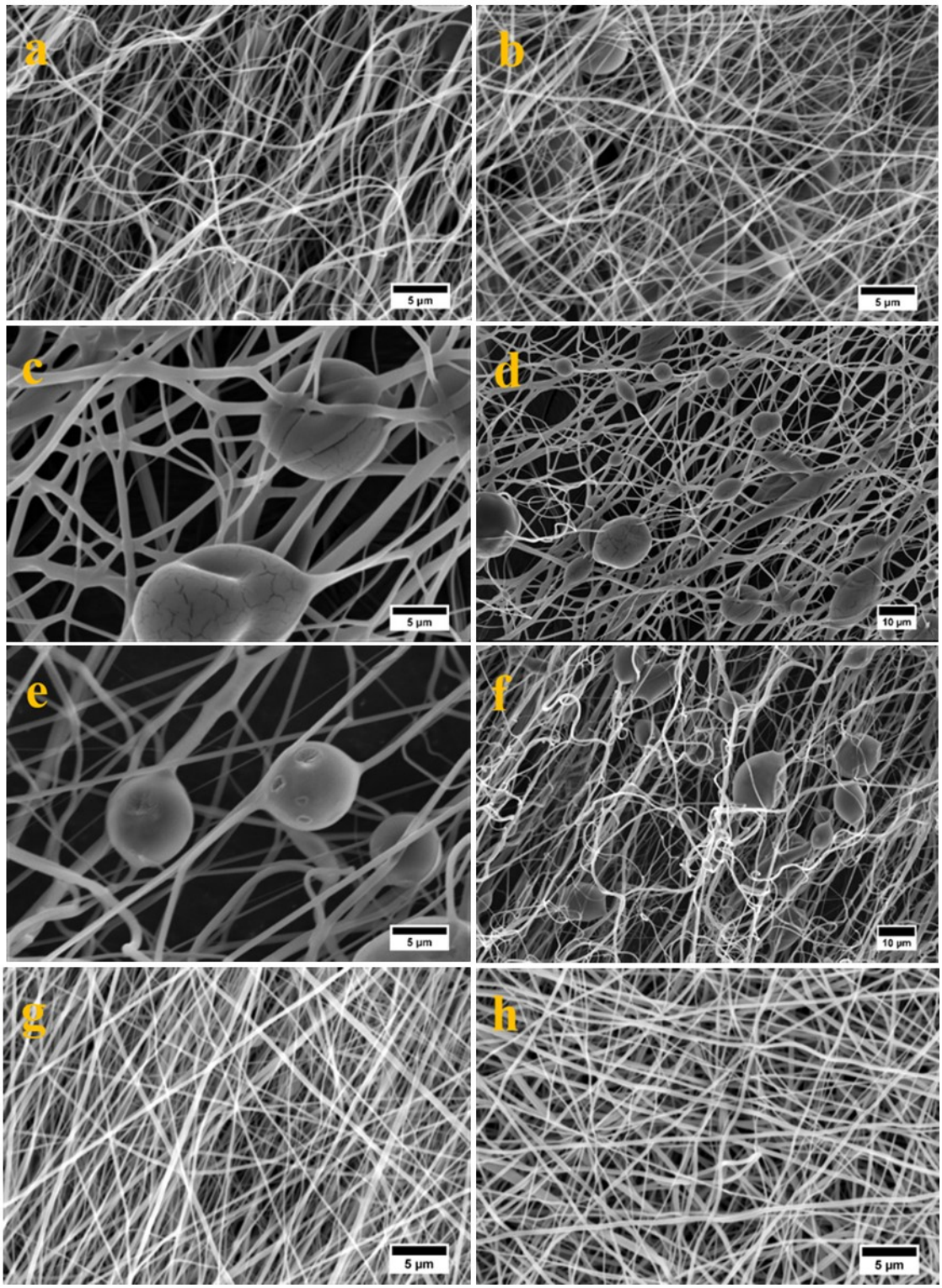

Figure 5-3 SEM images of (a) PVP-1 (b) PVP-2 (c-d) PANI-EB-5/PVP irregularly-shaped undissolved polymer particles are attached to nanofibres (e-f) PANI-EB-11/PVP irregularly-shaped undissolved polymer particles are attached to nanofibres (g) PANI-ES-5/PVP (h) PANI-ES-11/PVP.

Polyaniline / polyvinylpyrrolidone nanofibres via nozzle-free electrospinning

In contrast to PANI-EB/PVP, PANI-ES/PVP fibres display a different morphology. These nanofibres do not have any particles attached. This change in morphology might be attributed to the nano-sized fibrillar structure of PANI-ES, see Figure 5.1 (b). Colloidal stabilization can be achieved by electrostatic repulsion due to particle surface charge and/or steric repulsion (by introduction of a polymer or a surfactant as stabilizer) [20]. The backbone of the emeraldine form of polyaniline is positively charged by a protonic acid (H+A-). Therefore, a stable colloid could be formed through electrostatic repulsion without using steric stabilizer if particle size is very small or by steric repulsion via adsorbed PVP [21, 22].

The fibre morphology for PANI-ES-5/PVP and PANI-ES-11/PVP was smooth, uniform, and randomly oriented with a fibre diameter of 189 ± 61 nm and 219 ± 57 nm, respectively, see Figure 5.3 (g-h). As the amount of PANI-ES was increased from PANI-ES-5 to PANI-ES-11 in the PVP solution, a small increase in fibre diameters was observed, as presented in the histogram in Figure 5.4 (e-f). The polyaniline emeraldine salt content, viscosity, and strength of the electric field were the main parameters in determining the fibre diameters. The incorporation of salt increased the polymer jet stretching and reduced the incidence of bead formation by distributing the charges consistently to control the fibre uniformity [23-25].

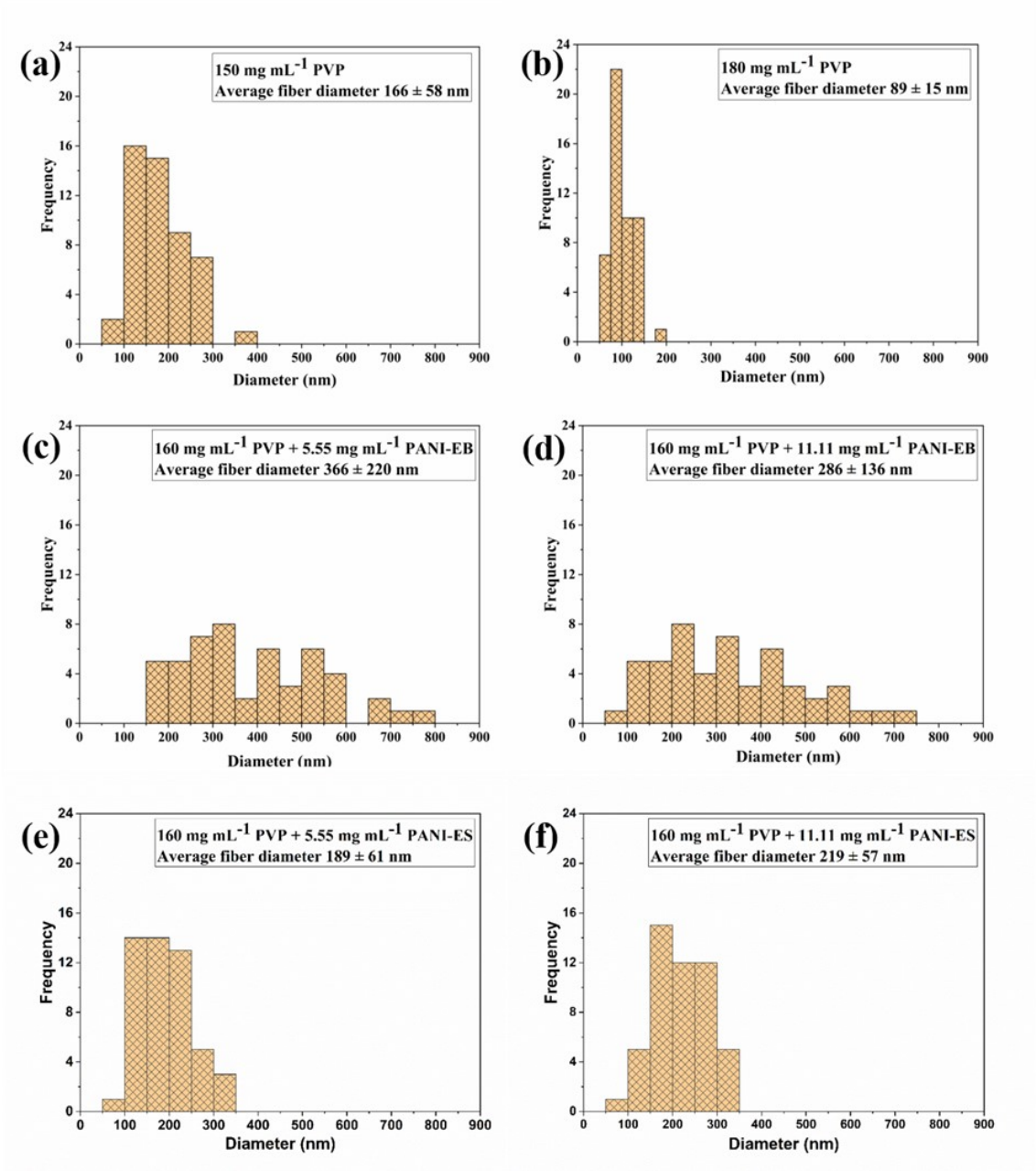

Figure 5-4 Histogram of the fibre diameters and average fibre diameters of electrospun composite (a) PVP-1 (b) PVP-2 (c) PANI-EB-5/PVP (d) PANI-EB-11/PVP (e) PANI-ES-5/PVP (f) PANI-ES-11/PVP.

5.2.4 FTIR of PANI and electrospun nanofibres

FTIR spectra of PANI-EB, PANI-ES, and PANI/PVP electrospun fibres are shown in Figure 5.5. The spectra of PANI-ES show two maxima bands of quinoid and benzenoid ring stretching vibrations at 1570 cm^{-1} and 1480 cm^{-1}, respectively. The band at 1243

cm^{-1} is C-N^{+}. stretching vibrations in the polaronic structure. The prominent band ~1136 cm^{-1} has been assigned to vibrations of the —NH^{+}═ structure [14, 26-28]. FTIR spectrum of PANI-EB powder demonstrates the vibrational bands groups at 824 cm^{-1} and 1141 cm^{-1}. The bands of quinonoid and benzonoid ring vibrations were revealed at 1495 cm^{-1} and 1585 cm^{-1}. The peak at 1377 cm^{-1} was attributed to C–N stretching in the neighbourhood of a quinoid ring [3, 5, 27, 29]. The PVP spectrum shows two main bands elongation of the accompanying OH is visible as a broadband at approximately 3400 cm^{-1}, and the strong band at 1644 cm^{-1} was also linked to the stretching vibrations of the free carbonyl groups in PVP. In addition, several bands are also seen in the range between 1245 and 1520 cm^{-1}. Both the band at 1443 cm^{-1} and the band at 1292 cm^{-1} are caused by the stretching of the molecules -(N-C)=O and -(C-N)-C, respectively [30, 31].

The PVP and PANI/PVP nanofibres spectrums are almost identical because higher concentrations of PVP are used to prepare the PANI/PVP electrospinning solution. The pure PVP nanofibre spectra exhibits one characteristic band at 1644 cm^{-1}, which corresponds to free carbonyl, while the PANI powder spectra is transparent and exhibits no absorptivity in the carbonyl region. In PANI/PVP nanofibres spectrums, this band gradually shifted to a mode of lower frequency stretching. This shift can be attributed to a rise in the stiffness of PVP rings and may also be seen as proof of the existence of a hydrogen connection between PVP and PANI [28, 30].

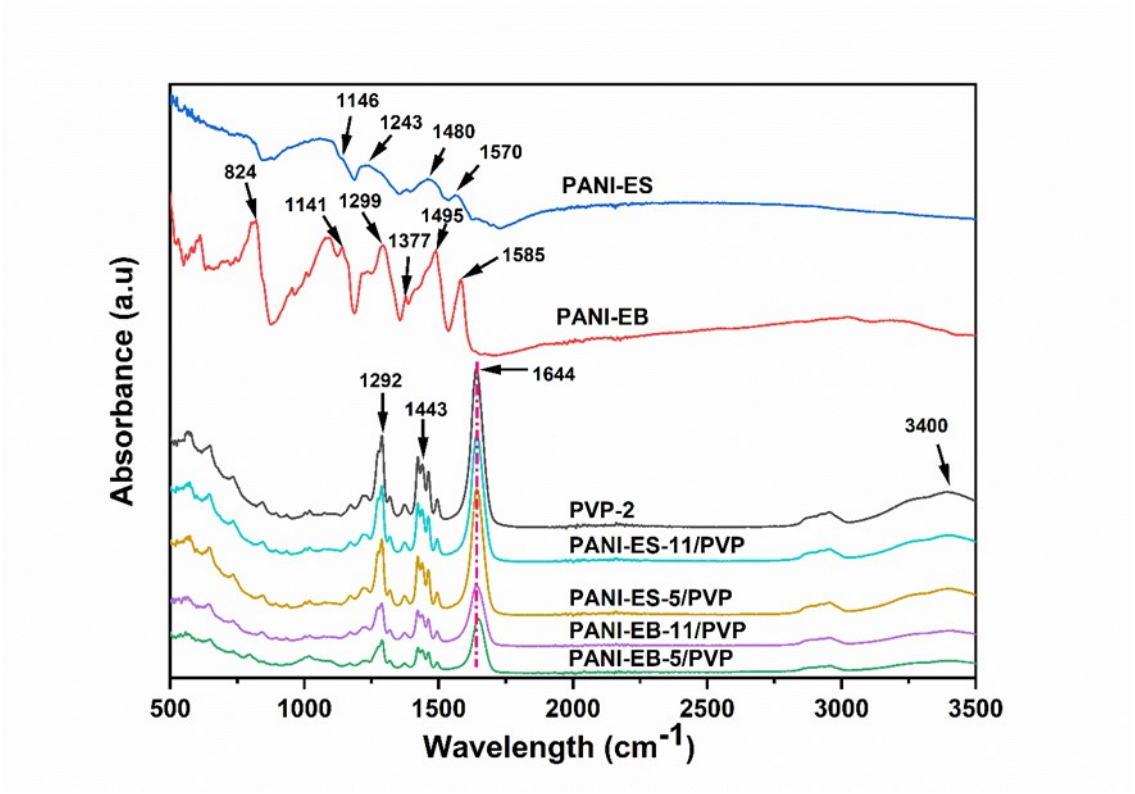

Figure 5-5 FTIR spectra of PANI-EB, PANI-ES powders and PANI-PVP electrospun fibres in the 500-3500 cm^{-1} region.

5.2.5 Elemental analysis of electrospun nanofibres

To identify the chemical composition of the particles attached to the PANI-EB/PVP nanofibres composite, an elemental analysis was carried out using Energy-Dispersive X-ray spectroscopy (EDX). Three different EDX spectra were obtained during the EDX analysis and are shown in Figure 5.6. Both PVP and PANI have C, H and N atoms in their chemical structures. PVP contains the O atom, whereas PANI does not. The EDX spectrum in Figure 5.6 (b) on the irregular-shaped polymer particle at position b in Figure 5.6 (a) shows the elements of carbon (C), chlorine (Cl), hydrogen (H) and gold (Au). The 6.1% amount of Cl proves that PANI was synthesised in an acidic medium (HCl) [5, 32]. The electrospun nanofibres were sputter-coated and this is the source of Au. A focused ion beam was used to cut an irregularly shaped polymer particle cross-sectionally (position c), and the EDX analysis was performed on that exposed surface. The spectrum at position c in Figure 5.6 (a) presented in Figure 5.6 (c) exhibits lower levels of Au, but matches closely the levels of C, H and Cl shown

Polyaniline / polyvinylpyrrolidone nanofibres via nozzle-free electrospinning in Figure 5.6 (b), providing further verification that these irregular particles are PANI-EB particles attached/incorporated to the electrospun fibres. However, the EDX spectrum at position d of Figure 5.6 (a) on electrospun fibres shown in Figure 5.6 (d) has peaks of C, H and O, and the percentage of C is reduced to 69%, indicating that these are the PVP/PANI blend electrospun fibres [5, 33].

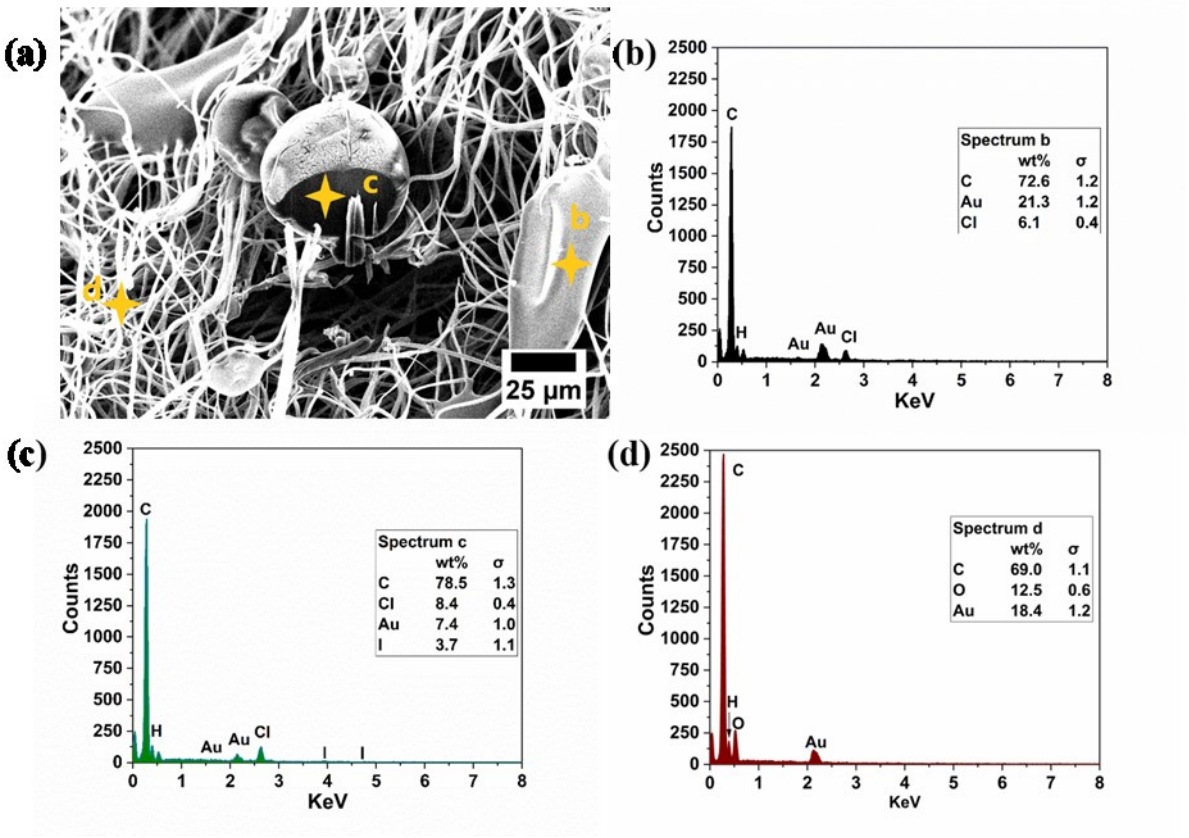

Figure 5-6 EDX analysis of PANI-EB-11/PVP (a) SEM image showing the positions b, c and d (b, c and d) corresponding EDX spectra of PANI-EB-11/PVP corresponding to positions b, c, and d, respectively.

5.3 Synthesis of laminate using electrospun fibres coated on carbon fibre fabric

PANI-EB/PVP and PANI-ES/PVP electrospun nanofibres were directly deposited on carbon fibre fabric. From a manufacturing perspective, direct deposition of electrospun nanofibres has benefits since it allows electrospinning to be integrated into production

lines, speeding up the manufacturing process and reducing cost [34]. Electrospun veils are very thin (few microns) with low areal weight and have minimal effect on the weight or thickness of the final product. The nanofibres do not move once inside a laminate and do not increase the viscosity of the matrix resin. The higher porosity of the electrospun veils makes it easy for the resin to flow through them while still keeping the nanofibres in place between the two layers. The mechanical properties of nanofibres can be much higher than those of the same material in its bulk state [35].

The polymeric solution's characteristics (polymer's molecular weight, solution's viscosity, and conductivity), process parameters, and environmental conditions are the same as presented in Chapter 3. The thickness of the PANI/PVP electrospun veils was in the range of 50-120 μm. Many researchers used nanofibre veils with an average thickness of 20-150 μm [35]. Generally, the thickness of nanofibre veils affects the interlaminar toughening due to varying loading levels, porosity, and adhesion of the nanofibre veil to the primary reinforcement fabric, i.e., carbon and glass fabric. Higher porosity of the veil can lead to higher permeability, which makes it easier for polymer resin to flow through the plies. Electrospun nanofibres are highly suited to infusion processing, as the nanofibres and the thermoset resin do not react until after the infusion process and phase separate during cure. This makes the two layers stick together better, which is good for interlaminar toughening. As the thickness of the nanofibre mat goes up, the porosity might go down, or it might be hard to separate the nanofibre mat from the main reinforcing fabric. Each laminate system may have its own optimal thickness, and nanofibres morphological properties. Therefore, complicated interlaminar toughening mechanisms make it hard to compare these results to each other [34, 35].

Table 5-2 Average thickness of PANI/PVP electrospun veils deposited on carbon fibre fabric. All the measurements taken are listed in Table B1 of Appendix B.

Composition of electrospinning solution in DMF	Name of samples	Average veil thickness (µm)
5.55 mg mL^{-1} PANI-EB	PANI-EB-5/PVP	69 ± 4
11.11 mg mL^{-1} PANI-EB	PANI-EB-11/PVP	90 ± 23
5.55 mg mL^{-1} PANI-ES	PANI-ES-5/PVP	92 ± 28
11.11 mg mL^{-1} PANI-ES	PANI-ES-11/PVP	76 ± 24

The electrospun nanofibres cover around 15 cm × 15 cm area of carbon fibre fabric. These electrospun-coated carbon fibre fabrics were used to produce electrospun interleaved CFRP laminates. The unidirectional (UD) laminates were made using a hand layup technique with a stack of 5 plies $[0]_5$ of electrospun coated carbon fibre fabric see Figure 5.7. For each composition, two laminates were made. After being hand laid up, the laminates were consolidated in a press at 1 bar of pressure and left to cure for 24 hours at room temperature. The resulting composites were post-cured for 2 hours at 40 °C, 2 hours at 50 °C, and 4 hours at 60 °C. Unfortunately, the conductivity of the fabricated PANI/PVP electrospun nanofibre veils were not measurable by our set-ups (Metrohm, Autolab PGSTAT204 and Sciospec ISX-3v2 electrical impedance spectroscopy). This could be due to the low amount of polyaniline in the electrospinning solution and the insulating nature of PVP. The presence of an insulating carrier polymer restricts the nanofibre veils to reach required conductivity percolation threshold and their possible use in those applications requiring higher electrical conductivity. Consequently, laminates prepared with PANI/PVP electrospun nanofibre veils were also electrically non-conductive.

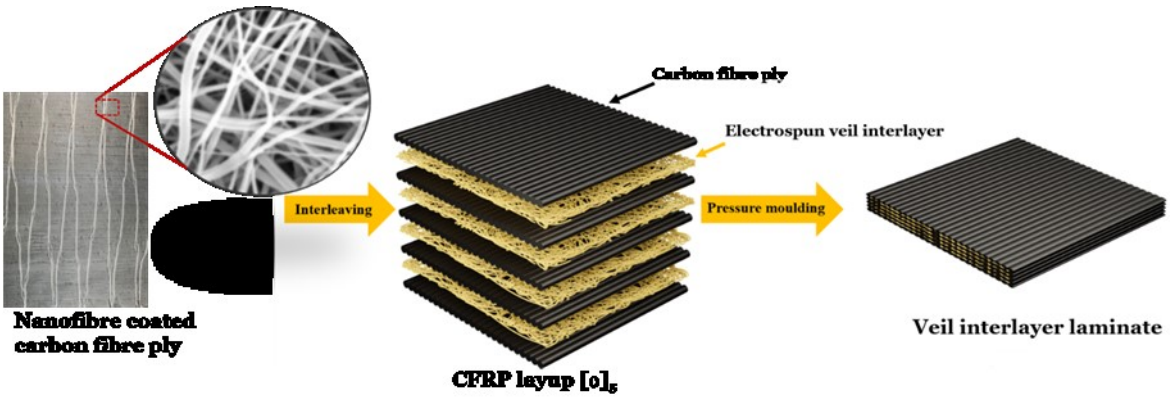

Figure 5-7 Schematic of electrospun nanofibre veil interlayer CFRP laminate preparation.

In summary, this approach of using electrospun nanofibre veils to increase the electrical conductivity of CFRP composites was not successful, as the veils made from PANI/PVP were not conductive possibly due to the low amount of polyaniline in the electrospinning solution, and the insulating nature of PVP. It has be noted that PVP in sufficient amounts is required for the successful electrospinning process.

5.4 Conclusions

In this chapter, polyaniline (PANI) in its emeraldine base (PANI-EB) and salt (PANI-ES) forms was combined with polyvinylpyrrolidone (PVP) to produce nanofibres in a one-step electrospinning process using a nozzle-free electrospinning setup. There has been no filtration of the PANI/PVP solution before electrospinning or any other chemical modification performed on PANI/PVP electrospun nanofibres. The different morphology of PANI-ES and PANI-EB affected the PANI/PVP solution properties and influenced the electrospinning process, morphology, and diameters of the electrospun nanofibres. The electrospinning of the PANI-EB/PVP solution is easy to perform compared to the solution containing PANI-ES because the addition of PANI-ES changes the solution's ionic conductivity. A higher voltage was applied for PANI-ES/PVP solutions during electrospinning to avoid electrospraying, which resulted in slightly thinner nanofibres. The PANI-ES/PVP electrospun fibres are well formed, smooth, and uniform exhibiting diameters of ca. 200 ± 60 nm. The PANI-EB/PVP nanofibres have PANI-EB irregular shaped microparticles attached to the fibres, which

Polyaniline / polyvinylpyrrolidone nanofibres via nozzle-free electrospinning are discontinuous and randomly oriented. However, similar fibre morphology was not observed for PANI-ES/PVP electrospun fibres due to nanofibril morphology of PANI-ES. The higher surface area of PANI/PVP electrospun nanofibres and encapsulation of PANI-EB particles around nanofibres make them promising materials for gas sensing, filtration, and membrane applications. However, the PANI/PVP electrospun nanofibres interlayers were not suitable for enhancing the through-thickness electrical conductivity of CFRP composites.

To achieve the aim of my PhD, I have shifted to a pre-fabricated carbon fibre-based veil material system. The carbon fibre (CF) or nickel-coated carbon fibre (NiCF) veils, were used as interlayers between standard carbon fibre reinforcement fabrics. The CF and NiCF veils were proprietary products of Technical Fibre Products Ltd., UK. Further research on the effect of carbon fibre-based veils on enhancing the through-thickness electrical conductivity of CFRP composites will be discussed in the next chapter.

5.5 References

1. Angelopoulos, M., R. Dipietro, W. G. Zheng, A. G. MacDiarmid, and A. J. Epstem, Effect of selected processing parameters on solution properties and morphology of polyaniline and impact on conductivity. 1997. 84(1-3): p. 35-39.

2. Huang, J., and Richard B. Kaner, The intrinsic nanofibrillar morphology of polyaniline. Chemical communications, 2006(4): p. 367-376.

3. Abdolahi, A., Esah Hamzah, Zaharah Ibrahim, and Shahrir Hashim, Synthesis of Uniform Polyaniline Nanofibers through Interfacial Polymerization. Materials, 2012. 5(8): p. 1487-1494.

4. Rahy, A., Mohamed Sakrout, Sanjeev Manohar, Sung June Cho, John Ferraris, and D. J. Yang, Polyaniline Nanofiber Synthesis by Co-Use of Ammonium Peroxydisulfate and Sodium Hypochlorite. Chemistry of Materials, 2008. 20(15): p. 4808-4814.

5. Yılmaz, F., and Zuhal Küçükyavuz, The influence of polymerization temperature on structure and properties of polyaniline e-Polymers, 2009. 9(1): p. 005.

6. Rahy, A. and D.J. Yang, Synthesis of highly conductive polyaniline nanofibers. Materials Letters, 2008. 62(28): p. 4311-4314.

7. Stejskal, J., and R. G. Gilbert, Polyaniline. Preparation of a conducting polymer (IUPAC technical report). Pure and applied chemistry, 2002. 74(5): p. 857-867.

8. Kamarudin, S., Mohd Saiful Asmal Rani, Masita Mohammad, Nor Hasimah Mohammed, Mohd Sukor Su'ait, Mohd Adib Ibrahim, Nilofar Asim, and Halim Razali, Investigation on size and conductivity of polyaniline nanofiber synthesised by surfactant-free polymerization. Journal of Materials Research and Technology, 2021. 14: p. 255-261.

9. Agrawal, P. and K. Pramanik, Chitosan-poly(vinyl alcohol) nanofibers by free surface electrospinning for tissue engineering applications. Tissue Eng Regen Med, 2016. 13(5): p. 485-497.

10. Lee, K., Shinuk Cho, Sung Heum Park, A. J. Heeger, Chan-Woo Lee, and Suck-Hyun Lee, Metallic transport in polyaniline. Nature, 2006. 441(7089): p. 65-8.

11. Chen, C.-H., Thermal and Morphological Studies of Chemically Prepared Emeraldine-Base-Form Polyaniline Powder. Applied Polymer Science, 2003. 89(8): p. 2142-2148.

12. Merlini, C., Alessandro Pegoretti, Thiago Medeiros Araujo, Sílvia DAS Ramoa, Wido H. Schreiner, and Guilherme Mariz de Oliveira Barra, Electrospinning of doped and undoped-polyaniline/poly (vinylidene fluoride) blends. Synthetic Metals, 2016. 213: p. 34-41.

13. Yang, Q., Zhenyu Li, Youliang Hong, Yiyang Zhao, Shilun Qiu, C. E. Wang, and Yen Wei, Influence of solvents on the formation of ultrathin uniform poly(vinyl pyrrolidone) nanofibers with electrospinning. Journal of Polymer Science Part B: Polymer Physics, 2004. 42(20): p. 3721-3726.

14. Wu, J.C.-C., Sudip Ray, Marija Gizdavic-Nikolaidis, Jianyong Jin, and Ralph P. Cooney, Effect of polyvinylpyrrolidone on storage stability, anti-oxidative and anti-bacterial properties of colloidal polyaniline. Synthetic Metals, 2016. 217: p. 202-209.

15. Yalcinkaya, F., Baturalp Yalcinkaya, and Oldrich Jirsak, Dependent and Independent Parameters of Needleless Electrospinning, in Electrospinning - Material, Techniques, and Biomedical Applications. 2016.

16. Gañán-Calvo, A.M., Cone-jet analytical extension of Taylor's electrostatic solution and the asymptotic universal scaling laws in electrospraying. Physical review letters, 1997. 79(2): p. 217.

17. Wei, M., Junseok Lee, Bongwoo Kang, and Joey Mead, Preparation of Core-Sheath Nanofibers from Conducting Polymer Blends. Macromolecular Rapid Communications, 2005. 26(14): p. 1127-1132.

18. Menzel, V.C., and Ignacio Tudela, Additive manufacturing of polyaniline-based materials: an opportunity for new designs and applications in energy and biotechnology. Current Opinion in Chemical Engineering, 2022. 35: p. 100742.

19. Meng, N., Xiangqin Wang, Binjie Xin, Zhuoming Chen, and Yan Liu, Preparation, structure and electrochromic behavior of PANI/PVA composite electrospun nanofiber. Textile Research Journal, 2019. 89(12): p. 2490-2499.

20. Hunter, R.J.W., L.R. Chan, D.Y.C., Foundations of Colloid Science. 1987: Clarendon Press.

21. Li, D., and Richard B. Kaner, Processable stabilizer-free polyaniline nanofiber aqueous colloids. Chem Commun (Camb), 2005(26): p. 3286-8.

22. Wang, Y.-Y., Wen-Jin Sun, Hao Lin, Ping-Ping Gao, Jie-Feng Gao, Kun Dai, Ding-Xiang Yan, and Zhong-Ming Li., Steric stabilizer-based promotion of uniform polyaniline shell for enhanced electromagnetic wave absorption of carbon nanotube/polyaniline hybrids. Composites Part B: Engineering, 2020. 199: p. 108309.

23. Abd Razak, S.I., Izzati Fatimah Wahab, Fatirah Fadil, Farah Nuruljannah Dahli, Ahmad Zahran Md Khudzari, and Hassan Adeli, A Review of Electrospun Conductive Polyaniline Based Nanofiber Composites and Blends: Processing Features, Applications, and Future Directions. Advances in Materials Science and Engineering, 2015. 2015: p. 1-19.

24. Raeesi, F., M. Nouri, and A.K. Haghi, Electrospinning of polyaniline-polyacrylonitrile blend nanofibers. e-Polymers, 2009. 9(1).

25. Sengupta, P., Aritri Ghosh, Navonil Bose, Sampad Mukherjee, Amit Roy Chowdhury, and Pallab Datta, A comparative assessment of poly (vinylidene fluoride)/conducting polymer electrospun nanofiber membranes for biomedical applications. Journal of Applied Polymer Science, 2020. 137(37): p. 49115.

26. Radoičić, M., Zoran Šaponjić, Jovan Nedeljković, Gordana Ćirić-Marjanović, and Jaroslav Stejskal, Self-assembled polyaniline nanotubes and nanoribbons/titanium dioxide nanocomposites. Synthetic Metals, 2010. 160(11): p. 1325-1334.

27. Nuzhnyy, D., J. Petzelt, I. Rychetský, M. Trchová, and J. Stejskal, High-frequency dielectric response of polyaniline pellets as nanocomposites of metallic emeraldine salt and dielectric base. Synthetic Metals, 2015. 209: p. 561-569.

28. Zhang, Y., Yuping Duan, Jia Liu, Guojia Ma, and Mingliang Huang, Wormlike Acid-Doped Polyaniline: Controllable Electrical Properties and Theoretical Investigation. The Journal of Physical Chemistry C, 2018. 122(4): p. 2032-2040.

29. Blinova, N.V., Jaroslav Stejskal, Miroslava Trchová, and Jan Prokeš, Polyaniline prepared in solutions of phosphoric acid: Powders, thin films, and colloidal dispersions. Polymer, 2006. 47(1): p. 42-48.

30. Atia, S., Khaled Zeggagh, Slimane Hadjout, Agustin Etxeberria, and Zitouni Benabdelghani, Enhancement of semiconducting and thermomechanical properties of materials based on polyaniline and polyvinylpyrrolidone. Journal of Polymer Research, 2022. 29(4): p. 138.

31. Kuo, S.W., and Feng Chih Chang, Studies of Miscibility Behavior and Hydrogen Bonding in Blends of Poly(vinylphenol) and Poly(vinylpyrrolidone). Macromolecules, 2001. 34(15): p. 5224-5228.

32. Molina, J., M. F. Esteves, J. Fernández, J. Bonastre, and F. Cases, Polyaniline coated conducting fabrics. Chemical and electrochemical characterization. European Polymer Journal, 2011. 47(10): p. 2003-2015.

33. Liu, W., Tuhua Zhong, Tuan Liu, Jinwen Zhang, and Hang Liu, Preparation and Characterization of Electrospun Conductive Janus Nanofibers with Polyaniline. ACS Applied Polymer Materials, 2020. 2(7): p. 2819-2829.

34. Palazzetti, R. and A. Zucchelli, Electrospun nanofibers as reinforcement for composite laminates materials – A review. Composite Structures, 2017. 182: p. 711-727.

35. Wang, G., Demei Yu, Ajit D. Kelkar, and Lifeng Zhang, Electrospun nanofiber: Emerging reinforcing filler in polymer matrix composite materials. Progress in Polymer Science, 2017. 75: p. 73-107.

36. Shakil, U.A., Shukur BA Hassan, Mohd Y. Yahya, and Saad Nauman, Mechanical properties of electrospun nanofiber reinforced/interleaved epoxy matrix composites—A review. Polymer Composites, 2020. 41(6): p. 2288-231

Chapter 6 Carbon fibre interleaving conducting veils in carbon fibre reinforced polymer composites

6.1 Introduction

This chapter presents detailed investigations using microfibrous carbon fibre-based conducting veils as interleaving materials to improve the through-thickness electrical conductivity of carbon fibre-reinforced composites. In Chapter 5, PANI/PVP electrospun mats were produced using nozzle-free electrospinning. These electrospun mats were not conductive enough to be used as conducting interleaving in CFRP composites. Carbon fibre (CF) or nickel-coated carbon fibre (NiCF) veils were used as interlayers between standard carbon fibre reinforcement fabrics. The through-thickness electrical conductivity of the interleaved composites with CF or NiCF veils improved over 50 fold, compared to the control specimens. However, the interleaved specimens exhibited a ca. 20-24% reduction in their interlaminar shear strength (ILSS) and flexural strength. The introduction of conducting veils facilitated establishing an electrical pathway between the carbon fabric plies by reducing the non-conducting resin rich zone in the interlaminar region. This established an electrically conductive pathway across the thickness of the laminate. This study reveals that conducting veil-

interleaved composites can meet a functional integration requirement of the aerospace sector for electrical properties, and can find applications in lightning protection, EMI shielding, and structural health monitoring.

6.2 Results and discussion

6.2.1 Interlaminar shear strength and flexural properties

Interlaminar shear strength (ILSS) for the control and veil-interleaved composites samples are plotted in Figure 6.1. The introduction of the NiCF veils in the interlaminar regions decreased the shear strength by ca. 22%, from 66 MPa to 51.5 MPa, see Figure 6.1 (d). Specimens interleaved with CF veils also exhibited a 24% drop in shear strength compared to the control sample. Pristine CFRP samples exhibited a standard linear trend up to the shear failure, where the ILSS value corresponded to 66 MPa. The interleaved samples showed two distinctive phases. Initially, a stiff response was noted, followed by a second softer behaviour, typical to yielding, before failure. It is interesting to note that the interleaved samples experienced a displacement of 0.6 mm until failure, which is about three times greater than the displacement of the control samples. The interlaminar shear strength was lower in the interleaved composites that might be due to weaker interlaminar regions.

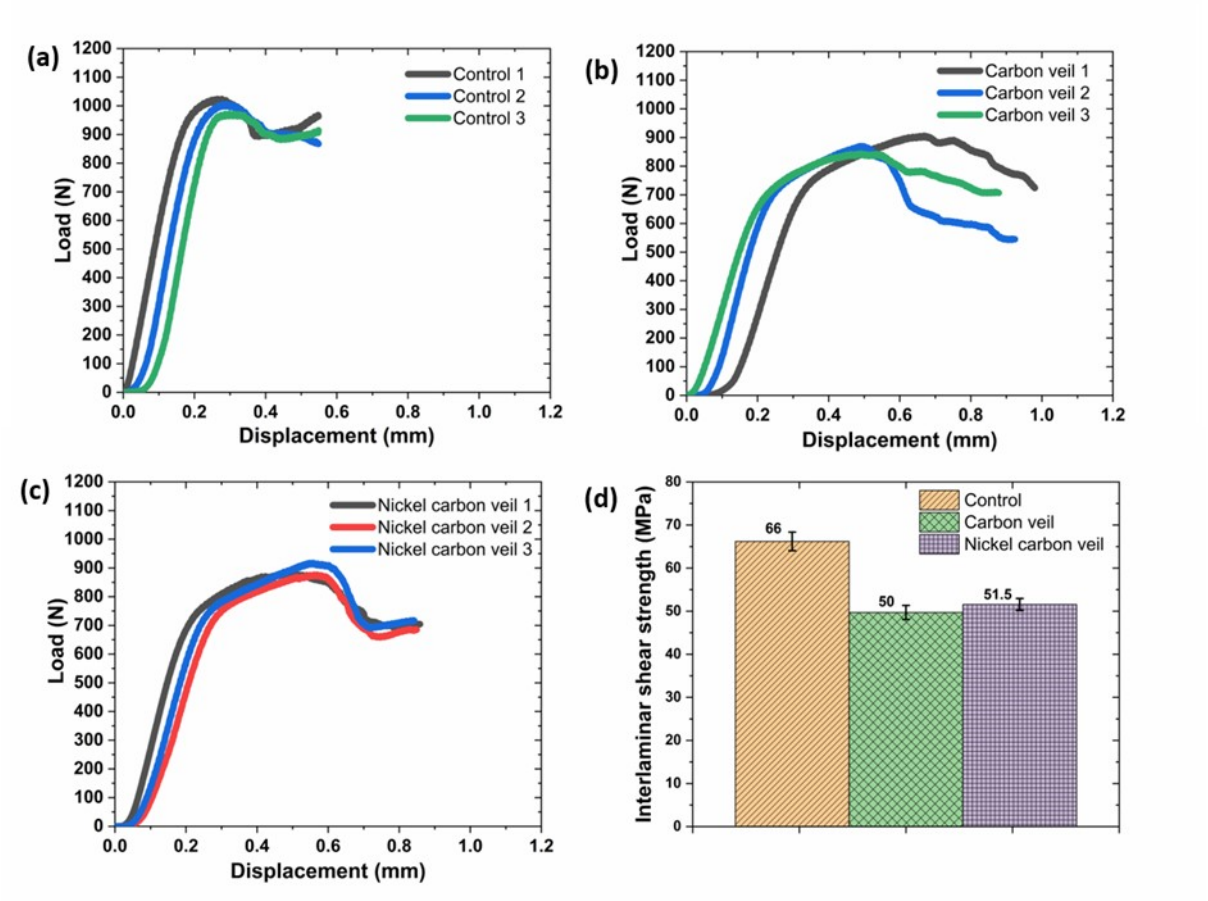

Figure 6-1 Interlaminar shear strength (ILSS) of control and veil-interleaved composites (a-c) Load-Displacement plots (d) Summary of interlaminar shear strength (ILSS).

The respective stress-strain curves for the flexural tests are shown in Figure 6.2 (a-c). The tensile and compressive stresses experienced during flexural testing may cause bending failure, and the effect of shear can be neglected for thin specimens. The flexural stress increased linearly for the control laminate. These graphs indicate that interleaved veil specimens fail at lower stresses, indicating a sudden loss of load-carrying capacity. Flexural testing revealed that the veil samples have lower flexural strength than the control specimens by 20% for the CF veil and 23% for the NiCF veil, as shown in Figure 6.2 (d). Interleaving causes a reduction in flexural performance of CFRP, since the embedded veil has a lower stiffness and strength. The flexural strength of both veil-interleaved laminates is almost equal. Yuan and Bard [1, 2] also reported

that the interlayer had a negative impact on the flexural strength of the laminates regardless of the interlayer fibre type, diameter, or length.

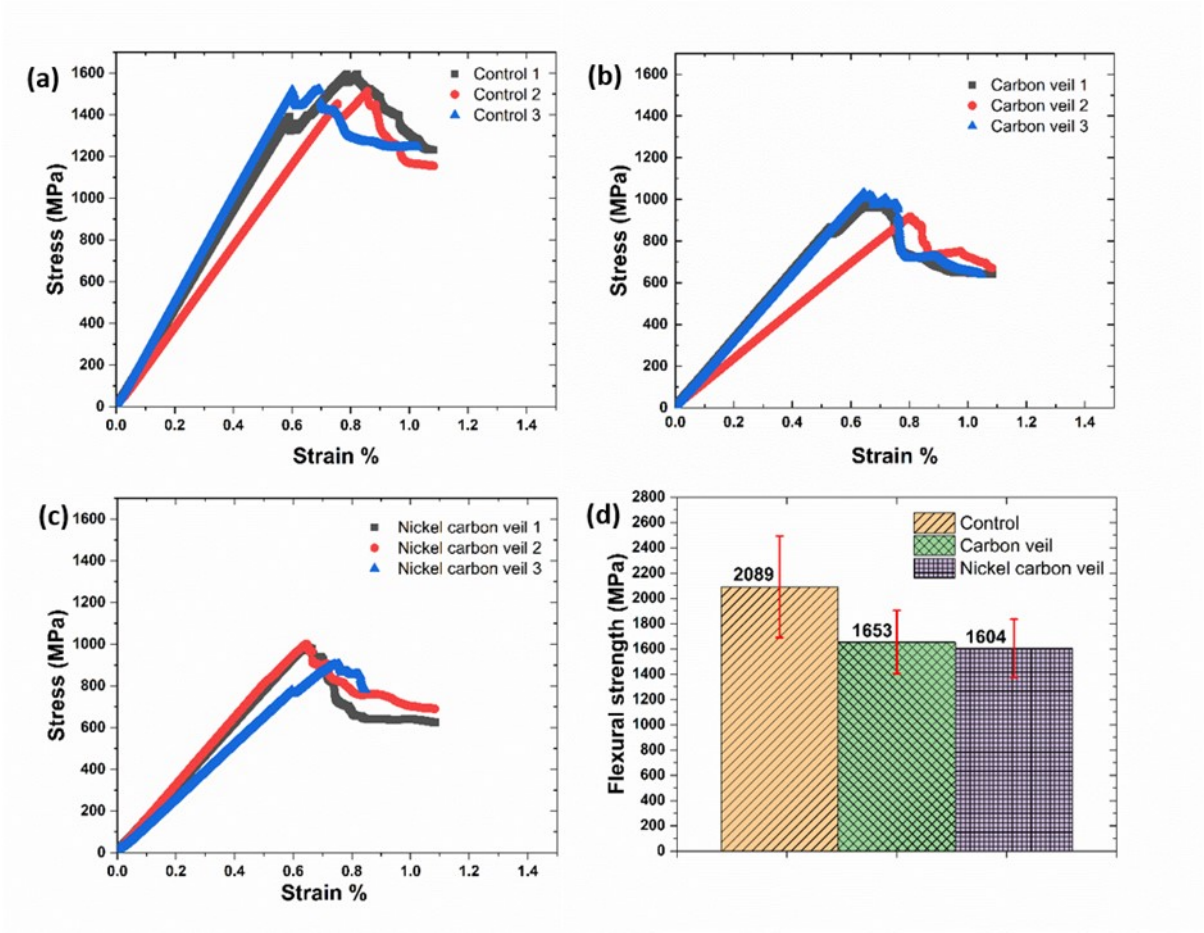

Figure 6-2 Flexural properties of control and veil-interleaved composites (a-c) flexural stress-strain plots (d) summary of flexural strength.

6.2.2 Dynamic mechanical properties

The dynamic mechanical properties of the interleaved laminates were evaluated in three-point bend mode. The tanδ (damping parameter) results are shown in Figure 6.3 as a function of temperature. The tanδ is the ratio of the viscous response to the elastic response of the material. The tanδ peak height, breadth, and glass transition temperature of the interleaved laminates were compared with the control laminate in Figure 6. The highest tanδ peak was observed in NiCF veil-interleaved CFRP samples, followed by CF veil-interleaved and control samples. Tanδ refers to the internal energy

dissipation within the material. The tanδ height for interleaved samples was higher compared to the control CFRP but with narrower peaks, indicating that the CFRP had a stronger fibre-matrix interface. The presence of binders and Ni coating on the CF veils might have an adverse effect on the bonding of epoxy resin with the veils. This resulted in higher chain mobility leading to higher energy dissipation, as seen with higher tanδ peak heights.

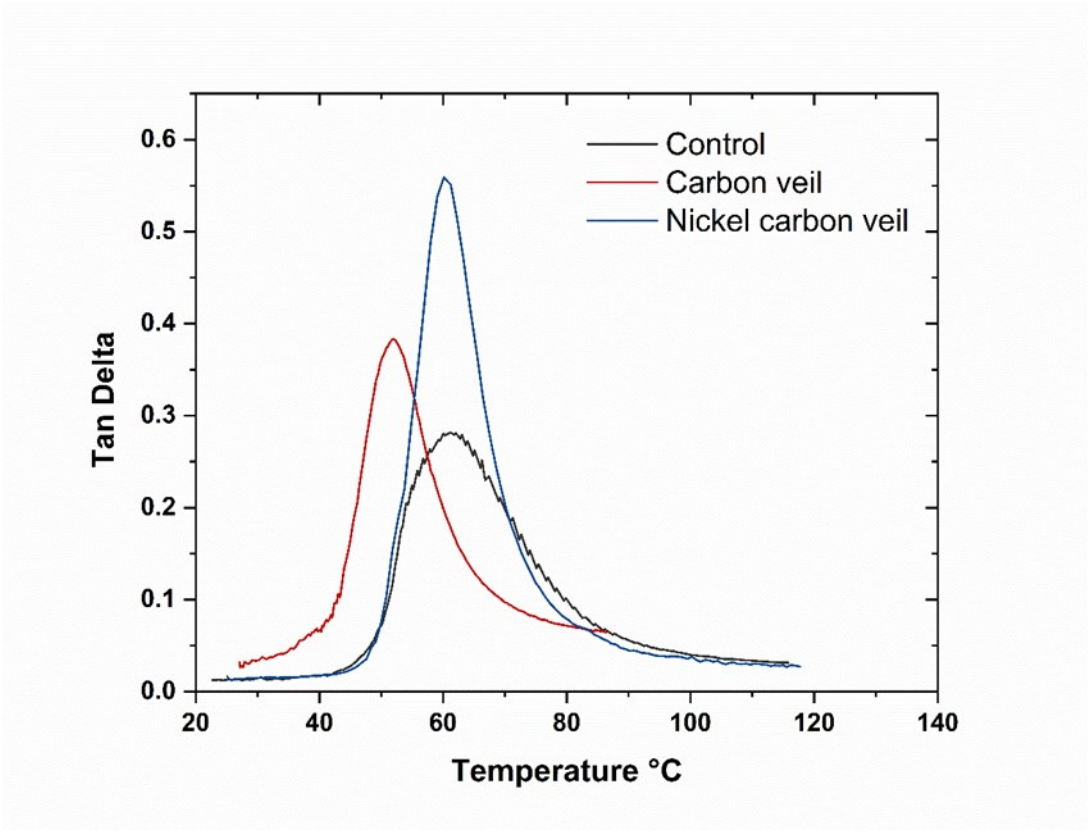

Figure 6-3 Tan δ of control and veil-interleaved composite samples in temperature sweep

6.2.3 FTIR spectroscopy

FTIR spectra of control, CF veil and NiCF veil-interleaved composites are shown in Figure 6.4. The binder present on the CF veil is cross-linked styrene-acrylic resin. In the CF veil-interleaved composite, the peak at 1727 cm^{-1} might be attributed to the C=O stretching of the ester side group of the acrylic component in the binder [3]. But the binder is hydrophobic in nature and is not likely to have any interaction with the hydrophilic epoxy resin. On the other hand, NiCF veil has a cross-linked polyester resin as the binder. The ester linkages present in the backbone of the polyester resin might have an H-bonding interaction with the OH groups of the epoxy resin. The OH stretching vibrations of the cured epoxy resins are observed in the range of 3200-3500 cm^{-1} in all the samples. The prominent peak observed at 2920 cm^{-1} in the NiCF veil-interleaved composite might be attributed to the stretching vibration of C–H bond in aromatic hydrocarbons in the cross-linked polyester binder. The ring skeleton vibration absorption peak at 1599 cm^{-1} represents the stretching vibration of the C = C bond in the benzene ring, consistent with the characteristic peak of polyester resin reported in the literature [4, 5]. The band at 1284 cm^{-1} in the spectrum of polyester is caused by the twisting and vibration of the CH_2 groups [6]. The presence of binders are therefore evident in the FTIR analysis. But binders are generally present in very small amounts on the veils and in this study, they are not chemically compatible with the epoxy resin. Hence, they are not likely to play any role in changing the interaction between the veil and the matrix resin. This is supported by the fact that the ILSS values observed were very similar in both the interleaved composites and the ILSS values were lower than the control laminate.

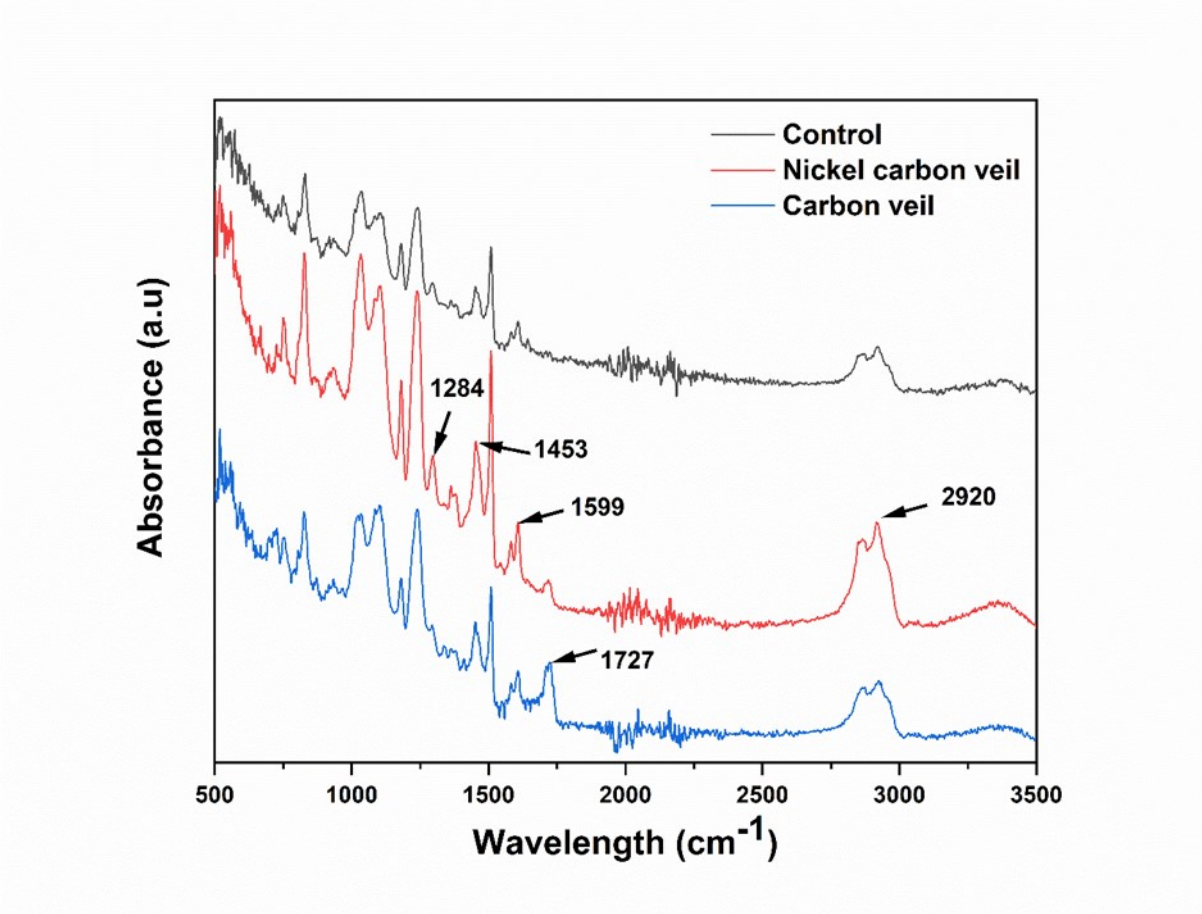

Figure 6-4 FTIR spectra of control and veil-interleaved composites.

6.2.4 SEM analysis

The SEM images of the interleaved laminates show that the veil interlayers are almost parallel to the carbon fibre plies and create a periodically laminated structure (see orange dashed lines in Figure 6.5). The carbon fibre plies and veil interlayers are well compacted, albeit some voids and imperfections can be seen, specifically within the veil interlayer regions. More SEM images of as prepared veil interleaved composites are shown in appendix C. The veil to fabric thickness ratios remained the same throughout the composite thickness. The average thickness of the carbon fibre ply in CF veil-interleaved laminate is around ca. 235 ± 37.46 µm, and the CF veil interlayer thickness is ca. 50 ± 3.88 µm. In the NiCF veil-interleaved laminate, the average thickness of carbon fibre ply is ca. 226 ± 23.56 µm, and the NiCF veil interlayer is ca.

56 ± 4.55 µm. All the measurements of carbon fibre ply and veil interlayer in the matrix are described in Table C1 of appendix C.

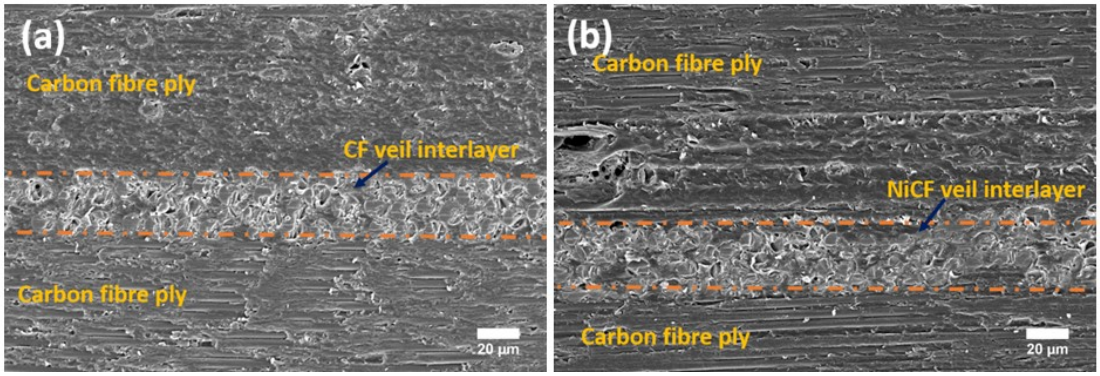

Figure 6-5 Representative SEM images of as prepared veil-interleaved composites in a longitudinal direction (a) CF veil and carbon fibre ply in matrix of CF veil-interleaved composites (b) NiCF veil and carbon fibre ply in matrix of NiCF veil-interleaved composites (Note that images are captured from the x-y plane and the position of the veils is given by the orange dashed lines).

The failed ILSS specimens were examined under SEM to determine their failure behaviour. The fracture surfaces of a pristine CFRP exhibited brittle behaviour, as shown in Figure 6.6 (a-b). Multiple shear fractures can be seen after the ILSS test. The fracture surfaces of the veil-interleaved CFRP in Figure 6.6 (c-f) show a noticeable difference as compared to the control laminate. The number and extension of cracks in the interleaved laminates are diminished. This might be due to the fact that the veil fibres take part in energy absorption in the interlayer region. The cracks in the matrix of the veil-interleaved laminates are shown by the red arrows. Some voids and cavities can be seen in the veil-interleaved regions in Figures 6.6 (d, f). These might be caused due to random orientation of the veil fibres, which forms a porous network. As the areal density increases, the probability of weak points through the veil also increases and presumably stress transfer efficiency also decreases because of added weak interlayer with lower stiffness, which is likely responsible for the reduction in mechanical properties [2, 7, 8].

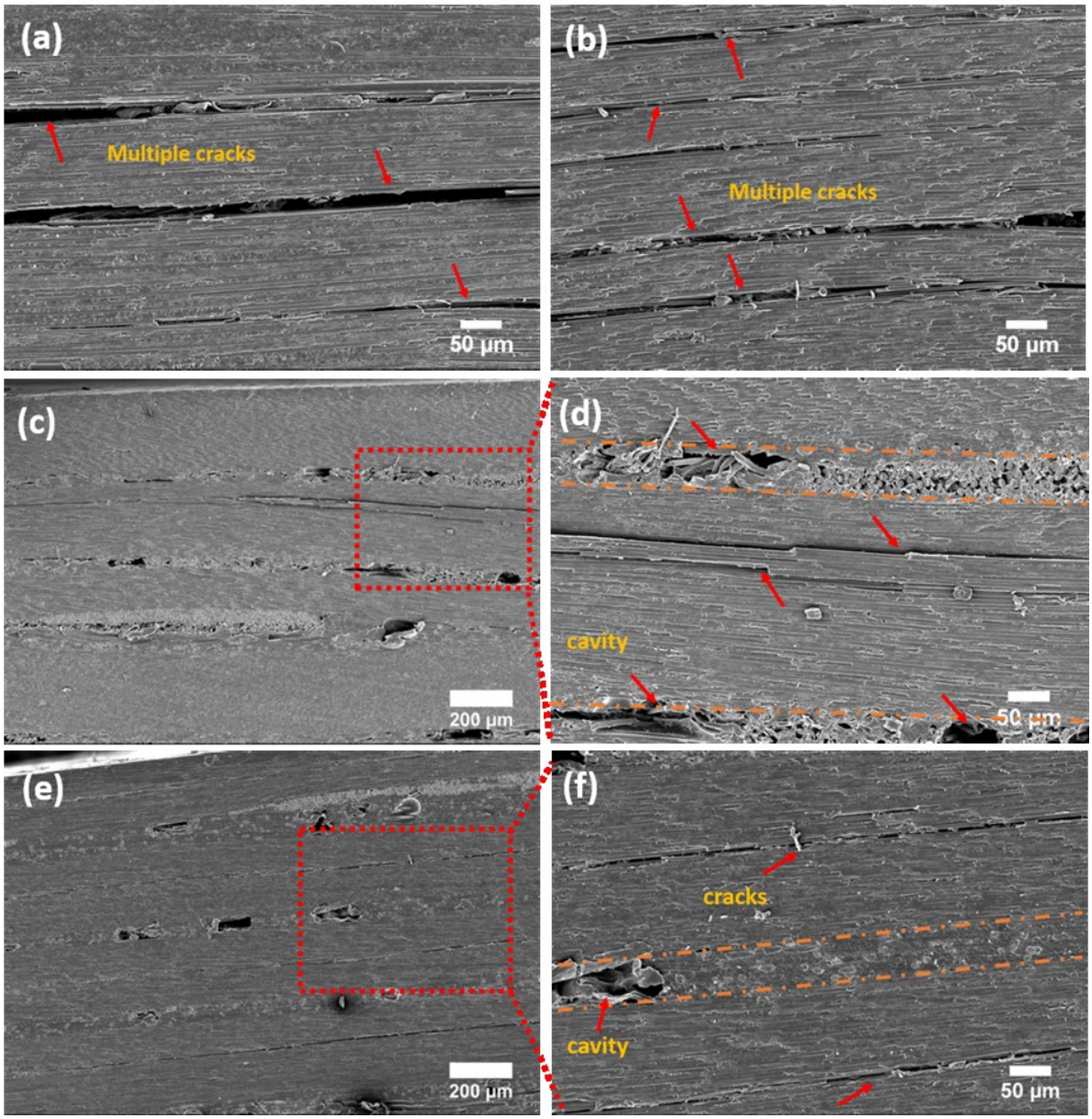

Figure 6-6 Representative SEM images of ILSS tested samples in a longitudinal direction (a-b) control (c-d) CF veil-interleaved composites (e-f) NiCF veil-interleaved composites (Note that images are captured from the x-y plane, and the position of the veils is given by the orange dashed lines).

6.2.5 Through-thickness electrical conductivity

The through-thickness electrical conductivity of the composite specimens was measured using the two-probe method [9]. The top and bottom surfaces of the laminates were polished to remove the excess epoxy resin and expose the conductive

path. A conductive silver epoxy adhesive and hardener (Circuit Works© CW2400) were mixed at a 1:1 ratio and painted onto the plates at 9 equally distributed points with 23 AWG copper wire on both sides prior to curing overnight see Figure 6.7 [7].

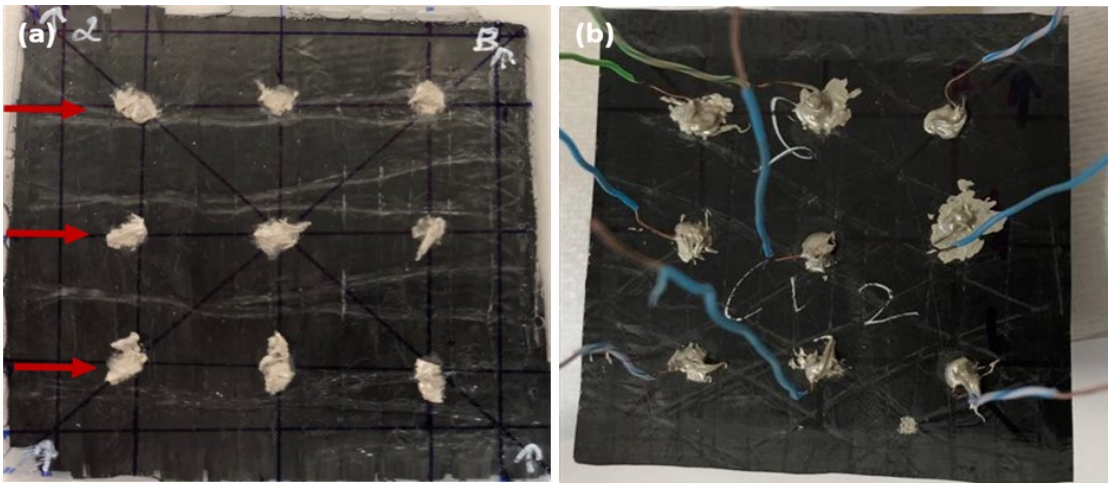

Figure 6-7 Representative images of the test laminates for through-thickness electrical conductivity measurement (a) conductive silver epoxy applied at 9 locations on a laminate, indicated via red arrows (b) copper wires attached to a laminate.

A Sciospec ISX-3v2 electrical impedance spectroscopy was used to measure the electrical impedance. One thousand data points were collected for a point electrical resistance in the through-thickness direction. The volume conductivity σ was determined by equation 3.1 [10-14]:

$$\sigma = \frac{1}{\rho} = \frac{L}{RA} \qquad \text{Equation 3.1}$$

Where ρ is the volume resistivity, L is the thickness of the specimen, R is the measured electrical resistance of the specimen, and A is the area of the sample.

The through-thickness electrical conductivity of the CF/epoxy laminates interleaved with CF or NiCF veils were measured and compared to the control CFRP as a reference. The average through-thickness electrical conductivity of the interleaved laminates was ca. 51 times higher, from 0.181 S/cm for the control CFRP sample to 9.46 S/cm for the CF veil-interleaved laminates see Figure 6.8 The conductivity of the NiCF veil-interleaved composite, on the other hand, was found to be 9.16 S/cm. This

substantial increase in through-thickness electrical conductivity was attributed to the presence of the conductive veil interlayers.

The through-thickness electrical conductivity of carbon fibre based veil-interleaved composites were not consistent across all 9 points as shown by Table 6.1. The highest and lowest conductivity achieved for CF veil-interleaved laminates is 17.357 S/cm, 3.302 S/cm, respectively. The highest and lowest conductivity achieved for NiCF veil-interleaved laminates is 16.915 S/cm, 3.105 S/cm, respectively. The highest and lowest values of electrical conductivity were almost same for both NiCF and CF veil interleaved composites. According to Brown et al. [11], a higher through-thickness conductivity with UD CFRP, is likely a result of the ability of the fibres to pack better reaching higher fibre volume fractions. A strong interfacial bonding is required when using interleaves, a weak interaction can greatly reduce the electrical conductivity. A highly conductive interlayer would improve overall conductivity. However, the bulk conductivity of carbon fibres, the composite's volume fraction, and the structural characteristics of conductive interleaves (thickness and areal density) also play an essential role. The matrix interpenetration into the interleaves is important for electrical conductivity and mechanical properties. The NiCF veil has a higher areal density than the CF veil. Therefore, resin-rich zones might exist above and below a denser interleave that does not create an inter-penetrative network with the insulating resin.

Table 6-1 The through-thickness electrical conductivity of CF and NiCF veil interleaved CFRP composites across 9 points.

Through-thickness electrical conductivity (S/cm)			
CF veil interleaved laminate	17.317	17.357	11.697
	3.302	4.4.876	12.953
	4.172	8.262	5.283
NiCF veil interleaved laminate	16.915	11.076	11.302
	9.251	3.105	7.016
	9.048	6.804	7.898

The spacing between the particles is crucial for electron transport for heterogeneous materials. With the inclusion of the conductive veils, the electron's ability to jump throughout the entire sample from one interlayer to the next was considerably boosted by following the least resistance path. The sudden rise in electrical conductivity due to incorporation of conductive veils in the interlayer regions indicates that the percolation threshold has been reached. Because of the porous nature of the veil, the conductive paths replace the conventional resin-rich regions in the interlaminar area and break the insulating barriers in through-thickness directions [2, 7, 8].

As a result, when compared to CF veil-interleaved composite, the laminate interleaved with NiCF veil has a slightly reduced through-thickness electrical conductivity. Another reason for this behaviour is because the average thickness of the NiCF veil interlayer is marginally higher (ca. 6 μm) compared to the CF veil interlayer that might have influenced the continuous electrical pathway.

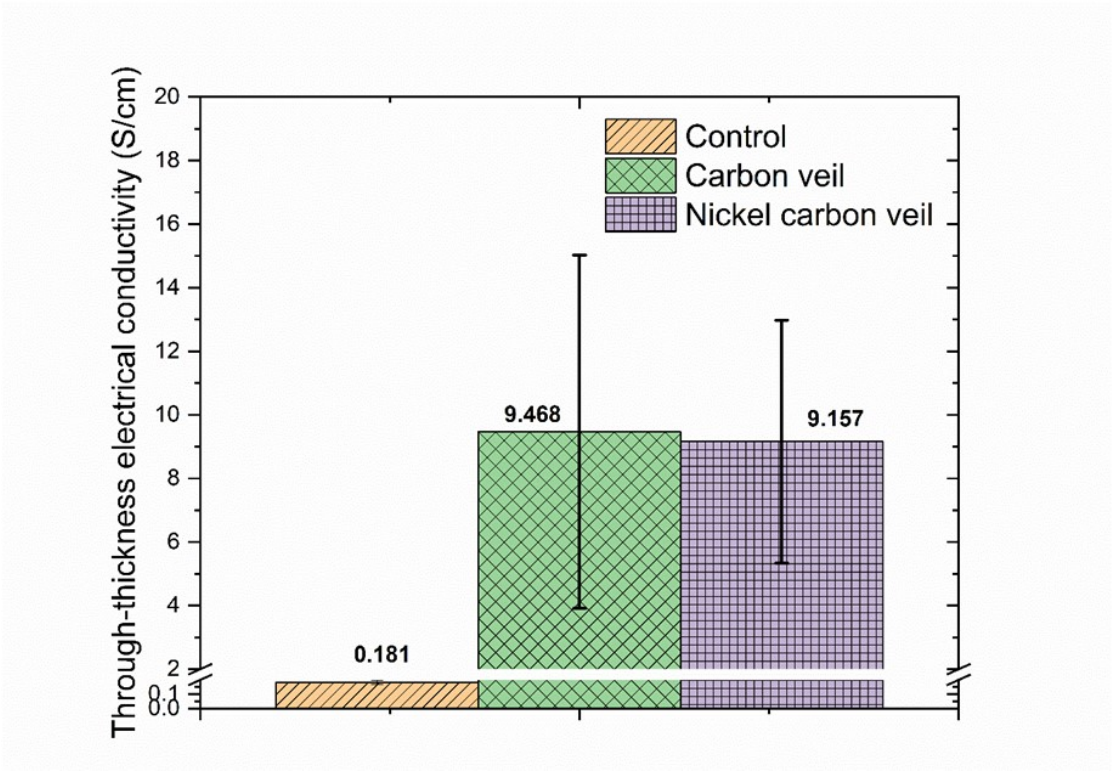

Figure 6-8 Through-thickness electrical conductivity of control, CF and NiCF veil-interleaved CFRP composites. Veil interlayer laminates have a ca. 51 fold increase in electrical conductivity compared to the control specimen.

6.3 Conclusions

CFRP composites were produced with interleaved CF or NiCF veils. A hand layup technique was used for the fabrication of the composites. The interleaved conductive veils incorporated in the resin-rich interlaminar regions between the carbon fibre plies improved the through-thickness electrical conductivity of the laminates. The through-thickness electrical conductivities of CF and NiCF interleaved composites increased from 0.181 S/cm (control) to 9.46 S/cm and 9.16 S/cm, respectively. The interlaminar shear strength was reduced by ca. 22-24% compared to that of the control specimen. The control sample underwent extensive shear failures at multiple locations, but the interleaved composites did not follow this pattern. Although electrical conductivities were enhanced, the incorporation of veils might have induced some weakness in the interlaminar regions, leading to a drop in the mechanical properties. This drop can be minimized with a suitable reactive binder on the veils and by keeping the veil areal weight as low as possible. The results show that the CF or NiCF veil based CFRP composites can provide a cost-effective and efficient way to meet the structural and functional integration requirements of the aerospace industry for electrical properties, presenting a wide range of potential applications in the field of lightning protection, EMI shielding, and structural health monitoring.

6.4 References

1. Yuan, B., Mingxin Ye, Yunsen Hu, Fei Cheng, Xiaozhi Hu., Flexure and flexure-after-impact properties of carbon fibre composites interleaved with ultra-thin non-woven aramid fibre veils. Composites Part A: Applied Science and Manufacturing, 2020. 131.

2. Bard, S., Florian Schönl, Martin Demleitner, Volker Altstädt., Copper and Nickel Coating of Carbon Fiber for Thermally and Electrically Conductive Fiber Reinforced Composites. Polymers (Basel), 2019. 11(5).

3. Jia, F., Emmanuel Oluwaseyi Fagbohun, Qianyu Wang, Duoyin Zhu, Jianling Zhang, Bin Gong, and Yanbin Cui, Improved thermal conductivity of styrene acrylic resin with carbon nanotubes, graphene and boron nitride hybrid fillers. Carbon Resources Conversion 2021. 4: p. 190-196.

4. Cecen, V., Yoldaş Seki, Mehmet Sarikanat, and Ismail H. Tavman, FTIR and SEM analysis of polyester- and epoxy-based composites manufactured by VARTM process. Journal of Applied Polymer Science, 2008. 108(4): p. 2163-2170.

5. González, M.G., Juan Carlos Cabanelas, and Juan Baselga, Applications of FTIR on epoxy resins-identification, monitoring the curing process, phase separation and water uptake. Infrared Spectroscopy-Materials Science, Engineering and Technology, 2012. 2: p. 261-284.

6. Chukwu, M., C. Madueke, and L. Ekebafe, Effects of Snail Shell as Filler on the Mechanical Properties of Terephthalic Unsaturated Polyester Resin. Niger. Res. J. Chem. Sci, 2019. 6: p. 21-32.

7. Hu, D., Xiaosu Yi, Minqiang Jiang, Genghong Li, Xiaoye Cong, Xiaoling Liu, Chris Rudd., Development of highly electrically conductive composites for aeronautical applications utilizing bi-functional composite interleaves. Aerospace Science and Technology, 2020. 98.

8. Elias, V.A.R., Effect of nonwoven veil architectures on interlaminar fracture toughness of interleaved composites, in School of Materials. 2015, University of Manchester. p. 287.

9. Koirala, P., Nekoda van de Werken, Hongbing Lu, Ray H. Baughman, Raquel Ovalle-Robles, and Mehran Tehrani., Using ultra-thin interlaminar carbon nanotube sheets to enhance the mechanical and electrical properties of carbon fiber reinforced polymer composites. Composites Part B: Engineering, 2021. 216.

10. Prabhu, R., T. Jeevananda, Kakarla Raghava Reddy, Anjanapura V. Raghu, Polyaniline-fly ash nanocomposites synthesized via emulsion polymerization: Physicochemical, thermal and dielectric properties. Materials Science for Energy Technologies, 2020. 4: p. 6.

11. Brown, S.C., Colin Robert, Vasileios Koutsos, and Dipa Ray., Methods of modifying through-thickness electrical conductivity of CFRP for use in structural health monitoring, and its effect on mechanical properties – A review. Composites Part A: Applied Science and Manufacturing, 2020. 133.

12. Guo, M., Xiaosu Yi, Chris Rudd, Xiaoling Liu., Preparation of highly electrically conductive carbon-fiber composites with high interlaminar fracture toughness by using silver-plated interleaves. Composites Science and Technology, 2019. 176: p. 29-36.

13. Chung, D.D.L., Polymer-Matrix Composites: Structure and Processing, in Carbon Composites. 2017. p. 161-217.

14. Nguyen, D.A., Anjanapura V. Raghu, Jin Taek Choi, Han Mo Jeong., Properties of Thermoplastic Polyurethane/Functionalised Graphene Sheet nanocomposites Prepared by the in Situ Polymerisation Method. Polymers & Polymer Composites, 2010. 18(7): p. 8.

Chapter 7 Conclusions and Future Work

7.1 Concluding remarks

In this thesis, the aim was to enhance the through-thickness electrical conductivity of CFRP composites using conductive veil interlayers. Recalling the information provided previously (Chapter 1), the specific goals of this thesis were the following.

The research work carried out in this thesis was focused on investigating the use of conductive electrospun nanofibres and carbon fibre-based micro fibrous veils interleaved in carbon fibre-reinforced polymer composites and assessing the potential of the veils to improve through-thickness electrical and mechanical properties. The research was planned to develop a method for efficiently collecting, evenly distributing, and manipulating the electrospun fibres on carbon fibre fabric. A nozzle-free electrospinning device was designed and constructed for the production of conductive electrospun nanofibrous veils on carbon fibre fabric. The conductive electrospun veils were synthesised using polyaniline (PANI) and polyvinylpyrrolidone (PVP), and the effects of varying PANI concentrations on the structure and characteristics of the fibres were investigated. The pre-fabricated carbon fibre-based microfibrous veils were also used to produce veil-interleaved CFRP composites. The resulting CFRP laminates with interleaved conductive veils were characterised in terms of their electrical and mechanical properties. Overall, the research aims to

improve the electrical conductivity of CFRP materials through the use of interleaving conductive veils.

7.2 Design and build of a nozzle-free electrospinning setup

The development of the nozzle-free electrospinning setup provided an economical route for needleless electrospinning research, and the higher production rate of electrospun fibres was achieved in a short time. Nozzle-free electrospinning has the ability to overcome limitations and drawbacks associated with single and multi-nozzle spinneret configurations, such as low yield, limited production capacity, non-uniform electric field distribution, and clogging. Most importantly, this lab-scale high-throughput device can provide an alternative, economical route for needleless electrospinning research, in contrast to the high costs associated with industrially available upscaling equipment. This research work started with the design and construction of a nozzle-free electrospinning setup using an existing set-up which was not in working condition and it lacked key components and integration. A few fundamental changes were made to the device's technical features. A rectangular glass tank (aquarium) of 5 mm glass thickness (dimensions: 610 mm (length) × 308 mm (width) × 380 mm (height)) was used. In total, 13 holes were carefully drilled in various compartments of the glass aquarium, taking into account the fragility of the glass material. A multi-channel gas chamber with layered glass lid was created. The ambient humidity is a critical factor that can directly affect the electrospinnability of a polymer solution as well as the subsequent morphology of the fibres. For instance, high humidity can affect the morphology of the fibres by forming defects (e.g., beads), secondary morphologies (e.g., net-like spider webs), or by completely halting a solution from being electrospun. The layered glass lid assembly allows for the uniform distribution of gas (hot air, nitrogen) onto the collector assembly, controlling the humidity and temperature within the electrospinning chamber. Each rectangular glass plate was of the following size: 590 mm (length) × 295 mm (width) × 5 mm (thickness). The outermost glass layer had 55 holes of 3 mm diameter arranged in the five rows and 11 columns, similar to perforated glass. This allowed for the uniform distribution of air/nitrogen across the glass aquarium, at a constant flow across the holes.

The two metallic collectors were made, a cryo-collector mandrel (diameter 64 mm and length 500 mm) and a small collector (48 mm and length 500 mm). The cryo-collector mandrel had a PEEK disc attached on the right side for insertion of dry ice into collector. Cryogenic electrospinning is a technique that uses a sub-zero (in °C) temperature collector to facilitate the simultaneous formation of nanofibres and ice crystals. The scaffold's pore size can be adjusted from 10 μm to 500 μm, depending on various controllable factors, such as size and the amount of ice crystals. The ice crystals are then removed by freeze-drying the fibrous scaffolds, leaving large void spaces that create an ultra-porous material with wide pores that can permit cell infiltration or resin. In addition, results from experiments using the nozzle-free electrospinning device to produce nanofibres using different polymer solutions are presented in chapter 4. The SEM images of these electrospun NFs are shown in Figure 4.10 (a-f). The nozzle-free electrospinning setup can produce homogenous and uniform electrospun mats over a large area. The higher production rate of electrospun fibres can be achieved in a very short time, 1.45 g of nanofibres collected on an aluminium foil in just 18 minutes, as shown in Figure 4.10 (g). These results demonstrate the device's ability to produce high-quality nanofibres with uniform diameter and morphology, as well as its high production yield and throughput.

As stated in Chapter 4, this setup has been successfully tested using several polymers, solvent systems and further validated by published papers in the fields of drug formulation [1], tissue engineering [2, 3], wound healing [4], energy storage [5], and energy harvesting [6]. By using this system, high-throughput nanofibres manufacturing may be accomplished effectively and affordably. This can help electrospun materials advance research in health care, energy, and a wide range of industrial sectors. All the drawings of the setup are available in the supplementary files of the published paper. So, for a low cost of 2000-2500 $, any research scientist can build a similar setup.

7.3 Electrospinning of Polyaniline and Polyvinylpyrrolidone

Chapter 5 was focused on the production of polyaniline and electrospinning of conductive polymer solutions, starting with the optimization of the solution and the identification of the working parameters and ambient conditions that would result in nano fibrous veils from the nozzle-free electrospinning setup. The first experiment set involved the synthesis of polyaniline. Chemical oxidative polymerization of aniline is the traditional method for preparing polyaniline. Polyaniline emeraldine base (PANI-EB) prepared using ammonium peroxydisulfate has a highly aggregated morphology and typical fluffy granular powder morphology. The electrical conductivity of PANI-EB is very low, and was not measurable by our set-ups (Metrohm, Autolab PGSTAT204, and Sciospec ISX-3v2 electrical impedance spectroscopy) that were used in this research. Green-coloured polyaniline emeraldine salt (PANI-ES) was synthesised after mixing aniline with two oxidants, potassium biiodate, and hypochlorite, in a 1 M HCl solution. The synthesized PANI-ES consists of an irregular mixture of thinner and longer nanofibrils and a few granular particles. The electrical conductivity of PANI-ES is 13.1 ± 1.71 S/cm which is ca. 7 times less than the value reported by A.Rahay. Stejskal et al. reported that a 40% standard deviation in polyaniline's conductivity is possible for a set of polymerization even after following the same method [7]. Variable electrical conductivity could be caused by differences in reaction conditions, sample processing, and electrical measurement conditions, such as pellet size and pressure applied to a compressed pellet. The electrical conductivity of polyaniline can be greatly influenced by varying the different parameters of

polymerization. To achieve maximum electrical conductivity by optimization of reaction speed, temperature, oxidant ratio, acid ratio, and time reaction of PANI polymerization are critical. The average diameter and length of synthesised PANI-ES nanofibrils were 124 ± 24 nm, and 1.16 ± 0.28 μm, respectively.

PVP, PANI-EB/PVP, and PANI-ES/PVP electrospun fibre veils were prepared employing nozzle-free electrospinning with varying fractions of PANI and PVP in the solution system. The electrospinning process of PANI/PVP solutions can be affected by the different morphologies of PANI and the ionic conductivity of the solution. Electrospinning of PANI-EB/PVP solutions was easier to perform than those containing PANI-ES, resulting in thinner nanofibres. The PANI-ES/PVP electrospun fibres have a smooth and uniform morphology with diameters around 200 nm, while the PANI-EB/PVP nanofibres have irregularly shaped microparticles attached to the fibres. The high surface area and encapsulation of PANI-EB particles make these nanofibres promising for applications such as gas sensing, filtration, biocompatibility, and membrane applications. These findings are valuable for researchers interested in exploring the potential of nozzle-free electrospinning for the production of conductive nanofibres for a wide range of applications.

PANI-EB/PVP and PANI-ES/PVP electrospun nanofibres were directly deposited on carbon fibre fabric. From a manufacturing perspective, direct deposition of electrospun nanofibres has benefits since it allows electrospinning to be integrated into production lines, speeding up the manufacturing process and reducing cost. Electrospun veils are very thin (few microns) with low areal weight and have minimal effect on the weight or thickness of the final product. The nanofibres do not move once inside a laminate and do not increase the viscosity of the matrix resin. The higher porosity of the electrospun veils makes it easy for the resin to flow through them while still keeping the nanofibres in place between the two layers. Unfortunately, the conductivity of the fabricated PANI/PVP electrospun nanofibre veils was not measurable by our set-ups (Metrohm, Autolab PGSTAT204, and Sciospec ISX-3v2 electrical impedance spectroscopy) that were used in this research. This could be due to the low amount of polyaniline in the electrospinning solution and the insulating nature of PVP. It has been noted that PVP in sufficient amounts of PVP compared to PANI (18:1 W/W) was

required for the successful electrospinning process. Consequently, laminates prepared with PANI/PVP electrospun nanofibre veils were also electrically non-conductive.

The cost of the polymer, its electrospinning ability, mechanical properties, glass transition temperature (T_g), and interaction with the matrix, i.e., epoxy, all influenced the choice of carrier polymer. Initially, three polymers polyethylene oxide, polyacrylic acid, and polyvinylpyrrolidone (PVP) were considered. Glass transition temperature was a key factor, and it should be as close as possible to or higher with respect to the highest temperature achieved in the post-curing of laminate. The electrospun veils with lower glass transition temperature polymer might completely melt and dissolve into the epoxy resin during the curing process rather than remaining as a nanofibre veil. It can compromise the structural and mechanical properties of laminates. PVP had better chemical, mechanical properties, and a higher glass transition temperature than other polymers.

7.4 Synthesis of carbon fibre-based veil interleaved laminates

Chapter 6 of this thesis presents the use of carbon fibre-based conducting veils as interleaving material to improve the through-thickness electrical conductivity of carbon fibre-reinforced polymer (CFRP) composites. The carbon fibre (CF) or nickel-coated carbon fibre (NiCF) veils, were used as interlayers between standard carbon fibre reinforcement fabrics. The CF and NiCF veils were proprietary products of Technical Fibre Products Ltd., UK. The unidirectional (UD) laminates were made using a hand layup technique with a stack of 5 plies $[0]_5$ of carbon fibre fabric, and interleaving veils positioned between each ply as shown in Figure 7.1.

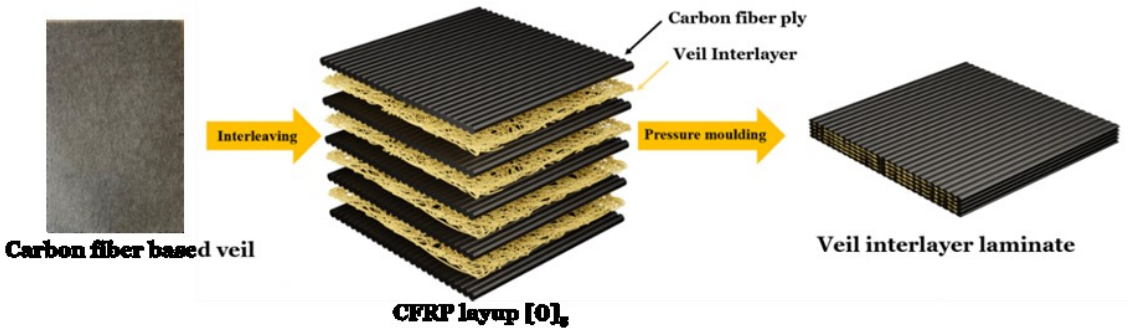

Figure 7-1 Schematic of overall CF based veil interlayer CFRP laminate preparation.

Interlaminar shear strength (ILSS) and flexural strength for the control and veil-interleaved composites samples were measured on Instron 3369. The ILSS testing has shown that the veil interleaved samples have lower interlaminar shear strength than the control specimens by 24% for the CF veil and ca. 22% for the NiCF veil laminates. The interleaved samples showed two distinctive phases. Initially, a stiff response was noted, followed by a second softer behaviour, typical to yielding, before failure. It is interesting to note that the interleaved samples experienced a displacement of 0.6 mm until failure, which is about three times greater than the displacement of the control samples. The interlaminar shear strength was lower in the interleaved composites which might be due to weaker interlaminar regions. Flexural testing revealed that the veil samples have lower flexural strength than the control specimens by 20% for the CF veil and 23% for the NiCF veil laminates. Interleaving causes a reduction in flexural performance of CFRP, since the embedded veil has a lower stiffness and strength. The flexural strength of both veil-interleaved laminates was almost equal.

FTIR spectroscopy was performed on control, CF veil and NiCF veil-interleaved composites for any possible chemical interaction between the veil binder and epoxy. The CF veil was made of carbon fibre loosely connected with a cross-linked styrene acrylic binder. The NiCF veil was made of nickel-coated carbon fibre loosely connected with a cross-linked polyester binder. The random orientation of the veil fibres forms a uniform porous network structure, which aids in resin impregnation. The binder present on the CF veil is cross-linked styrene-acrylic resin binder that is hydrophobic in nature and is not likely to have any interaction with the hydrophilic

epoxy resin. On the other hand, NiCF veil has a cross-linked polyester resin as the binder and no prominent peaks were observed. But binders are generally present in very small amounts on the veil and in this study, they were not chemically compatible with the epoxy resin. Hence, they are not likely to play any role in changing the interaction between the veil and the matrix resin. This is supported by the fact that the ILSS values observed were very similar in both the interleaved composites and the ILSS values were lower than the control laminate.

The failed ILSS specimens were examined under SEM to determine their failure behaviour. The fracture surfaces of a pristine CFRP exhibited brittle behaviour with multiple shear fractures after the ILSS test. The fracture surfaces of the veil-interleaved CFRP showed a noticeable difference as compared to the control laminate. The number and extension of cracks in the interleaved laminates have diminished. This might be due to the fact that the veil fibres take part in energy absorption in the interlayer region. The cracks in the matrix of the veil-interleaved laminates are shown by the red arrows. Some voids and cavities can be seen in the veil-interleaved regions. These might be caused by the random orientation of the veil fibres, which form a porous network. As the areal density increases, the probability of weak points through the veil also increases, and presumably stress transfer efficiency also decreases because of the added weak interlayer with lower stiffness, which is likely responsible for the reduction in mechanical properties.

The through-thickness electrical conductivity of the composite specimens was measured using the two-probe method. A Sciospec ISX-3v2 electrical impedance spectroscopy was used to measure the electrical impedance. One thousand data points were collected for a point electrical resistance in the through-thickness direction. The through-thickness electrical conductivity of the CF/epoxy laminates interleaved with CF or NiCF veils were measured and compared to the control CFRP as a reference. The average through-thickness electrical conductivity of the interleaved laminates was ca. 51 times higher, from 0.181 S/cm for the control CFRP sample to 9.46 S/cm for the CF veil-interleaved laminates. The conductivity of the NiCF veil-interleaved composite, on the other hand, was found to be 9.16 S/cm. This substantial increase in through-thickness electrical conductivity was attributed to the presence of the

conductive veil interlayers. A higher through-thickness conductivity with UD CFRP, is likely a result of the ability of the fibres to pack better reaching higher fibre volume fractions. However, the bulk conductivity of carbon fibres, the composite's volume fraction, and the structural characteristics of conductive interleaves (thickness and areal density) also play an essential role. The matrix interpenetration into the interleaves is important for electrical conductivity and mechanical properties.

The use of interleaving conducting veils in CFRP composites has been shown to provide a number of benefits, including the establishment of an electrically conductive pathway across the thickness of the laminate and the reduction of the non-conducting resin-rich zone in the interlaminar region. The results show that the CF or NiCF veil based CFRP composites can provide a cost-effective and efficient way to meet the structural and functional integration requirements of the aerospace industry for electrical properties, presenting a wide range of potential applications in the fields of lightning protection, EMI shielding, and structural health monitoring.

The findings reported throughout this thesis, as well as the challenges that were identified but remained unaddressed, offer only a glimpse of what can be achieved when electrospun structures are used to enhance the through-thickness electrical conductivity of CFRP composites. The project evolved through several stages, initially focusing on the material aspect, and eventually progressing to an application oriented evaluation of their electrical properties. The interdisciplinary work presented in this thesis opens up new pathways for exploration in regards to the fields of materials science, nanotechnology, lightning strike and structural health monitoring.

7.5 Limitations

The work presented in this thesis had some inevitable limitations. The project involved several areas, including materials science, electrical engineering, mechanical engineering, and CFRP composites engineering. This made it challenging; considerable time and effort were dedicated to using all the necessary equipment, undergoing training, conducting diverse experiments and characterisation, and analysing data.

Most of the research activities mentioned were conducted in the Nano Materials and Composites laboratories of the School of Engineering. This lab's nozzle-free electrospinning apparatus produced nano-fibrous electrospun materials. The nozzle-free system lacked some accessories and features that could have made electrospinning more efficient and exhaustive. The revolutions per minute (RPM) controller for the nozzle-free electrospinning works fine; however, the device appears to be incapable of handling speeds beyond 1000 RPM for an extended period of time. The device shakes at high RPM and puts considerable mechanical stress on the electrospinning chamber walls if left running. We could have tested whether electrospinning at high RPMs produced dense structures with mainly aligned fibres.

Another limitation at times was the availability of electrical conductivity measurement setups such as Metrohm, Autolab PGSTAT204, and Sciospec ISX-3v2 electrical impedance spectroscopy. Both were not available in the nanomaterials laboratory; thus, it was necessary to arrange the training for using these devices and also check the availability of these devices in other laboratories. This would work out fine most of the time, but often resulted in the interruption of my experimental work when the device was under the constant use of the device owner. It was extremely difficult to gain access to Metrohm, Autolab PGSTAT204, and Sciospec ISX-3v2, but this problem was solved by collaborating with other students.

The effect of the previous limitations was further exacerbated by the COVID-19 pandemic. Laboratory closures and the restrictive working policies enforced once people were allowed back into the buildings resulted in the experimental work

presented in this thesis slowing down severely. There were significant delays in getting access to labs for the characterization of samples from different labs, i.e., XRD characterization (School of Chemistry), and EDX (School of Physics). The unidirectional (UD) laminates were made using a hand layup technique with a stack of 5 plies $[0]_5$ of electrospun coated carbon fibre fabric. After being hand laid up, the laminates were consolidated in a press at 1 bar of pressure and left to cure at room temperature. Overall, this hand layup method was not ideal, and vacuum-assisted resin transfer moulding (VARTM) could have been used for laminate synthesis for a significant improvement in laminate quality. Future work

7.6 Future work

The work carried out in this thesis allowed me to experiment with several polymers, pre-fabricated veils, and methods for improving the through-thickness electrical conductivity of CFRP composites. While this work was going on, several improvements were identified, some of which were addressed in previous chapters. However, some of the aspects that were identified posed greater challenges and would require more extensive work. The following propositions represent the main lines of work that could be of interest for further investigation.

1 The PVP has good solubility, film forming, electrospinability, adhesive, compatibility with other polymers, and mechanical properties. Because of these properties, the PVP chemical interaction with resin could provide good mechanical properties in CFRP composites. In the current study, a higher amount of PVP (18:1 W/W) was used compared to PANI to electrospun the PANI/PVP solutions. The results from Chapter 5 showed that due to the insulating nature and higher concentration of PVP used in PANI/PVP solution used to produce their electrospun veils, they were not electrically conductive. Therefore, substituting the carrier polymer PVP with any other piezoelectric polymer, i.e., PVDF, could produce PANI/PVDF conductive electrospun veils. It would also be interesting to investigate the potential of using other conductive polymers, such as polypyrrole and polythiophene, in the

electrospinning process. Additionally, it would be fascinating to investigate the potential of using other conductive materials, such as carbon nanotubes and graphene, in conjunction with conductive polymers to produce conductive veils.

2 Electrospun nano-fibres are deposited at the collector as randomly aligned non-woven veils. The mechanical properties of nanofibres can be much higher than those of the same material in its bulk state. The alignment of nanofibres in the polymer matrix can increase the mechanical properties of composite materials. Aligned PANI/PVP electrospun nano-fibres deposited on carbon fibre fabric may form a strong interfacial bonding with the polymer matrix, which could lead to good load transfer from the polymer matrix to the reinforcing nano-fibres and overall better mechanical properties of the resultant polymer composites. Investigating the effect of PANI/PVP electrospun veils on impact damage resistance, fracture toughness, and delamination behaviour would be worthwhile.

3 Interlaminar toughening is generally affected by the thickness of nanofibre veils, porosity, and adhesion of the nanofibre veils with the primary reinforcement (i.e., carbon or glass fabrics). Higher porosity in the veils can make them more permeable, allowing polymer resin to flow through the plies more easily. This, in turn, improves the adhesion between the two layers, which is advantageous for interlaminar toughening. If the nanofibre veil thickness increases, there might be reduction in veil porosity. Different researchers have used thicknesses ranging from 20 µm to 150 µm, and the average areal density (mass per unit surface area) of the fibre layer has been between 0.7 g/m^2 and 45 g/m^2. Because of the way that the interlaminar toughening operates, it is difficult to compare these results. Each laminate system may have its own morphological characteristics of electrospun nanofibres, such as an ideal thickness.

4 In carbon fibre polymer composites, mode-I and mode-II fracture toughness tests can be used to determine the resistance of the composite material to crack growth in different directions. These tests can provide valuable information about the material's performance in real-world applications, where cracks can develop in a variety of orientations. The Mode-I fracture toughness test, also known as the "crack-opening" or "tensile" mode, measures the ability of a material to resist crack

propagation when a crack is present and the material is subjected to an external loading that tends to open the crack. This test is typically used to measure the fracture toughness of materials in the presence of a crack that is perpendicular to the direction of applied loading. The Mode-II fracture toughness test, also known as the "shear-opening" or "in-plane shear" mode, measures the ability of a material to resist crack propagation when a crack is present and the material is subjected to an external loading that tends to slide the crack surfaces past each other. This test is typically used to measure the fracture toughness of materials in the presence of a crack that is parallel to the direction of applied loading. In this study, flexural and short beam shear testing were performed on carbon fibre-based veil interleaved laminates. Further mechanical testing of mode-I and II fracture toughness should also be performed to assess the effect of the insertion of veils in the interlaminar region of CFRP laminate fracture toughness.

5 Tomography of CFRP laminates interleaved with carbon fibre-based veils could be conducted. For the purpose of early diagnosis of scarcely perceptible impact damage, electrical resistance tomography (ERT) should be taken into consideration as a structural health monitoring technology. Electrical resistance tomography (ERT) is a soft-field tomographic method that can map a spatial representation of electrical conductivity. Tomography measurements are based on the boundary voltages that show up when an electrical constant-value current flows. One of the biggest benefits is that ERT can be used in-situ because it doesn't require as much equipment as other methods. The results in Chapter 6 showed that carbon fibre-based veil interleaved laminates are highly conductive in the through-thickness direction. Further study should also be performed with a damage-detection capability assessment using ERT in the area of CFRP composites involving relevant conductive paths.

7.7 References

1. Keirouz, A., Norbert Radacsi, Qun Ren, Alex Dommann, Guido Beldi, Katharina Maniura-Weber, René M. Rossi, and Giuseppino Fortunato., Nylon-6/chitosan core/shell antimicrobial nanofibers for the prevention of mesh-associated surgical site infection. Journal of nanobiotechnology, 2020. 18(1): p. 51.

2. Keirouz, A., Giuseppino Fortunato, Mei Zhang, Anthony Callanan, and Norbert Radacsi, Nozzle-free electrospinning of Polyvinylpyrrolidone/Poly(glycerol sebacate) fibrous scaffolds for skin tissue engineering applications. Med Eng Phys, 2019. 71: p. 56-67.

3. Muenwacha, T., Oratai Weeranantanapan, Nuannoi Chudapongse, Francisco Javier Diaz Sanchez, Santi Maensiri, Norbert Radacsi, and Wiwat Nuansing, Fabrication of Piezoelectric Electrospun Termite Nest-like 3D Scaffolds for Tissue Engineering. Materials, 2021. 14(24): p. 7684.

4. Keirouz, A., Mariia Zakharova, Jaehoon Kwon, Colin Robert, Vasileios Koutsos, Anthony Callanan, Xianfeng Chen, Giuseppino Fortunato, and Norbert Radacsi, High-throughput production of silk fibroin-based electrospun fibers as biomaterial for skin tissue engineering applications. Mater Sci Eng C Mater Biol Appl, 2020. 112: p. 110939.

5. Radacsi, N., Fernando Diaz Campos, Calum RI Chisholm, and Konstantinos P. Giapis, Spontaneous formation of nanoparticles on electrospun nanofibres. Nat Commun, 2018. 9(1): p. 4740.

6. Sanchez, F.J.D., Michael Chung, Muhammad Waqas, Vasileios Koutsos, Stewart Smith, and Norbert Radacsi, Sponge-like piezoelectric micro- and nanofiber structures for mechanical energy harvesting. Nano Energy, 2022. 98: p. 107286.

7. Stejskal, J., and R. G. Gilbert, Polyaniline. Preparation of a conducting polymer (IUPAC technical report). Pure and applied chemistry, 2002. 74(5): p. 857-867.

Appendix A

Table A-1 List of the assembled and connected parts/material used for the manufacturing nozzle-free electrospinning setup.

Category	**Designator**	**Component**	**Material source**	**Material type**
Glass aquarium	Glass, fish tank	Rectangular glass unit for nozzle-free electrospinning setup	Porton Garden Aquatic & Pets, UK	Glass
		Safety Interlock	RS Components Ltd. UK	Steel and plastic
		Rectangular bars for lid support	Direct Plastics Online Limited, UK	Acrylic

	Layered glass assembly	Rectangular glass plates	Saint-Gobin Limited, UK	Glass
		Swagelok connector for air passage	RS Components Limited, UK	Stainless steel
		Circular diamond-tipped drills	RS Components Limited, UK	Aluminium
		Transparent epoxy	Bostik Limited, UK	Adhesive
Heating assembly	Heating unit	Copper tubing	RS Components Limited, UK	Copper
		Metallic hose clamp	RS Components Limited, UK	Steel
		Ultra-high-temperature heating tape	Omega Engineering, UK	Samox insulated
		Swagelok connector for air passage	RS Components Limited, UK	Stainless steel
		Glass fibre yarn ladder tape	RS Components Limited, UK	Glass fibre

		Hollow round pipe	-	Aluminium
		Silicone pipe	RS Components Limited, UK	Silicone
	Analogue Heating controller	MC242 heating controller	Electrochemical, Cole-Palmer, UK	-
Collector assembly	Fabricated/machined parts	PEEK disc	-	PEEK
		Flexible Beam Coupling, Bore A 6mm Bore B 10mm.	Enrgtech Limited, UK	Glass Fibre Reinforced Polyamide
		PEEK connector	-	PEEK
		Ball-bearing dia. 8mm	RS Components Limited, UK	Stainless steel
		Round hollow collector diameter 64 mm, 48 mm	-	Stainless steel pipe

		M3 screws	RS Components Limited, UK	Plastic
		M2 screws	RS Components Limited, UK	Metal
Spinneret assembly	Fabricated/machined parts	Spinneret of 60 mL, 40mL, 2 mL	_	Teflon
		PEEK connector	-	PEEK
		Metallic electrode	-	Stainless steel
		Metallic electrode with spiral steel coil	_	Stainless steel
		Flexible Beam Coupling, Bore A 6mm Bore B 10mm	RS Components Limited, UK	Aluminium
		Connecting rod	-	Teflon

Electronics	Spinneret assembly	DC motor, 6 V, 5 RPM	RS Components Limited, UK	-
	Collector assembly	Bosch DC Motor, 28 W, 12 V dc, 6 Ncm, 4500 RPM, 6mm Shaft Diameter	RS Components Limited, UK	-
		adjustable DC power supply Model HCS	Manson Engineering Industrial Ltd.	-
	Power supply	5kV-35kV DC Universal power supply	Information Unlimited, New Hampshire, USA	-
		High Voltage wires	RS Components Limited, UK	

Appendix B

Table B-1 Average thickness of PANI/PVP electrospun veils deposited on carbon fibre fabric. (PANI-EB: Polyaniline emeraldine base, PANI-ES: Polyaniline emeraldine salt, PVP: Polyvinylpyrrolidone, SD: Standard deviation)

No	**5.55 mg mL^{-1} PANI-EB** (μm)	**11.11 mg mL^{-1} PANI-EB** (μm)	**5.55 mg mL^{-1} PANI-ES** (μm)	**11.11 mg mL^{-1} PANI-ES** (μm)
1	63.254	84.67	100.0451	63.23
2	65.26	116.003	109.035	42.286
3	69.715	123.228	91.106	59.212
4	65.972	114.009	87.406	81.059
5	70.439	140.868	104.86	134.317
6	64.082	129.09	107.17	98.005
7	79.89	140.976	109.86	132.299
8	70.018	127.36	122.572	82.589

9	68.014	81.722	114.62	84
10	66.687	79.147	142.52	81.722
11	63.453	59.427	106.261	69.147
12	62.832	67.576	71.47	59.427
13	70.04	56.488	68.91	57.576
14	72.1	60.503	69.09	56.488
15	73.81	67.523	64.909	60.503
16	74.21	57.819	63.094	57.523
17	70.6	68.35	51.315	47.819
18	66.25	95.31	98.64	66.29
19	75.29	105.23	88.62	71.79
20	69.74	79.45	77.31	98.123
Mean	69.327	91.845	90.373	76.122
SD	4.439	28.181	23.963	24.09

Appendix C

Additional figures:

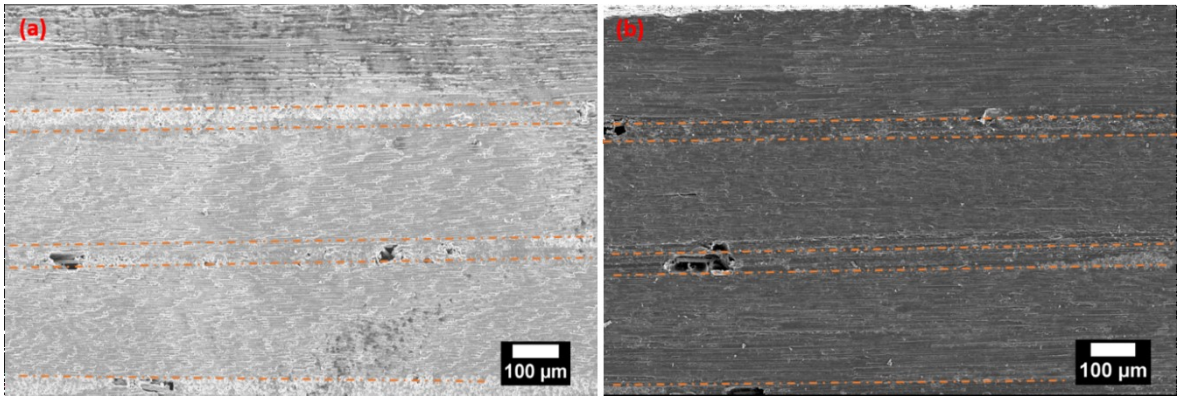

Figure C-1 SEM images of as prepared veil-interleave composites: (a) CF veil-interleaved composites, (b) NiCF veil-interleaved composites (Note that images are captured from the x-y plane and the position of the veils is given by the orange dashed lines).

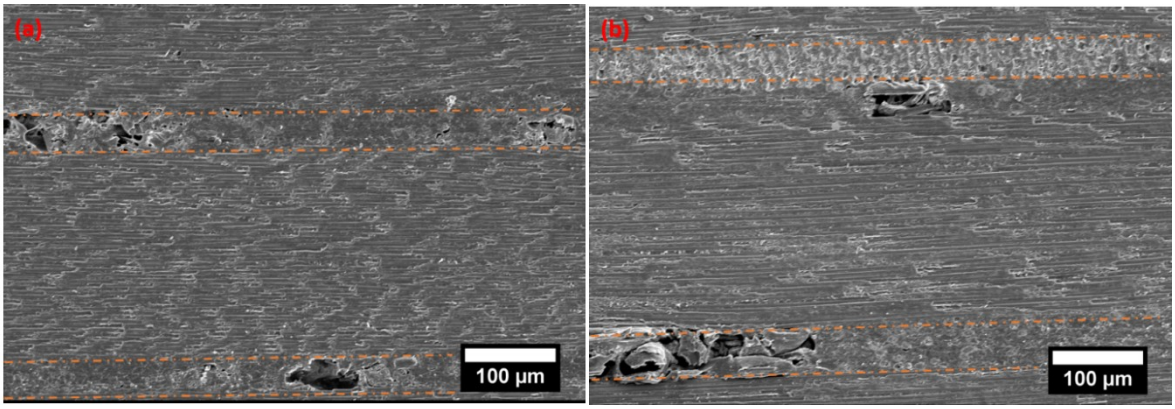

Figure C-2 SEM images of as prepared veil-interleaved composites: (a) CF veil-interleaved composites, (b) NiCF veil-interleaved composites (Note that images are captured from the x-y plane and the position of the veils is given by the orange dashed lines).

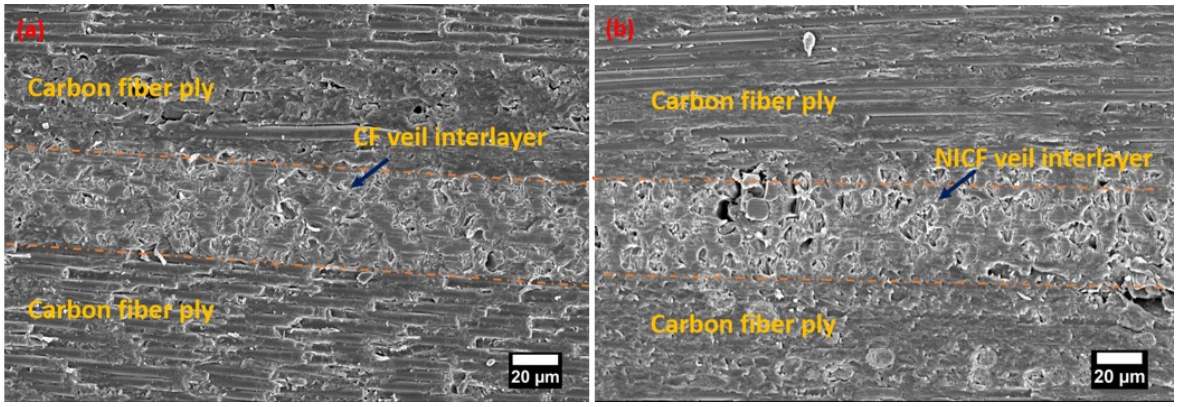

Figure C-3 SEM images of as prepared veil interleaved composites: (a) carbon fibre ply and CF veil and in matrix of CF veil-interleaved composites (b) carbon fibre ply and NiCF veil in matrix of NiCF veil-interleaved composites (Note that images are captured from the x-y plane and the position of the veils is given by the orange dashed lines).

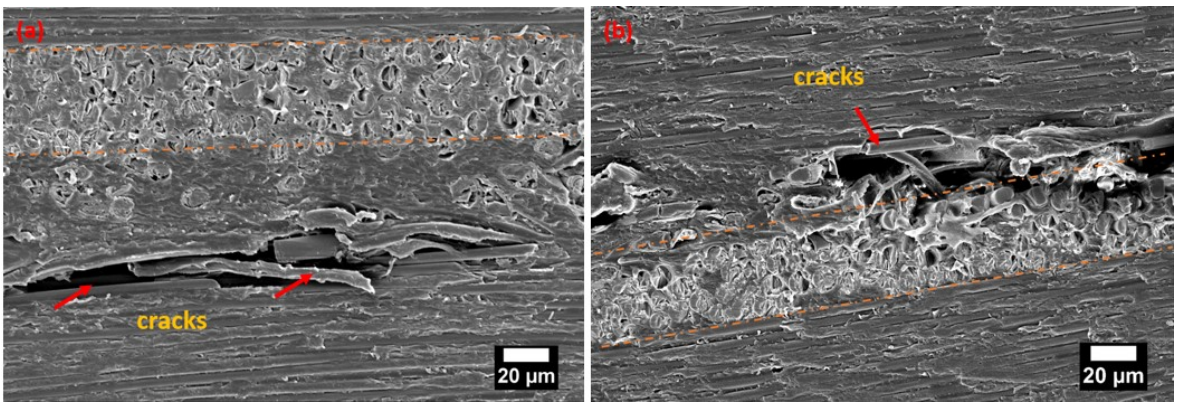

Figure C-4 SEM images of ILSS tested samples; cracks are shown by red arrows (a) CF veil-interleaved composites (b) NiCF veil-interleaved composites (Note that images are captured from the x-y plane and the position of the veils is given by the orange dashed lines).

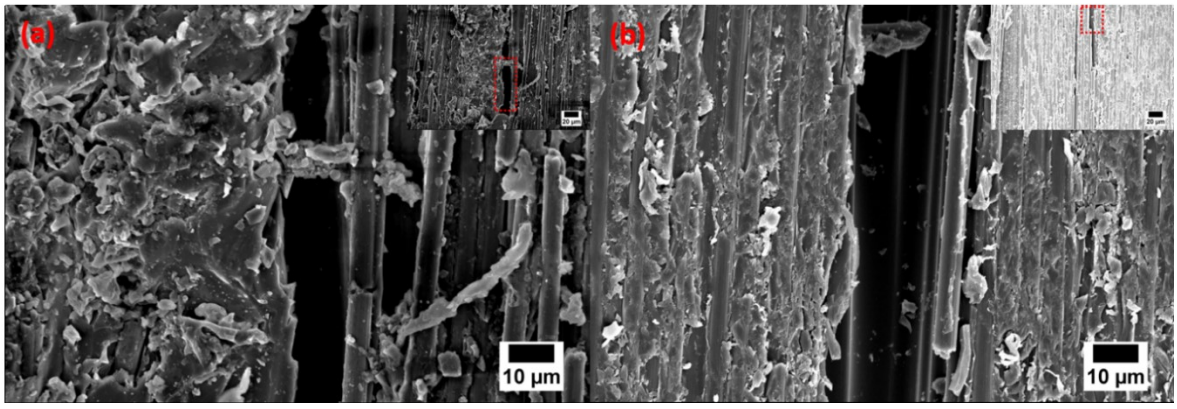

Figure C-5 SEM images of ILSS tested samples (a) CF veil-interleaved composites (b) NiCF veil-interleaved composites.

Table C-1 Measurements of the thickness of carbon fibre ply and veil interlayer in the matrix. (CF: carbon fibre, NiCF: nickel carbon fibre. SD: Standard deviation)

No	Carbon fibre ply of CF veil laminate (μm)	CF veil interlayer (μm)	Carbon fibre ply of NiCF veil laminate (μm)	NiCF fibre veil interlayer (μm)
1	255.015	50.000	195.359	59.131
2	258.835	48.248	190.276	56.161
3	249.422	46.804	181.728	57.556
4	237.348	51.261	183.000	57.556
5	241.701	49.256	255.838	48.146
6	253.347	50.651	251.247	49.146
7	236.06	51.051	245.284	55.122
8	246.796	48.251	247.504	47.115
9	233.394	53.453	214.767	52.202
10	260	49.051	216.317	59.841
11	253.46	51.852	199.612	54.342
12	238.76	57.658	236.000	51.971
13	216.411	55.688	226.014	55.271
14	232	57.906	222.081	51.271
15	174.794	46.543	231.695	60.531

16	140	53.561	223.701	59.034
17	129.443	48.431	209.441	64.231
18	276	46.900	229.940	53.764
19	274.718	46.411	226.375	66.310
20	288.745	48.804	235.287	58.775
21	264.484	44.621	237.070	59.775
22	260	49.600	239.743	56.256
23	255	46.067	225.484	56.189
24	262	56.620	247.765	54.770
25	288.722	51.044	232.675	54.509
26	248.247	48.382	238.859	55.819
27	258.247	47.680	232.613	53.219
28	244.237	49.717	222.854	52.670
29	258.647	49.012	243.308	53.933
30	171.69	53.894	244.200	53.601
31	178.722	54.675	243.349	54.690
32	300.752	56.016	229.048	50.699
33	306.306	50.251	189.000	55.602
34	230.23	49.230	185.500	51.480
35	216.216	50.368	188.851	54.392

36	242.242	55.681	246.548	54.211
37	244.264	54.176	266.600	52.773
38	228.228	56.441	269.075	56.719
39	196.196	45.106	205.082	54.953
40	202.212	48.309	220.718	55.729
41	200.2	50.094	225.650	55.444
42	206.216	52.550	223.553	50.961
43	196.206	55.434	230.547	67.476
44	260.26	55.771	236.534	61.660
45	182.156	51.023	272.606	58.052
46	242.242	52.056	255.003	68.659
47	235.740	55.170	230.060	62.036
48	190.620	44.071	240.040	55.660
49	232.242	42.426	198.080	60.000
50	248.680	44.173	176.721	55.020
Mean	234.95	50.63	226.372	56.09
SD	37.46	3.885	23.56	4.55

Table C-2 Typical uncured resin (IN2 epoxy infusion resin, Easy Composites Ltd., UK) and hardener properties.

Property	Units	Resin	Hardener	Combined
Material		Epoxy resin	Formulated amine	Epoxy
Appearance		Clear liquid	Amber liquid	Clear liquid
Viscosity @ 20 ºC	mPa.s	500-800	10-20	200-500
Density @ 20 ºC	g/cm^3	1.08-1.18	1.07-1.13	1.12-1.18
Molecular weight	g/mol	=<700	-	-

Table C-3 Typical cured resin (IN2Epoxy resin + AT30 Slow) properties.

Property	Units	IN2 Epoxy resin + AT30 SLow
Colour		Pale yellow
Machinability		Excellent
Density @ 25 ºC	g/mL	1.08-1.12
Hardness @ 20 ºC	Shore D/15	84.5-88.5
Maximum T_g	ºC	92-98

Water absorption (24h RT)	%	0.12-0.20
Water absorption (2hr @ 100 ºC)	%	0.58-0.70
Flexural strength	MN/m^2	112-124
Maximum strength	%	5-7
Strain at break	%	6-8
Flexural modulus	MN/m^2	3150-3550
Tensile strength	MN/m^2	65.5-73.5
Elongation at break	%	6-8